Study of Drilling Properties in Bone Biomodel

Doctoral Thesis

Study of Drilling Properties in Bone Biomodel

A Dissertation Submitted for the Degree of Doctor of Philosophy (Biomedical Engineering)

Graduate School of Biomedical Engineering
TOHOKU UNIVERSITY

by

Yuta MURAMOTO

(ID No. B7WD1004)

February, 2020

TOHOKU UNIVERSITY

Graduate School of Biomedical Engineering

Study of Drilling Properties in Bone Biomodel

（骨モデルにおける切削特性に関する研究）

A Dissertation Submitted for the Degree of Doctor of Philosophy (Biomedical Engineering)

Department of Biomedical Engineering

by

Yuta MURAMOTO

February, 2020

修了年度	2020 年度	課程	博士課程後期 3 年の課程

英文 Abstract

Title: Study of Drilling Properties in Bone Biomodel
Author: Yuta MURAMOTO
Supervisor: Makoto OHTA

Drilling of bone is a fundamental surgical skill in orthopedics, dentistry, and neurosurgery. Bone biomodels are indispensable for surgical training and mechanical tests of medical devices, having their merits in the ease of handling and consistency of material properties. However, a bone biomodel produced under the standard specification is reported to show different drilling properties compared to those of cortical bone. Toward development of bone biomodels that cover drilling properties of bone, this thesis finds out the relationship among mechanical and drilling properties, and tactile feedback during drilling. To do so, acrylic composite materials including ceramic additives were fabricated, and the effects of additives on drilling properties were studied. Assuming that the alternation of drilling properties is related to the changes of mechanical properties dominant on drilling, mechanical tests were performed. Besides, tactile feedback was obtained through manual drilling by surgeons.
The experimental results suggest that additives can alter both drilling and mechanical properties. This effect becomes larger along the increase in additive amount up to 40 wt%. Acrylic composite materials exhibit the good similarity to bone in perceptual feedback during drilling. These results are considered to be attributed to changes of thrust force during drilling, which were brought by the changes of hardness and elasticity of acrylic resin due to additives.

和文アブストラクト

論文題目： 骨モデルにおける切削特性に関する研究
提出者氏名： 村元 雄太
指導教員： 太田 信

骨切削は整形外科，歯科，脳外科における基本手技である．骨切削の訓練や切削に関連する医療機器の力学試験のために骨モデルは必要不可欠であり，生体骨に比べて扱いの容易さや品質の恒常性に特徴がある．規格に沿って製造された骨モデルも存在するが，生体骨と異なる切削特性を示すことが指摘されている．本研究では，皮質骨の切削特性を再現する骨モデル材料の開発指針獲得のため，骨モデル材料に用いられるアクリル樹脂にセラミック系添加物を混合させた複合材料を作製し，これを用いた切削試験を行うことによって，添加物が切削特性に与える影響を解析した．また切削特性の違いは，切削に寄与する力学特性の違いに基づくと考え，切削に影響すると考えられる力学特性を解析した．更に，切削特性に付随する切削感覚との関連を解明するため，医師による複合材料切削時の感覚調査と切削特性の測定を行った．
試験の結果より，セラミック系添加物を混合することにより複合材料の切削および力学特性が変化することがわかった．混合量 40wt%まで調べると，混合比が高くなるに従い各特性は大きくなった．また複合材料は既存の骨モデルよりも皮質骨に近い切削感覚を示すとの評価を受けた．これらの結果は、添加物が複合材料の硬さや弾性を変化させ，医師が切削時のスラスト力を変化させたことによる可能性がある．

Table of Contents

Chapter 1: Bibliography Synthesis

This chapter presents the state of the art in drilling of bone biomodels, by reviewing the literatures concerning biomodel, bone, and drilling, followed by the description of the objective of this study and the research approach toward improvement of bone biomodels.

1.1. Introduction

Drilling of bone is one of the common surgical steps. Surgical treatment results are largely influenced by the surgical skills of surgeons and the performance of medical devices. Then, it is important especially in Japan, the most super-aged society in the world, that surgical training of doctors and development of high-performance medical devices should be carried out efficiently.

Biomodels can function to meet the rapidly increasing demands for medical resources. Bone biomodel is one of the biomodels that replicate human tissue, and known for its usage in surgical training for doctors or mechanical tests of medical devices.

A number of bone biomodels are currently available in the market, but the reproducibility of drilling of bone has little been paid attention and barely been in the research scope up until today. Therefore, conventional bone biomodels cannot fully reproduce the unique drilling behavior of natural bones. Besides, evaluation items among physical and mechanical properties of biomodels toward the replication of drilling of bone is uncertain.

Replication of drilling includes both drilling properties such as thrust force and torque, and tactile feedback during drilling. These aspects should be influenced by physical and mechanical properties of work materials. In order to improve the conventional bone biomodels, it is necessary to fabricate the alternative materials based on understanding of the correlation among mechanical and drilling properties, and tactile feedback during drilling.

Then, the objective of this study is to find out the relationship between mechanical and drilling properties, and also drilling properties and tactile feedback during drilling for the development of bone biomodels that cover drilling characteristics of natural bone.

To accomplish this objective, the present study adopts the fabrication of composite materials to look into the effects of additives on mechanical and drilling properties, and tactile feedback during drilling. Contrary to the conventional approach that relied on the tactile feedback of doctors, where there were a lot of trials and errors for improvement, quantitative characterization of mechanical and drilling properties from the standpoint of engineering are applied to drilling of bone biomodels as well as natural bones and conventional bone substitute materials.

In this chapter, backgrounds and literature studies focusing on biomodel, bone, and drilling are summarized, including the current limitations and challenges in the development of bone biomodels. The research objectives and approaches to achieve the objectives are also described as well as the outline of this thesis.

1.2. Biomodel

1.2.1. The role of biomodel to fulfill medical resources

In 2007, Japan has entered the "super-aged society", which is defined by the World Health Organization (WHO). The WHO defines the "aging rate" as the proportion of a society's population for those aged 65 or older. If a society has the aging rate more than 7%, the society is an "aging society". If the rate exceeds 14%, it is an "aged society", and a "super-aged society" in case that the rate surpasses 21%. Fig. 1-1 shows a demographic change in Japan from 1990 to 2065 as illustrated in the statement on the social welfare renovation by the Ministry of Health, Labour and Welfare [1]. Although it has been stressed for a long time since the Japan faced the super-aged society, the aging rate at the year of 2016 in Japan is about 27.3% as reported in the White Paper on Aging Society [2]. Moreover, according to the 15th estimated population reported in 2017 by the National Institute of Population and Social Security Research [3], the elderly over 65 years old can account for about 30% of the whole Japanese population in 2025, and almost 40% in 2065.

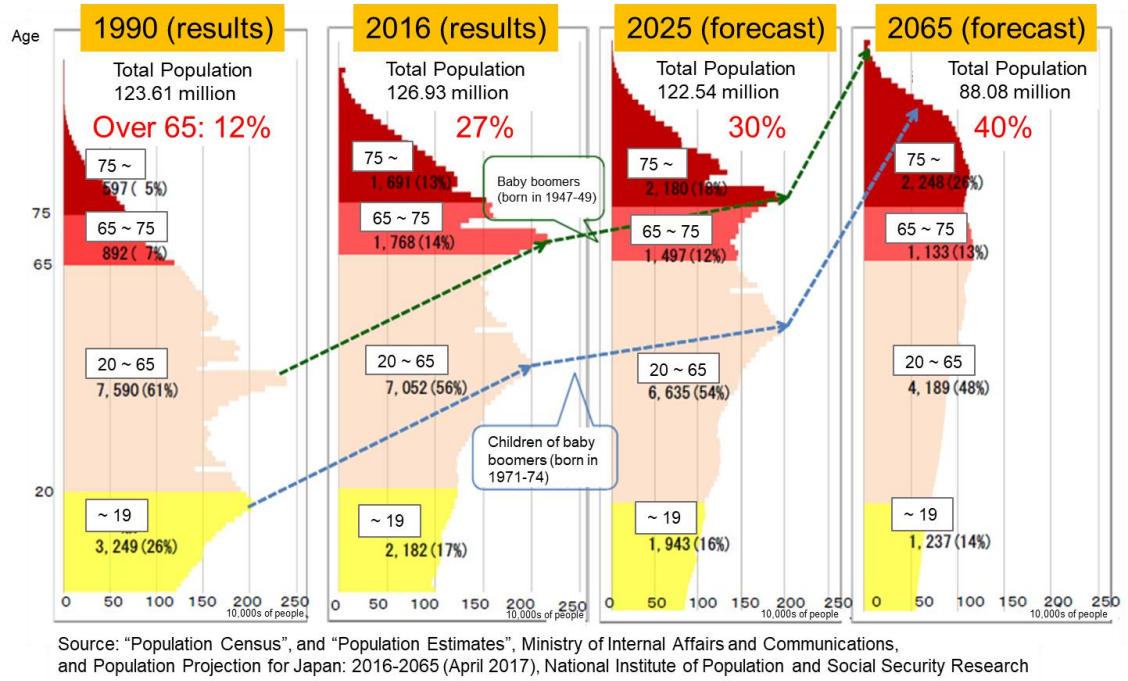

Fig. 1-1 Demographic change in Japan (Reprinted and translated from [1])

The advancement of the super-aged society holds problematic potentialities especially in medical and welfare support systems. A larger number of orthopaedic surgeries has been performed along the drastic increase in the proportion of the elderly. For example, the number of total joint replacement of hip, knee, and shoulder operated from April 2017 to March 2018 reached 220,000, which is 28.3% larger than that of the previous year period [4]. This trend is not only the case in Japan, but also in other developed countries. In the U.K., the number of joint replacement operations for hips, knees, ankles, shoulders, and elbows performed in 2018 statically came up to 240,163, marking 9.5% increase compared to 2017 as reported in the annual reports by the National Joint Registry (NJR) [5,6]. Also in the U.S., the number of primary total knee arthroplasty (TKA) performed from 2012 to 2017 was 650,674 according to the 5th annual report in 2018 by the American Joint Replacement Registry [7], and the number of such operation is estimated to increase by 3.48 million per year by 2030 [8].

As just described, the number of orthopedic operations is undoubtedly keep increasing all over the world in the future. To meet this rapidly increasing demands for medical care, the society is required to rapidly fulfill medical resources such as a sufficient number of skillful doctors, and good-quality medical devices. To do so, the joint effort has been made between the industry, government, and academia for enhancement of medical educational system, research and development of high-performance medical devices, and establishment of appropriate testing standards of medical devices or test materials for facilitation of evaluation procedure.

Biomodel is an attractive material that steadily supports the progress of medical technology in all the aspects mentioned above; enhancement of educational system, development of medical devices, and establishment of test standards. The use of biomodels will be detailed in the next sessions.

1.2.2. Definition and applications of biomodel

According to Lohfeld *et al*. [9], "A *biomodel* is an entity that replicates the geometry or morphology of a biological structure, which can be realized in either a computer-based form or a solid physical form." Based on this definition, there are two kinds of biomodels available; a *computer-based biomodel* and a *physical biomodel*. Computer-based biomodel covers not only a *virtual biomodel*, but also a *computational biomodel* [9]. A *virtual biomodel* shall be created for the purpose of visualization of biological structures, such as a skeletal model based on 3D computer-based images generated from computed tomography (CT) scans, normally used for preoperative planning. A *computational biomodel* indicates a finite element (FE) model of skeletal structure for the purpose of biomechanical

analysis on a biological structure, often used for determination of stress and strain distributions in reality [10].

A *physical model* is a biomodel in a solid physical form that can be fabricated by engineering technologies such as computerized numerical control (CNC) milling, injection molding, or rapid prototyping (RP) technologies [11,12]. Fig. 1-2 shows several examples of a *physical model* [13–15] mainly replicating the geometry or morphology of biological structures respectively. As far as engineering technology permits, all the parts of soft and hard physiological tissue can be generated. Recently, 3D printing technology is also applied in development of biomodel widely from blood vessels to bones [16–20].

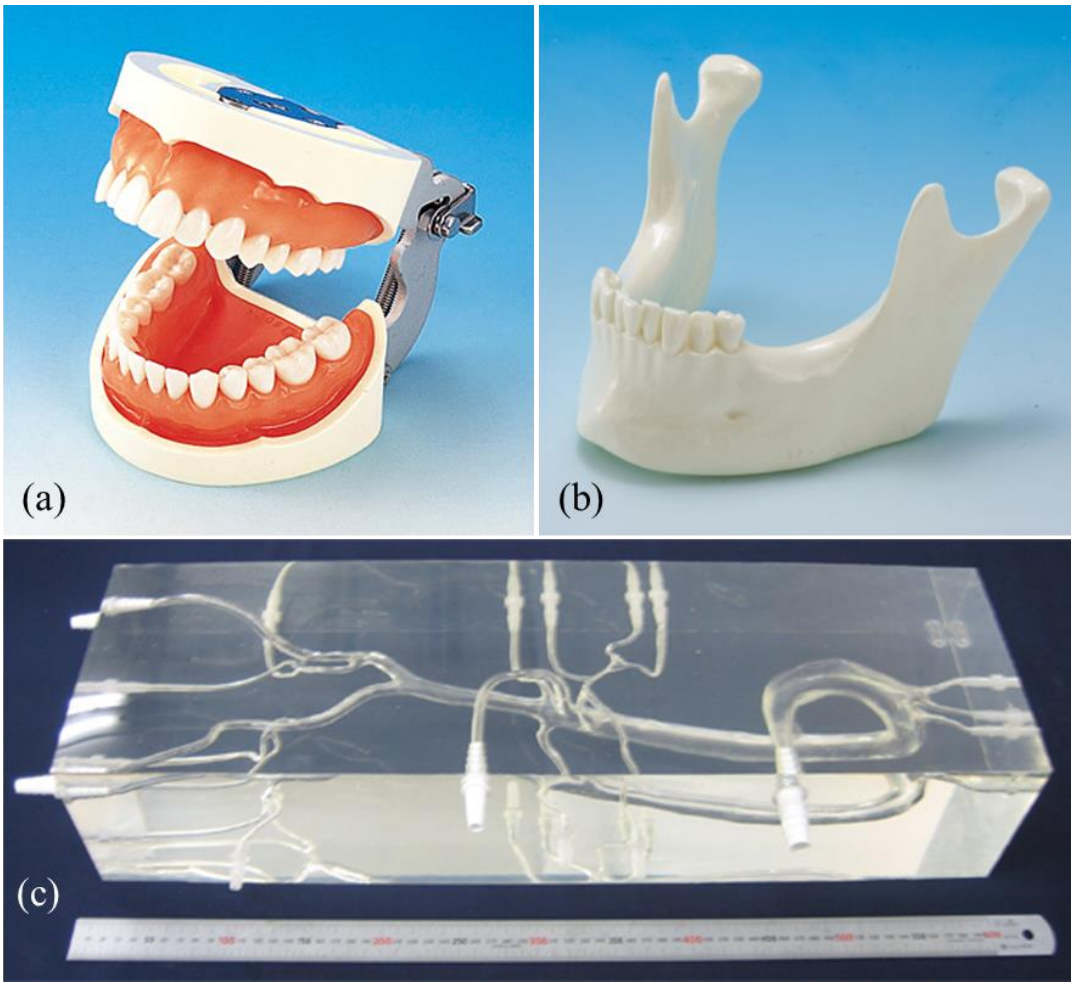

Fig. 1-2 Examples of physical biomodel. (a) A Prosthetic Restoration Jaw Model [13], (b) A Drilling Training Model [14], and (c) A blood vessel model [15].

Biomodel is used for a wide range of applications. Representative application is, for example, preoperative planning [21–23], surgical training [16,24–26], and mechanical tests as laboratory study for evaluation of medical devices [27–30]. The efficacy of preoperative explanation of surgical procedure using biomodel is also regarded as helpful to obtain informed consent about operation [11].

For each application, the intended role of biomodel is different. That is to say, the desired ability that biomodel has to exhibit should be well determined. For the purpose of preoperative explanation to patients, the realistic appearance of target tissue with its anatomical accuracy should be of its high priority, rather than its similarity of tactile feedback or physical properties. This application is relevant to the definition of biomodel in [9]. On the other hand, tactile feedback as well as anatomical structure should have high priority for surgical training, while physical and mechanical responses related to target function should be reproduced for the mechanical tests of medical devices. In these applications, the functional behavior of living tissue is more requested rather than the geometry or morphology of the biological structure over the conventional definition of biomodel. The functional characteristics of biomodel is the recently emerging aspect that should be replicated in the use of physical models, which used to be out of the scope of its use.

1.2.3. Biomodel in development of medical devices

In Japan, sales and production of medical devices are regulated by the Pharmaceuticals and Medical Devices Law (PMDL). Under the PMDL, the Pharmaceuticals and Medical Devices Agency (PMDA) is in charge of evaluation of medical devices in terms of quality, efficacy, and safety taking into account the current scientific and technological standards. In the U.S., these services are under the jurisdiction of the Food and Drug Administration (FDA). Fig. 1-3 shows the overview of PMDA's reviews and related services during product development procedure consisted of several stages; research and development, non-clinical tests, clinical trials, filing of application, approval, and marketing [31]. The PMDA provides various services at each stage of the procedure, such as consultation in relation to regulatory submission, compliance assessments focusing on Good Laboratory Practice (GLP), Good Clinical Practice (GCP), and Good Post-marketing Study Practice (GPSP) to ensure the submitted data shall be in accordance with the ethical and scientific standards, and inspections in terms of Good Manufacturing Practice (GMP), Quality Management System (QMS), and Good Gene, Cellular, and Tissue-based Products Manufacturing Practice (GCTP) in order to ensure the quality management of the manufacturing facility for the pending products.

As illustrated in Fig. 1-3, one of the characteristics in development of medical devices before distribution to a customer in comparison of other industrial products is the presence of clinical trials to obtain the approval. Since the intended purpose of medical devices is to help health care providers diagnose, prevent, and treat sickness or disease of their patients, with often influencing patients' anatomical structure or physiological function, clinical trials have been regarded as indispensable in Japan. What is essential in clinical trial is to see whether an emerging device has the capability to fulfill the intended purpose, balancing the benefits and the risks on patients' body. Therefore, newly developed medical devices are tested using living tissue either *in vivo* or *in vitro*.

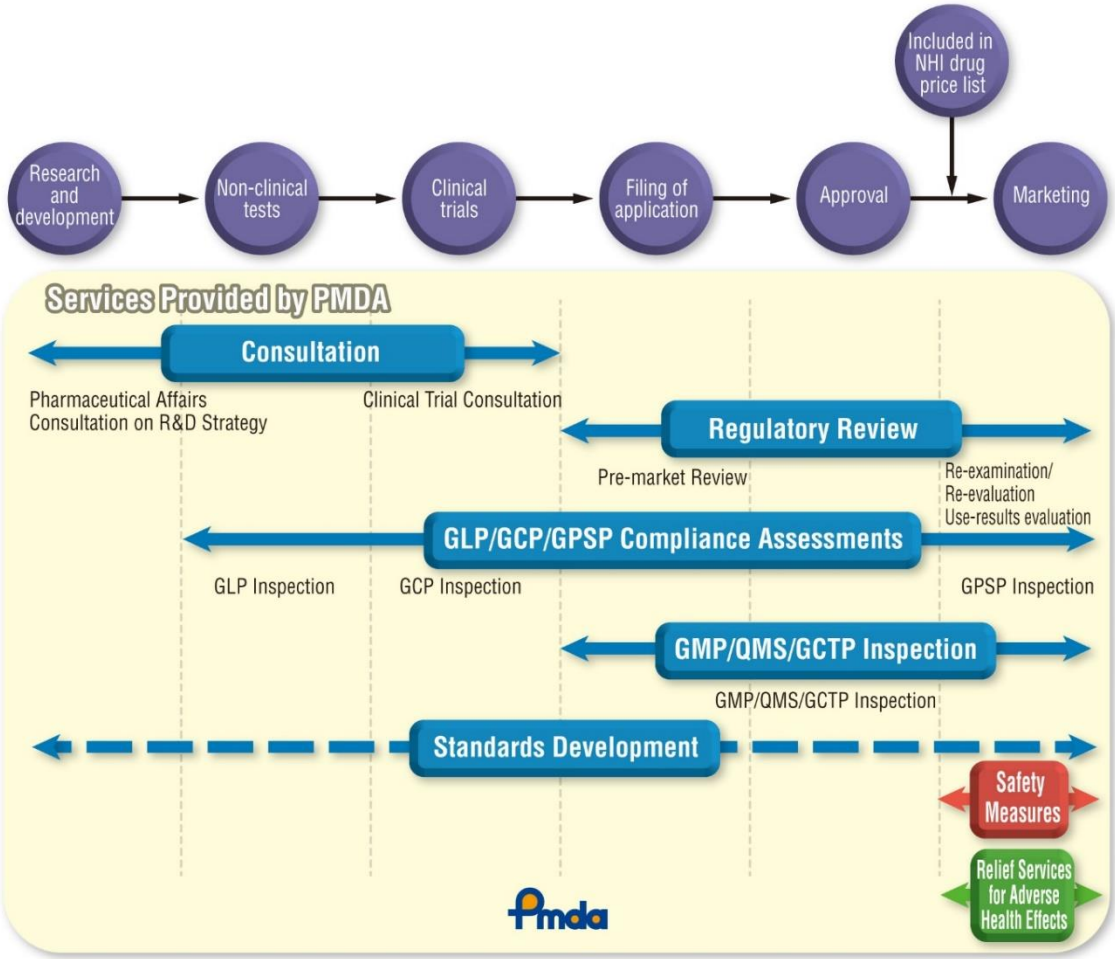

Fig. 1-3 Services of PMDA at each stage of product development (Reprinted from [31])

It is unsurprising that performing clinical trial is not easy. As developers of medical device, there are several steps to overcome, in order to obtain the approval. In addition to a number of administrative works, developers have to recreate the intended usage environments (e.g. a number of intact vascular systems surrounded by human soft tissue and bones), and prepare a sufficient number of test specimens and subjects. No matter what kind of living tissue is required, obtaining live specimens of acceptable sample size and quality, from the limited stock, within a reasonable time period, before environmental deterioration like dehydration or biological decay affects and alters the specimens [32,33], is a complicated and complex work. Besides, individual variance in material properties also make it difficult to obtain statically reliable data due to animal species, gender, anatomic location, food history, and the presence of disease [34,35]

Then, the use of inanimate biomodel can play a role as alternative materials to living tissue, somehow to mitigate these limitations and predict the biomechanical testing results. Compared to living tissue from cadavers or animals, the use of biomodel has two major advantages; ease of handling (biomodel does not require any special storage methods, licenses, or approvals from ethical committee and do not carry the risk of infection), and reproducibility (biomodel can provide statically reliable testing outcomes owing to the consistence of material composition, density, and geometry). Thanks to those advantages, the use of biomodel attracts more and more attentions over the world.

1.2.4. Biomodel as a standard test material

Another difficulty for evaluation of medical devices lies in the authorities' side. In Japan, PMDA is in charge of fixing up the testing methodology and requirements in the evaluation items for each medical device, but designing valid testing system could take time, especially in case that genuinely required evaluation items related to the accomplish of the intended function is not clear. The term "medical device" covers a wide range of devices used for health care, in various medical specialties. Nowadays, numerous types of medical devices have been invented, and thus evaluation methods are diverse. Therefore, PMDA is responsible to study the intended purpose of each medical device, and determine the most appropriate evaluation methodology to see if the medical devices can exhibit the desired function, taking into account the possibility of securement of a sufficient number of subjects, guarantee of long-run capability of products, uncertainty of surgical outcome depending on surgeons, and unique usage environments (particularly implantable devices such as artificial joint or artificial heart). In this regard, it is academically expected to provide a better understanding of the

relationship between the required properties of medical devices and the capacity of the medical devices to fulfill the intended function, for facilitation of the development of medical devices by helping to establish evaluation items composed of the bare minimum requirements.

Standards development is one of the services of PMDA as illustrated in the Fig. 1-3. In this service, testing methodology valid for evaluation of medical devices are established as standards. Standards are reviewed and protected by the International Organization for Standardization (ISO) and ASTM International (ASTM; American Society for Testing and Materials) over the world, and by the Japanese Industrial Standards (JIS) in Japan. Hundreds of standards have been already defined for medical devices, for example, about the implants for surgery [36–43]. By following the ASTM standard designated such as F543 [40], metallic bone screws for bone plates in orthopedics were evaluated by researchers [44–46], and comparable among the screws. Specification by the standards covers not only terminology and testing methodology, but also materials both for medical devices and test materials as well as their fabrication methods. The use of bone biomodel, which is made of polyurethane foam, is regulated by the specification F1839 [47], for determination of the axial pullout strength of metallic bone screws [40].

Sawbones® is one of bone biomodels commercially available around the world (Fig. 1-4) [48]. Among the products of Sawbones®, solid rigid polyurethane foam is defined as a standard test material (Fig. 1-5) [47]. Taking into account the specification, researchers have studied its static physical and mechanical properties [49–51]. However, as Hausmann described, obtaining clinically relevant data is limited for cases of biomechanical testing, due to the essential difference in mechanical properties compared to those of genuine bone, whereas the use of Sawbones® as a test material for comparable study between a series of identical devices can be agreeable [52]. Nevertheless, it is also true that there is still lack of quantitative information available regarding machining characteristics, such as cutting forces and cutting temperatures during drilling, whose information are essential for the assessment of orthopedic or other specialties dealing bone and prosthesis. Among limited literatures, Cseke reported that there is a large difference in machining characteristics between natural bones and Sawbones® test materials [53]. Therefore, only a comparable study between bone drills, bars, and prosthesis can be possible using the current bone biomodels. In order to improve the use of bone biomodel to evaluate the machining functions of medical devices, enhanced biomodel that can reproduce the machining properties of natural bone should be developed.

The use of biomodel as a standard test material caught the attention in a decade. However,

current technology for fabrication of biomodel permits only comparable studies among the same type of medical devices such as screws or pins. To take a further step, biomodel that equips with the realistic properties of natural bone, related to the assessment of intended purpose for each medical device is necessary.

Fig. 1-4 Sawbones® biomechanical test materials [48]

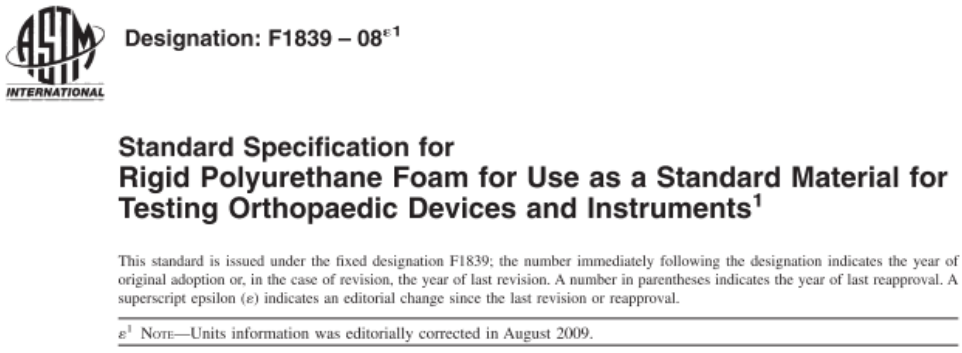

Fig. 1-5 Standard specification for rigid polyurethane foam regulated by the ASTM international [47]

1.2.5. Biomodel in surgical training

Surgical outcomes can be largely influenced by a user of medical devices or instruments, even though highly-performant products have been newly developed. In case that surgeons lack their knowledge and/or operational capability of surgical devices, medical accidents can possibly occur. In orthopedic surgery, surgeons would manually cut and remove patients' skins and other tissues using surgical knife and electric scalpel in order to expose the target inner organs. Here, surgeons are required to have a good command of surgical instruments to properly conduct operations as initially planned.

Regarding this point, there are certain surgical skills that are complicated and take time for mastery, such as clipping of aneurysms [54] or drilling of bone [55]. Drilling of bone is one of a series of surgical steps in dentistry or orthopedics, and often performed during dental implant surgery or artificial joint replacement. Therefore, dentists and surgeons are required to acquire the skill of drilling. In this regard, the surgeons are expected to accurately and steadily handle the surgical tool with controlling their level of force along the progress of drilling displacement depending on the bone structure and the individual difference of bone's characteristics, in order to avoid severe risks to their patients.

Medical and dental students can learn the basic knowledge about frequently occurring diseases and disorders, and their treatment methods. They have a chance to practice surgeries using actual instruments on dummies, and work as doctor-in-training in hospital under senior doctor at various specialties. In this manner, the students learn to conduct surgeries by following a proper procedure. In fact, however, the students do not have many chances to train themselves on living tissue while in school, because of the difficulty in handling as well as the limited accessibility. Besides, during internship, the students often only observe the surgeries and have less chance to give treatment [56]. The progress in medical technology has extended the surgical knowledge, and as a result increased the students' burden. The industry, government, and academia have been somehow responding to this trend by developing educational materials and increasing learning opportunities [57,58].

Basically surgical training for amateur doctors are performed in operating rooms in a hospital, but the currently increasing medical demands in our society require a number of experienced doctors and therefore amateur doctors are expected to do supplementary training away from hospital. Workshop using cadavers or animal models has been traditionally performed since long years, but nowadays clinical practice is becoming more and more difficult, because of the less tolerance of our

society against the use of cadavers or animals in medical research and education [59]. As alternative training methods, the advancement in technology brought computer-based training systems [60–62] and virtual reality (VR) simulators [63,64]. Although these emerging training systems show high efficiency in educational performance and have great advantages, the technology still has some room for improvement and also not many hospitals can introduce the systems because of its initial and maintenance cost [58].

For the purpose of surgical training, the use of biomodel has high potential. Similarly, as the use in mechanical tests of medical devices, inanimate biomodels possess strong advantages in ease of obtaining, conserving, and handling as well as reliability for repeated times of use over a long-duration. In a wide field of specialties, biomodel for surgical training has been developed. For biomodels of bone, there are many sorts of biomodels already available. One of the bone biomodels, made of acrylic resin and wood flour (Exsurg®, Tecno Cast Co., Ltd.) (Fig. 1-6) [65], has relatively better reputation among the existing models, but the reputation is by no means based on quantitative evaluation. Widely as for the evaluation of biomodels, there has been no specific criteria to determine a good biomodel except the perceptual feedback by doctors. Therefore, development of biomodel has been a series of trials and errors without concrete direction for improvement.

To address this situation, researchers aware of the gap between human tissue and conventional biomodels have been working on reproducing more realistic biomodels [66–69]. Recently, a bionic humanoid was invented in Japan in a framework of research and development program driven by the Japanese government [70–72]. The invented humanoid consisted of artificial living tissues and equipped with a series of sensors that enabled tactile force measurements of operators. Using this model, surgical training can be possible with quantitatively monitoring mechanical parameters and simultaneously assessing the surgical skill of the operator. However, the development of human bone tissue that can reproduce the realistic drilling haptics has no yet been its scope and no quantitative research can be found for the assessment of the tactile perception during drilling based on mechanical criteria.

Fig. 1-6 An example of mandibular biomodels for surgical training [65]

1.3. Bone

1.3.1. Physiological functions

Bone is one of human hard tissues, accounting for around 18% of the weight of our human body. Bone constitutes the skeletal system and six main functions are displayed in Table 1-1. In a microscopic level of view, bone, or osseous tissue, contains an abundant extracellular matrix that surrounds widely isolated cells. Those extracellular matrixes are composed of about 25% water, 25% collagen fibers, and 50% crystallized mineral salts [73]. The richest mineral salt is calcium phosphate, and it combines with another mineral salt, calcium hydroxide [$Ca(OH)_2$], to form crystals of hydroxyapatite [$Ca_{10}(PO_4)_6(OH)_2$]. Those crystals combine with other mineral salts, such as calcium carbonate, and ions such as magnesium, fluoride, potassium, and sulfate. Those mineral salts are generally embedded on the collagen fibers of the extracellular matrix, and the crystalizing process, which hardens the bone tissue, is called calcification.

Bone is not completely solid but has many small spaces between its cells and extracellular matrix components. Several spaces work as vascular channels which provide nutrients to bone cells. Other spaces function as storage area for red bone marrow. Bone is categorized as compact (or cortical) and spongy (or cancellous) bone, according to the size and distribution of the spaces. About 80% of the skeletal system is cortical bone and 20% is cancellous bone.

Fig. 1-7 shows an overview of both compact and spongy bones [73]. Compact bone, also called cortical bone, has strong and dense form of bone tissue. Cortical bone tissue forms the outer layer of

every bone and provides protection and support and endures the stresses induced by weight and movement. Blood vessels, lymphatic vessels, and nerves from the periosteum run through cortical bone inside perforating canal, often referred to as Volkmann's canals, and they connect with those of medullary cavity, periosteum, and central or Haversian canals. The central canals run longitudinally through the bone. Cortical bone tissue is composed of several repeating units called osteons or Haversian systems. Each osteon has a Haversian canal surrounded by several parts of lamellae, lacunae, osteocytes, and canaliculi. Osteons in cortical bone tissue are arranged in a parallel way to the lines of stress. The distribution of osteons is not settled and osteons remodel their structure according to the physical needs of the skeleton.

On the other hand, spongy bone, also called cancellous bone, tissue is light and has porous structure literally similar to sponge. Cancellous bone tissue forms interior part of bone, normally surrounded by cortical bone for protection. The bone tissue is composed of trabeculae, lamellae distributed in a random lattice of thin columns. Distribution of trabeculae appears to be arranged randomly, but in fact they are optimized precisely along lines of stress; the distribution helps bones endure and propagate stresses without breaking. The empty spaces between the trabeculae are often filled with red bone marrow.

Table 1-1 Functions of bone and the skeletal system [73]

1.	*Support.*	: The skeletal system works as the structural framework by supporting soft tissues.
2.	*Protection..*	: The skeleton protects internal organs from injury.
3.	*Assistance in movement.*	: Skeletal muscles attached to bones pull on bones to produce movement.
4.	*Mineral homeostasis (storage and release).*	: Bone tissue stores and releases several minerals, such as calcium and phosphorous.
5.	*Blood cell production.*	: Within certain bones, blood cells are produced.
6.	*Triglyceride storage.*	: Yellow bone marrow consists mainly of adipose cells, which store triglycerides.

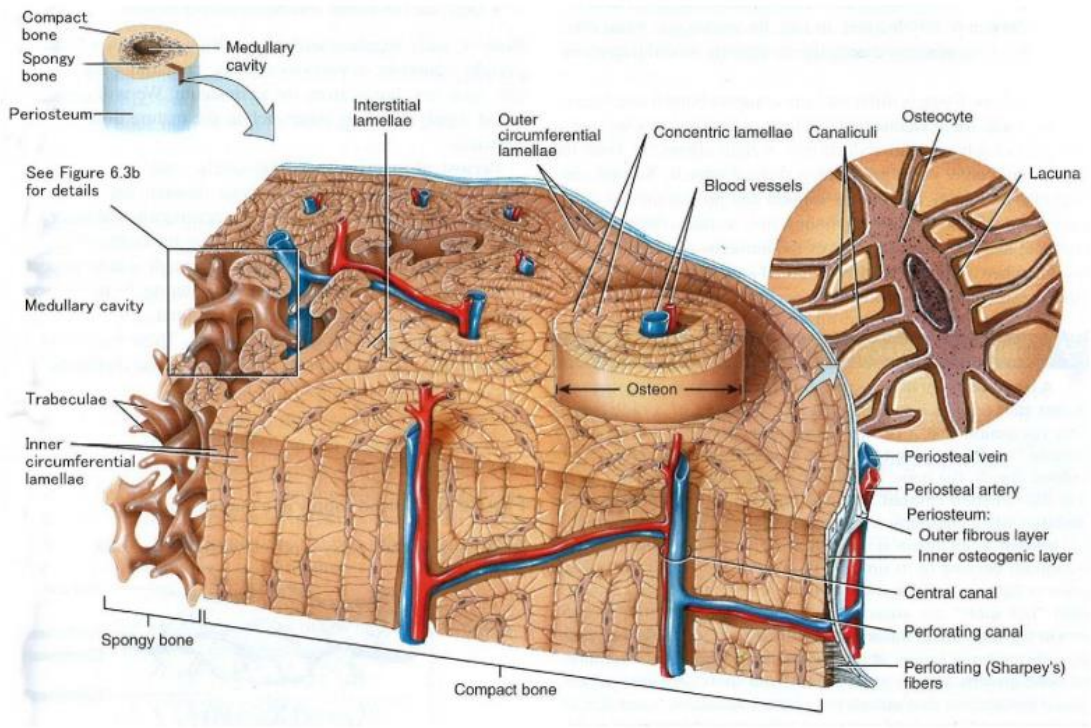

Fig. 1-7 Osteons (Haversian systems) in compact bone and trabeculae in spongy bone [73]

1.3.2. Biomechanical aspects

Biomechanics of bone have been widely studied since the middle of 20th century. The previous studies have shown the macroscale to microscale of mechanical properties of bone about tensile, compressive, and shear strength and elasticity or fracture and fatigue behavior with categorizing the anatomical location in both cortical and cancellous bone [33,74–81]. Particularly, Currey found that the stiffness of bone increases drastically with the mineral density of bone [74], while Bonfield *et al.* found the anisotropy of stiffness of bone using ultrasonic measurement technique [76]. It was the early days of the study of bone from the standpoint of material engineering.

The recent progress in measurement technique and the further research interests about bone in these three decades brought deeper understanding of bone [82]. Most famously, nanoindentation technique enabled researchers to measure the mechanical properties of bone precisely at nano-scale. Focusing on the effects of anisotropy of bone with distinguishing at the scale of osteons [83–88], the anisotropy in mechanical properties at the level of osteons was confirmed as the longitudinal moduli is higher than the transverse moduli [87,88]. General mechanical properties of bone such as tensile strength and elastic modulus are listed in Table 1-2 [32,49,75,83,89–91]. Human cortical bone shows

elastic modulus from 17.6 to 23.5 GPa in longitudinal direction, which is slightly higher in comparison with that of traverse direction as an anisotropic material. As shown in Table 1-2, cortical bone is superior to cancellous bone in mechanical properties. There is also difference in mechanical properties depending on animal types.

Moreover, research interests have been expanded to dominant factors on mechanical properties such as not only the effects of mineral contents [85,92] or experimental parameters as represented by strain rate [93,94], but also specimen size, wet or dry conditions [95,96], and conservation methods [97–100]. Taken together, bone specimen is recommended to preserve frozen rather than in chemical liquids in order to maintain its mechanical properties.

Numerical simulation by finite element method (FEM) also supports the biomechanical aspects of bone, as firstly introduced, for example, by Richmond *et al*. [101]. Currently, combining with scanning images at high resolution using CT, stress distribution of bone in a realistic geometry can be obtained [102,103]. The advance in computer processor made it possible to analyze numerically as far as the machining of bone [104,105].

Table 1-2 Mechanical properties of bone from [83][a], [89][b], [49][c], [32][d], [75][e], [90][f], and [91][g]

Material	Tensile strength [MPa]		Elastic modulus [GPa]	
	Axial (longitudinal)	Radial (traverse)	Axial (longitudinal)	Radial (traverse)
Human cacncellous bone			18.14 ± 1.7^{a}	
	84.9 ± 11.2^{b}		18.0 ± 2.8^{b}	
Human cortical bone			23.45 ± 0.21^{a}	16.58 ± 0.32^{a}
	107.9 ± 12.3^{b}		19.9 ± 1.8^{b}	
	132 ± 16.1^{c}	57.9 ± 5.5^{c}	17.7 ± 3.9^{c}	13.1 ± 3.1^{c}
	124 ± 1.1^{d}		17.6^{d}	
Canine cortical bone	108.3 ± 20.5^{e} (ultimate)		13.86 ± 1.17^{e}	
	251.0 ± 49.1^{f} (ultimate)		15.6 ± 2.6^{f}	
Porcine cortical bone	88 ± 1.5^{d}		14.9^{d}	
	194.5 ± 14.45^{g}		17.4 ± 1.11^{g}	

1.3.3. Bone among engineering materials

Bone can be regarded as a composite material consisting of organic (collagen) and inorganic (hydroxyapatite) tissues, having unique characteristics among engineering materials widely applied in industry. Fig. 1-8 shows the comparison of stress-strain curves for four representative engineering materials with different elasticities, such as steel, glass, bone, and rubber [106]. It indicates that bone exhibits higher stiffness rather than that of rubber, but lower than steel and glass, locating the curve of bone between those of rubber and glass. To the authors' knowledge, there is no such alternative materials that can show the similar mechanical response to that of bone.

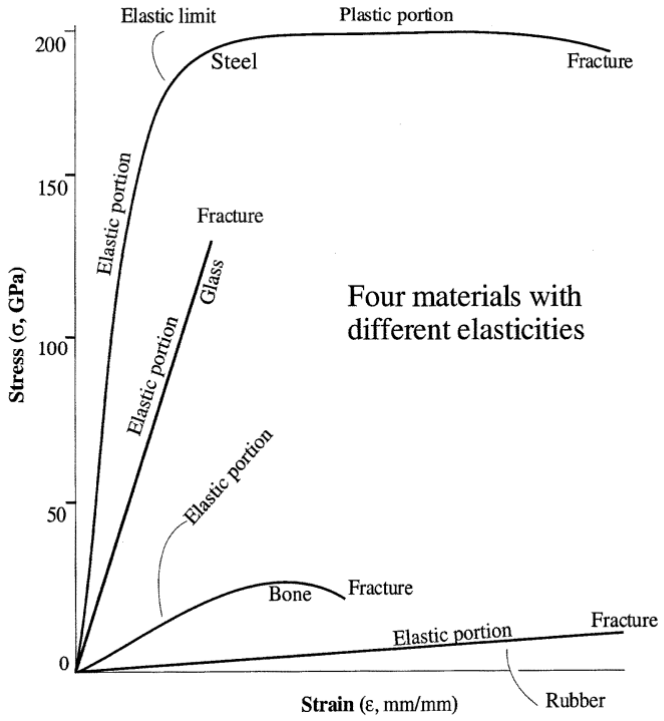

Fig. 1-8 Stress-strain curves of representative engineering materials [106]

On the other hand, development of new materials such as engineering plastics and fine ceramics have been undertaken in last decades in order to expand the area of use from plastics and ceramics respectively. In the fields of ceramics, the development of fine ceramics has enthusiastically progressed thanks to the advance in technique that allowed the accomplishment of highly refined materials and the control of resultant composition and geometry. In the early 20th century, fine ceramics

gradually came into practical realization as represented by the vehicle engines and semiconductors. Besides, the application for medical purpose caught attention at the late 20th century, though the primary use started even the late 18th century in dentistry and the late 19th in orthopedics for bone filling [107]. After that, the improvement in toughness and strength of fine ceramics, such as alumina (Al_2O_3) and zirconia in particular, led to the use into implantable devices. Eventually since 1990, a tremendous number of joint replacement, using alumina components and zirconia femoral heads, has been implanted across the world [107]. In addition to these "bioinert" ceramics consisted of alumina and zirconia, "bioactive" ceramics, mainly from hydroxyapatite (HAP) or tricalcium phosphate (TCP) because of the similarity of their compositions to the mineral part of bone, is known for the clinical use.

Reinforced plastics was also keenly developed since 1960s along the rapid industrial growth of petroleum chemistry for various applications. Glass or carbon fiber reinforced plastics (GFRP or CFRP) are the two representative products, having such characteristics in specific strength and specific stiffness, where epoxy resin and polyester have been mostly chosen for the majority of the matrix in previous studies [108]. CFRP is particularly applied to the constructional materials in aircrafts or vehicles as well as sports goods due to its advantage.

These fiber-reinforced plastics (FRPs) are categorized as composite materials. Not only for the improvement of mechanical properties of a matrix, but also for the adjustment of target characteristics, composite materials are fabricated. Exsurg® [65], one of the bone biomodel presented at the section 2.5, is also a composite material, which consists of acrylic resin as a matrix and wood flour as fillers. According to the inventors' patent, the inclusion of wood flour was intended for the adjustment of tactile perception during drilling to give the similarity to that of natural bone [109]. Like this case, polymeric (sometimes composite) materials are often used to replace human tissue.

1.4. Drilling

1.4.1. Environments surrounding drilling in industry

Drilling is one of the machining techniques for material removal similarly to milling or grinding, which is usually performed as finishing process in order to obtain the desired geometry of engineering materials. A drill bit is used to make a hole of circular cross-section in any solid materials such as wood, metal, ceramics, plastics, and composites. Rotated at a certain rate of revolutions per minute,

the drill bit is pressed against a work piece at a voluntary feed rate. The force conveyed through the drill bit makes the cutting chips from the drilled hole along the penetration of drill bit. Although the remarkable advancement in engineering technology brought the various machining methodology, the drilling process continuously stays as an indispensable technique for material removal in manufacturing.

Development of machining tool for drilling dates back to the time of ancient Egypt, but it is only since the late 18th century in England that the machining tool was renovated during the industrial revolution. Basic knowledge about cutting theory of our time was widely obtained in the middle of 20th century [110–114]. After that, machining tools became numerically controlled by a computer, making automatic machining possible for mass production with high precise machinability and productive efficiency. Cutting tools have been developed in response to the appearance of new materials such as strengthened alloy, reinforced plastics, and fine ceramics. A tremendous number of research works on drilling have been done along the increasing demands of improvement in machinability and due to the complexity of processing mechanism of emerging materials.

Contrary to the simple purpose of drilling, making a hole, drilling is known as a complex mechanical phenomenon because of various factors affecting the resultant outcome. Focusing on FRPs, both GFRP and CFRP show low machinability due to additives. In both cases, enhanced strength of the composite materials makes cutting tools difficult to penetrate and subsequently the used tools show short useful life, resulting in the increase in manufacturing cost. A number of researchers have been struggling to address the low machinability of FRPs [108,115–117]. In this regard, most of literatures are focusing on the accomplishment of good finish surface or drilled hole quality, by optimizing machining parameters such as spindle speed, feed rate and geometry of a cutting tool [118–125].

To investigate drilling outcomes, the correlation between those machining parameters and drilling responses such as thrust force, torque, temperature rise, and cutting chips morphology is often characterized for the analysis of drilling. However, it is barely quantitatively mentioned the relationship between drilling characteristics and mechanical properties of work materials, such as surface roughness, hardness, and strength, which are known dominant [114]

1.4.2. Surgical drilling for operations

Drilling performs a practical role for medical purpose. Surgical drilling on natural bone is often performed in several specialties such as dentistry, orthopedics, and neurosurgery. This section

summarizes case examples of bone drilling in operations and risks on human body carried by drilling. Previous findings on drilling of bone are also summarized.

Fig. 1-9 shows an example of typical surgical process in dental implant surgery [126]. Drilling is performed on maxillary or mandibular bone to make a pilot hole for dental prosthesis. After determination of drilling site, several kinds of drill bits are used with gradually increasing the diameter of drill bits before implantation of dental prosthesis. In orthopedics, bone pins, screws, and plates can be inserted as traumatic injury treatments wherever the anatomical location is (e.g. distal femur and proximal humerus as shown in Fig. 1-10 [127]). According to the surgical procedure manual for the insertion of NCB® bone screws as illustrated in Fig. 1-11, drilling shall be performed to make guide holes for bone screws [128]. The insertion of bone screws and plates is a fundamental procedure also for joint replacement and spine surgery. In neurosurgery, surgeons deal with diseases or disorders related to the nervous system including the brain, spinal cord, peripheral nervous system, and cerebrovascular system. Hence, neurosurgical treatments on the brain or cerebrovascular system accompany craniotomy procedure to reach the inner system through the skull, which makes drilling a mandatory step. As stated so far, various types of surgical operations require drilling technique.

It is obvious that drilling technique is an essential and still fundamental skill for surgeons, but drilling carries a large risk on patients' body:

- Firstly, there is a possibility that failure of implanted devices or bone fractures can accidentally occur in case of inappropriate fastening. As shown in Fig. 1-12, Natali *et al.* reported breakage of drill bit left inside bone tissue resulting from overloaded drilling [129]. Motoyoshi *et al.* suggested recommended values of fixation torque for tightening an orthodontic mini-implant to avoid failure of implant devices [130].
- Second risk is the accidental damages to the surrounding tissue because of the error in position of drilling site or in drilling depth. Especially when drill bits are penetrated deeper than needed, serious damage can occur in bone tissue as well as in nerves or vascular channels adjacent to bone tissue, which may bring medical accidents such as excessive bleeding, paralysis, or abnormality of sensation.
- Thirdly, bone necrosis, often referred as osteonecrosis, can be caused due to either exposure of excess force or high temperature attributed to drilling. Since osteonecrosis is regarded as a serious risk on mother body, due to not only delaying the regeneration of bone cells but also facilitating bone fracture, the effects of drilling on temperature elevation have been

extensively studied. After it was turned out as early as 1984 by Eriksson *et al.* that bone temperature must not be more than 47℃ for 1 min to avoid osteonecrosis [131–133], various aspects such as machining parameters [134–139], machining tools [140,141], and cooling methods [136,142–144] were the major scope of research topics. There are still rooms left for further research about the effects of application of surface coating or textile on drill bits and the improvement of numerical modelling of temperature rise during bone drilling [132,133,145].

Considering these risks, surgical education as well as mechanical tests of medical devices are important since surgical outcomes are strongly dependent on operators' command of medical devices. The advancement of information technology also offers significant benefits on surgeons, such as robot-assisted drilling systems [146–149] or remote controlled robots for surgery [150,151].

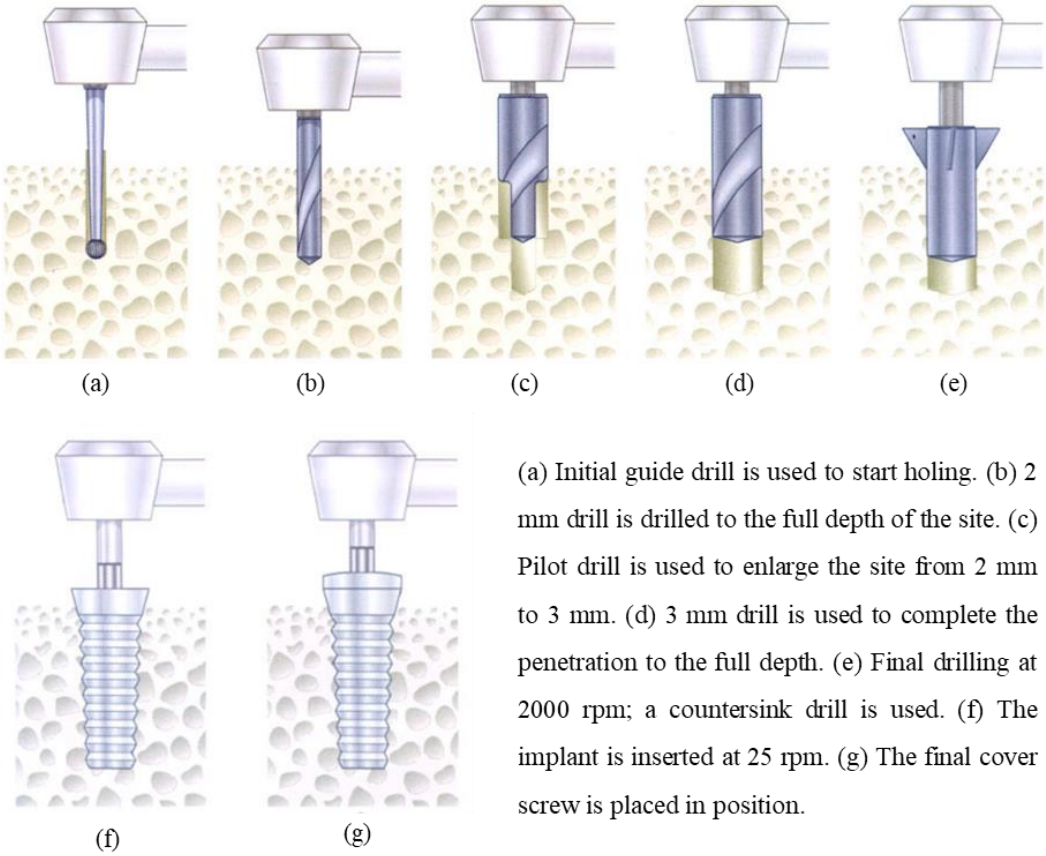

Fig. 1-9 Diagrams of surgical sequence using a bur and drill bits in dental implant placement [126]

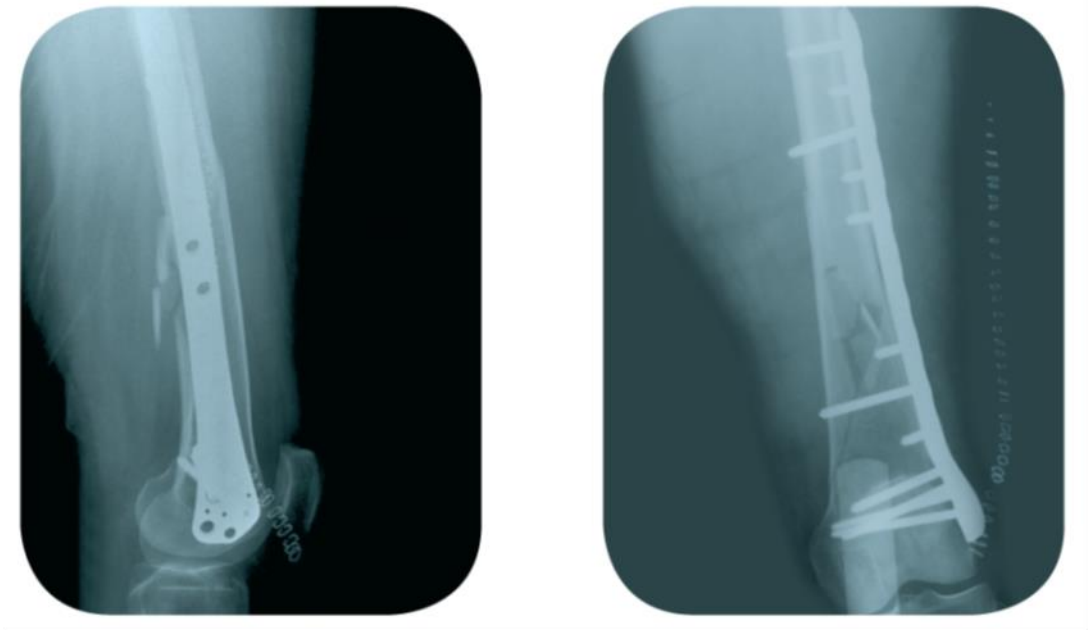

(a) Distal femur plate

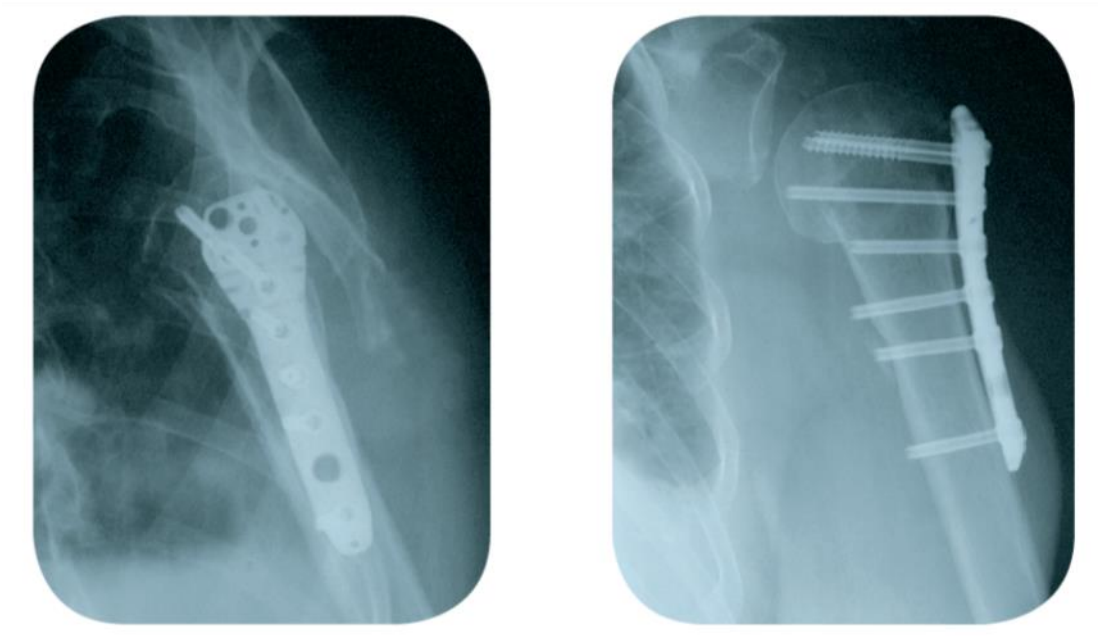

(b) Proximal humerus plate

Fig. 1-10 Postoperative radiographs after the insertion of orthopedic plates (Reprinted from [127])

Cortical Screws

1. If an *NCB* cortical screw is used, use the *NCB* Drill Guide (REF 02.00024.011) and drill with the drill bit 4.3 mm (REF 02.00024.002). Drill through both cortices. In the case of hard cortical bone, tap the cortex with the tapper (REF 02.00024.050).

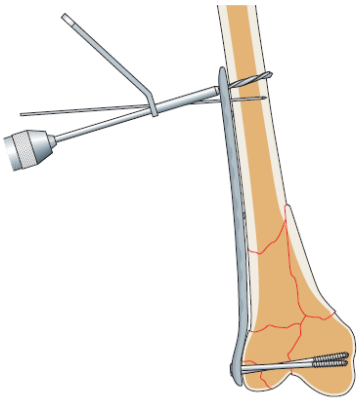

Drilling

2. Insert the *NCB* Screw using the *NCB* Screwdriver, (REF 02.00024.023).

3. To lock the screw proceed as for the cancellous screws: insert the locking cap (REF 02.03150.300) and tighten the cap with the *NCB* Torque Screwdriver, 6 Nm (REF 02.00024.021) until a clicking sound is heard.

4. In the diaphyseal area bone spacers are used to prevent close contact. After locking of the screws the spacers should be removed.

For the placement of the additional screws proceed as above.

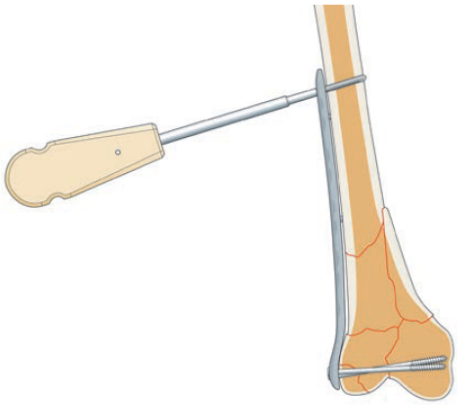

Insert the cortical screw

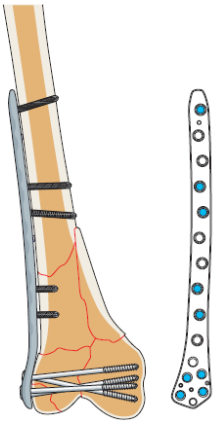

Final plate fixation (example)

Fig. 1-11 Procedure manual of the insertion of cortical screws (Reprinted from [128])

Fig. 1-12 An example of failure of drill bit left *in situ* [129]

1.4.3. Quantitative aspects in drilling

1.4.3.1. Geometry of a drill bit

Above all, a drill bit is an indispensable tool for drilling procedure. Fig. 1-13 illustrates a sketch of a drill bit, consisted of a shank, flutes, and cutting edges [152]. The shank is used to connect to a piece to a chuck of a hand-drill or a machining system. Material removal takes place by the cutting edge. Cutting chips and debris are extracted along the flutes in response to penetration of a drill bit. The cutting edges function to produce a series of slices as the drill bit progresses.

The cutting face can be divided into several parts, as shown in Fig. 1-13 (b). The chisel edge contributes seldom to cutting but largely to the axial thrust force of the drill bit. This is because of a relatively slow rotating velocity in the center of the drill bit and the rake angle nearly zero, meaning the cutting edge almost perpendicular to the work surface.

The point angle is the angle on the tip of the drill bit formed by both cutting chips (Fig. 1-14). Optimal point angles in the orthopedics for bone surface is recommended such as 90° and 118° by the literature [152]. Hillery *et al.* reported that there seems no significant difference in temperature elevation in bovine and cadaveric bone in vitro in their experiments investigating the effects of point angles between 70°, 80°, and 90° [135]. Similarly, Augustin *et al.* found trivial effects on drilling temperature using 2-fluted drill bits with 80°, 100°, and 120° [153]. Therefore, point angle has little effect on the increase in temperature during drilling.

The helix angle is the angle between the longitudinal axis of the drill bit and a tangent to the leading edge of the land. Surgical twist drill bits are often slow-spiral, which means the helix angle is relatively small. This small helix angle was assumed ideal for the drilling of bone [154].

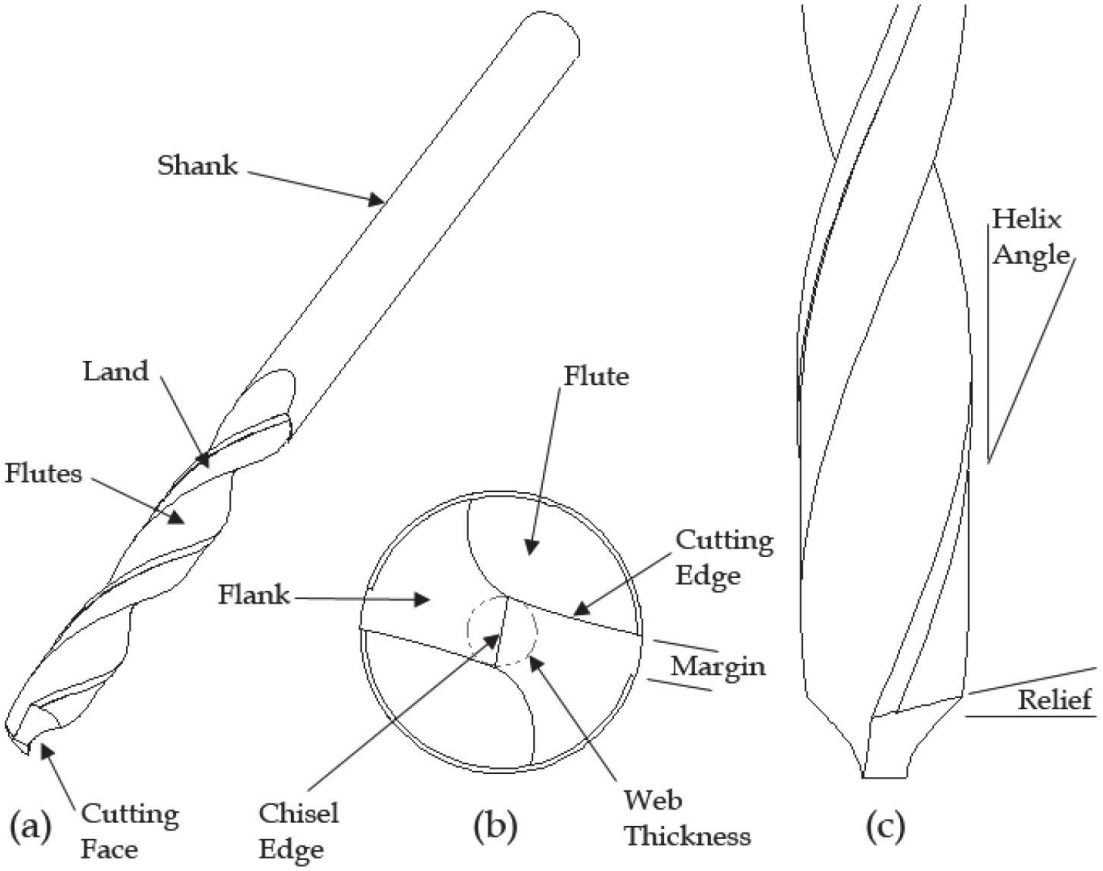

Fig. 1-13 Sketch of a drill bit. (a) Overview, (b) Point geometry, and (c) Relief and helix angles [152]

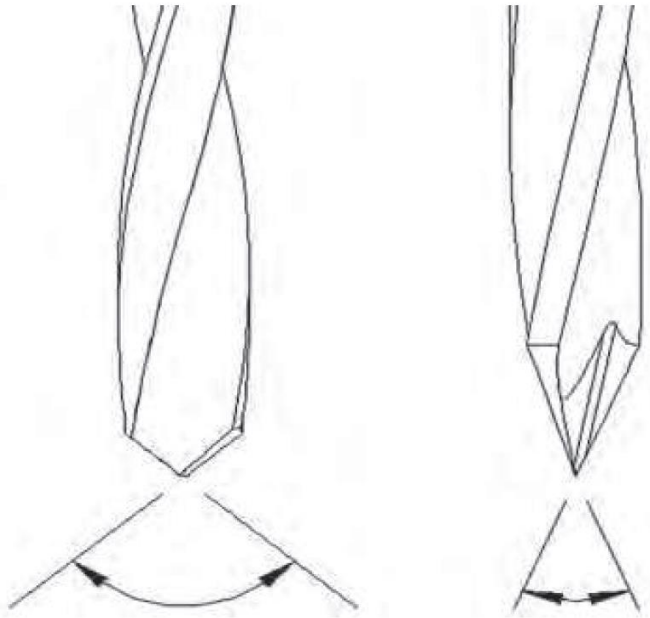

Fig. 1-14 Comparison of point angles between two drill bits [152]

1.4.3.2. Mechanism of drilling in bone

Drilling requires the mechanical input for the rotational motion (rpm) and torque (N・m), where torque means the moment of lateral force that is required for material removal by drill bits. These input are often exerted by the hand-drill or the machining system. Axial thrust force (N) is also loaded vertically to work material for material removal, which is applied manually by the operator or automatically by the machining device under numerical control (NC). The moving velocity of the drill bit through the work material is defined as the feed rate (mm/s).

In industrial manufacturing, a constant feed rate is normally applied under NC systems whereas in the clinical circumstances, a quasi-constant axial thrust force is applied to the hand-drill by the surgical operators. This distinction of the two drilling system is considered to be of crucial importance especially for the studies on surgical drilling of cortical bone.

The literature seems to suggest that drill bit diameter is an important variable that determines the magnitude of thrust force, in addition to the bone quality of drilling site as another contributing factor. Allotta *et al*. found the linear relationship between drill bit diameter and axial thrust force to produce a given feed rate [155]. Hobkirk *et al.* found the mean values applied during oral surgery between 4 and 19 N [156], and likewise Natali measured a maximum of between 10 and 20 N in case of 2.5-mm diameter drilling [129]. On the other hand, as much as 110-N mean thrust force was applied on drilling 3.2-mm diameter holes in cortical bone [157]. Altogether, previous studies focusing on dentistry generally applies axial thrust force no larger than 25 N [137], while orthopedic studies has a range between 20 and as much as 120 N [137,152,158,159].

An idealized illustration of the oblique cutting mechanism is shown in Fig. 1-15. The removal of bone at the cutting face takes place by the cutting edges that remove a certain thickness, t, with each rotation as they spiral through the bone, following a helical path. The work material being cut is associated with a unique cutting force, and this determines the optimal rake angle, which is around 25 to 35° for cortical bone [154]. Moreover, the unique anisotropy of bone gives a complexity to drilling characteristics because the cutting resistance vector is continuously changing along the rotation of the drill bit [53]. This dependency of the cutting process on the osteon direction in cortical bone was firstly demonstrated by Jacobs *et al.*, as the cutting forces were greatest when cutting perpendicularly to the longitudinal direction of osteon [154]. Based on this work related to the orthogonal cutting in bone, it was established that a rake angle of 45° was recommended because of the markedly reduced cutting force, regardless of the osteon direction.

Heat generation inevitably occurs during drilling. According to Fig. 1-15 [152], the primary heat sources pertain to shear deformation of work material (1), friction between the cutting chips from work material and the rake face of cutting tool (2), and friction between cutting edge and under surface of work material touching the relief face of the cutting tool (3). Secondary, indirect heat sources are driven purely by friction involving cutting chips, especially between bone chips and flutes, bone chips and drilled wall of work material when travelling the flute. In case of drilling of metals, almost 60 to 70% of the total heat are transferred to cutting chips [160]. In case of drilling of bone, approximately 60% of the heat energy generated during drilling can be converted to bone chips [152], transferring the rests to the surrounding tissues as well as the drill bit itself. Numerical and mathematical models have been currently developed for the analysis of heat generation and transfer during drilling of bone [104,105,161–164].

Thermal conductivity is a thermodynamic parameter that determines an ability of materials to conduct heat. Cortical bone has a relatively poor heat conductivity as a composite material. Recently, Feldmann *et al.* determined the thermal conductivity of cortical bone to be 0.64 W/mK for bovine, 0.68 W/mK for human [165], whereas that of surgical-grade stainless steel, often used to drill bits, is around 16.3 W/mK. Specific heat is also known as another material property that influences the temperature rise during drilling [165].

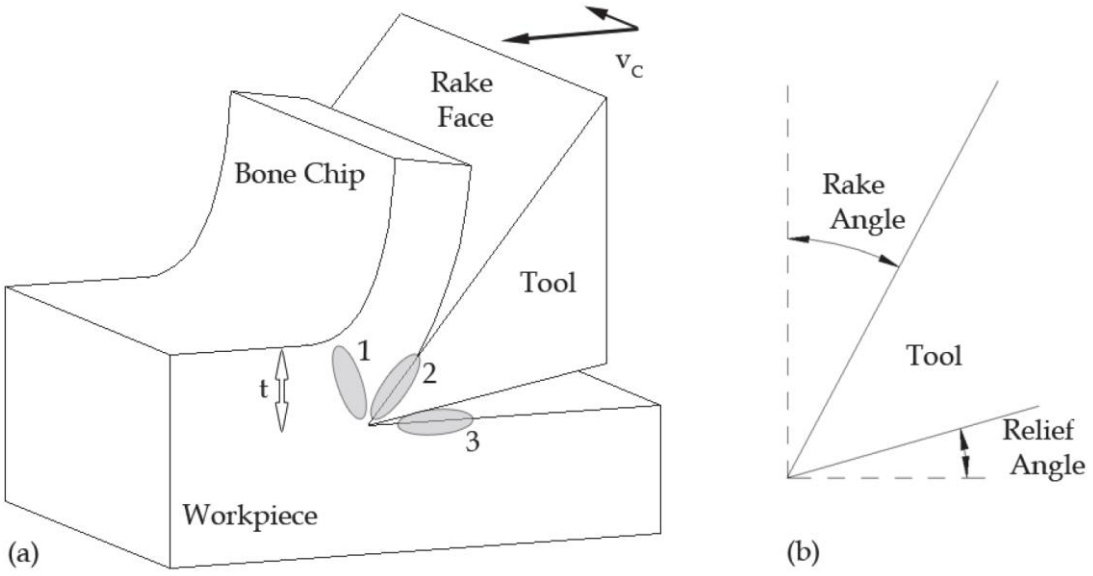

Fig. 1-15 Mechanism of material removal by a drill bit at the rake angle of oblique cutting, with regions of primary heat generation indicated; (1) shear deformation of the bone, (2) friction between the bone chip and cutting tool, and (3) friction between the tangential surface and cutting tool. (b) Rake and relief angles [152].

A relief angle is designed in cutting tools to relieve thermal dissipation and mechanical damages due to the friction between cutting tools and the emerging surface of work materials. Chacon *et al.* reported the significant effects of relief angle on the scale of the temperature elevation during drilling of bone [166].

1.4.3.3. Characterization of drilling in bone

Drilling behavior is the outcome deriving from variables such as cutting tools, machining conditions, and mechanical, thermal, and chemical properties of work materials. Drilling behavior can be characterized by cutting forces (thrust force and torque) and resultant temperatures. Under constant thrust force drilling, drilling time and feed rate are another key properties describing drilling. Drilling behavior can also be characterized by the cutting tool life observed in wear of cutting edge, quality of drilled holes seen in surface roughness and dimension accuracy, and cutting chips generated during drilling. Since these aspects cannot be directly converted from the mechanical properties of materials, drilling tests shall be carried out for the characterization of drilling behavior.

- **Cutting forces**

Thrust force and torque have been reported as the mechanical outputs in drilling to describe drilling characteristics of bone since as early as 1970s [154,167]. Until now, a large number of researchers have worked to find out the haptic aspects on drilling of bone [133,152,168–170]. Wang *et al.* reported the effects of rotation speed, feed rate and drill bit diameter on thrust force and torque under constant feed rate drilling, describing the decreased force and torque along the increase in rotation speed, and increased force and torque in case of increase in feed rate and drill bit diameter [171]. This trend is in a good agreement with other researchers [133,167,170]. Tuijthof *et al.* compared the thrust force between different surgical machining tools such as twist drill bits, round burrs, and kirschner wire in bones of pig and goat [172].

- **Cutting temperature**

Temperature elevation during drilling can be measured mainly by two major methods; thermal images obtained from infrared camera, or thermocouples placed in bone [173]. Both methods have advantage and drawback. In case of using the infrared camera, what can be obtained is thermal images on the very surface of work piece during drilling, thus temperature rise inside the drilled hole can be more accessible in case of using thermocouples. However, as cortical bone usually has a thickness of less than 5 mm in radial direction, placing thermocouples in cortical bone is not always appropriate

due to the limitation of spaces. It is important to distinguish the measurement purpose and select the suitable method.

Recently, a lot of researchers carry out experimental analysis of bone drilling as a validation method of their numerical models [174–177]. Lugnmani *et al.* particularly established a numerical model to predict thrust force and torque that were in a good accordance with obtained experimental results [176]. Feldmann *et al.* even established a numerical model that predicts temperature elevation during bone drilling [145].

- **Cutting chips**

Chip formation is another important factor in the characterization of drilling in bone. The morphology of cutting chips indicates fracture behavior of work specimens. There are certain literatures focusing on bone chips formation during drilling [178–180]. Apparently, bone often exhibits crack-typed cutting chips in drilling possibly due to its brittleness, which was different from those of synthetic materials, as flow-typed chips was observed for cutting epoxy-based bone biomodels [180]. In addition to the nature of bone, the progress of machining process accompanies temperature increase in bone, which consequently change the fracture mode of bone chips alternating the morphology of cutting chips from flow-typed to crack-typed [178,179]

- **Wear of cutting tools**

A repeated contact of the cutting edge on the emerging surface of work pieces causes wear and dulling of cutting edges, which subsequently requires the application of a higher thrust force for the progress of drill bit. Wear of cutting tools can cause defective cutting usually with higher elevation of temperature, and the initiation of vibration due to an increase in surface roughness of the cutting edges. Observation of cutting edges using optical microscope or Scanning Electron Microscope (SEM) is the imaging methodology to analyze wear of cutting edges. Literatures report that abrasive wear as well as plastic deformation can occur to alter the geometry of the chisel and cutting edges, and the rake face of the drill bit [181,182]. Allan *et al.* investigated the effects of various magnitude of wear on maximum temperature elevation in cortical bone *in vitro*. Three types of drill bits (1.5 mm diameter, 2-fluted Leibinger) were compared which were fresh, used in the drilling of 600 holes in porcine mandibular bone, and provided from operating theatres after the use for several months with measuring maximum temperatures during drilling tests [181]. They revealed that 600 holes was statistically sufficient to cause significant temperature rise compared to fresh drill bits with showing the images of three drill bits as shown in the Fig. 1-16.

There seems a large number of information available on drilling of bone, but in most cases machining parameters such as rotation speed, feed rate, tool geometry, animal species, and anatomical positions are diverse and those reported results cannot be always comparable. Therefore, in order to study the drilling characteristics of bone toward development of biomodel, it should be necessary to determine the information of target bone and machining conditions respectively.

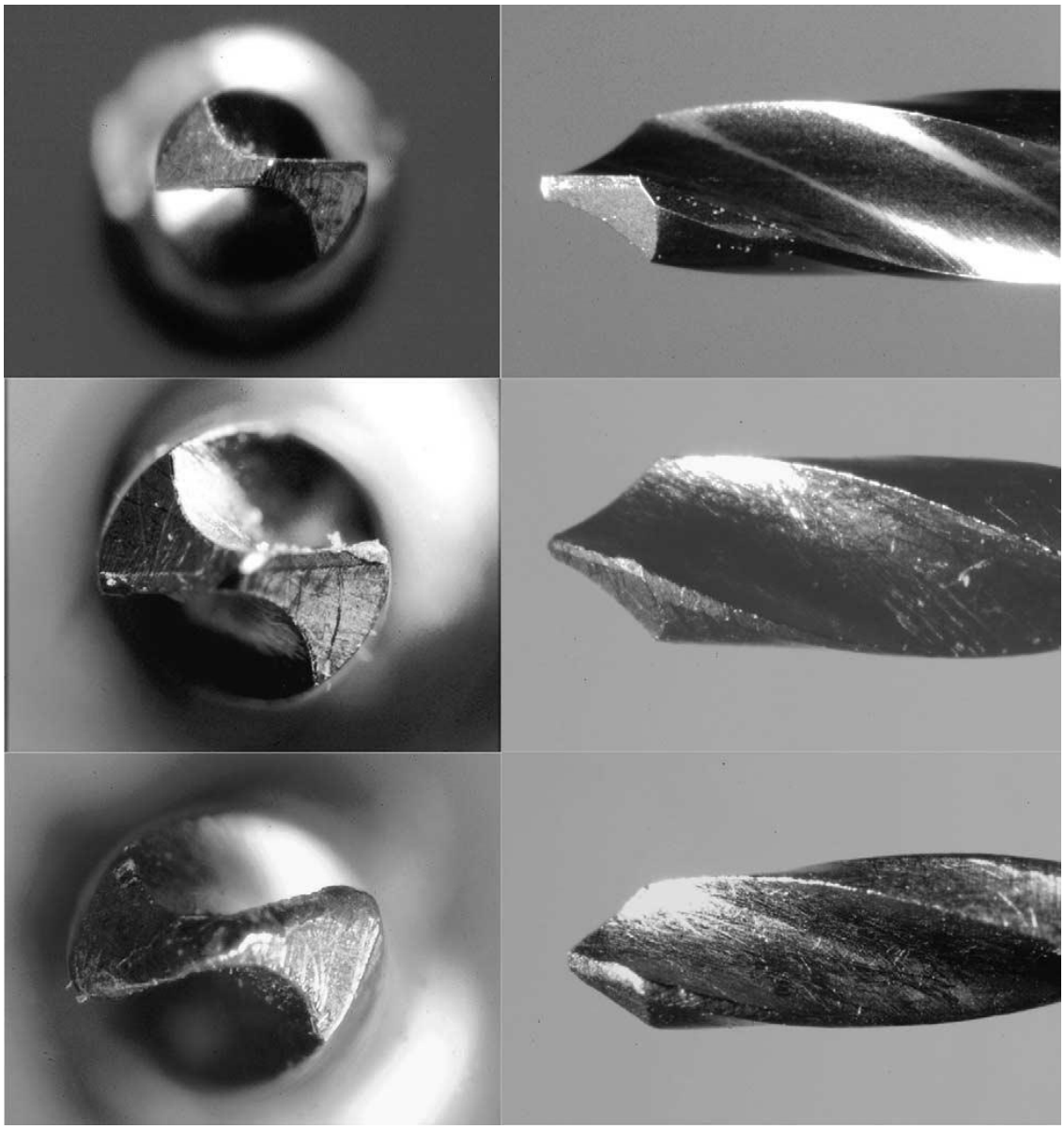

Fig. 1-16 Images of three drill bitsfrom side view and tip. Upper row: fresh, Middle row: used in the drilling of 600 holes, Bottom row: Drill bit from theatre [181].

1.4.3.4. Drilling of bone biomodels

Drilling characteristics of bone biomodels have not yet been reported until Cseke *et al.* reported the drilling of bone and Sawbones® test materials in comparison [53]. They described that drilling properties such as thrust force and torque of Sawbones® test materials under constant feed rate drilling are quite lower than those of porcine and bovine bones [53], implying a discrepancy under surgical training or evaluation of medical devices. No other literatures on drilling of Sawbones® test materials can be found at this moment.

Nonetheless, Tawara *et al.* pointed out the difference of mechanical properties between human bone and conventional bone biomodels and so manufactured a new bone biomodel made of polyurethane, whose drilling characteristics not yet available experimentally but pull-out strength [183,184]. Tai *et al.* developed a plaster-based material that showed the same order to bone in thrust force and torque under constant feed rate drilling, still having limitations in replicating cutting chips morphology [20,21]. In addition, there are two patents available for bone biomodels; acrylic-based composite materials with ceramic additives [186], and acrylic-based composite materials with wood fibers [109]. However, drilling characteristics of those models are not available in the patents but describing the accomplishments of good sensory feedback from doctors, thus lacking scientific grounds.

Bone biomodels are often made of plastics, ceramics, or composites of plastics and ceramics. Therefore, there should be the knowledge in those materials currently available that can be applied to drilling of bone biomodel. Drilling of plastics maybe especially applicable that has been studied along the development of FRPs for the components of industrial products [108,113,116–118,187–189]. Conventionally, thermoset polymers such as epoxies and polyesters are on the main scope of research works [116], but the usage of thermoplastic polymers is recently getting more and more attention for FRPs (CFRTP for carbon fiber-reinforced thermoplastic polymer, and GFRTP for glass fiber-reinforced thermoplastic polymer), thanks to their recyclability based on the thermoplasticity. Among thermoplastic polymers, polypropylene (PP), polycarbonate (PC), polyvinylchloride (PVC), and nylon (polyamide) are the main matrices often studied and applied to composite materials [188,190–193]. Regardless of the registration of patents as bone model, poly(methylmethacrylate) (PMMA) has not yet been a main focus of literatures. Since polymers show distinct material properties each other and thus different machinability, drilling characteristics of polymers shall be studied respectively for polymer species [188].

Among limited literatures, Kobayashi studied the three-dimensional drilling characteristics of PMMA [113], although studied machining conditions cannot necessarily be applied to surgical drilling. Apart from drilling, two-dimensional cutting, single point diamond turning (SPDT), on PMMA was reported for the frequent application of PMMA to optical lenses [194], but likewise, the cutting theory in two-dimensions cannot be always applicable in three-dimensional machining.

PMMA is known for its use as bone cement or teeth fixation in medical applications. Acrylic-based composite materials including ceramic additives can be found in literatures [195–197], but those acrylic composite materials are used for fixation of prosthesis or restoration of teeth, not yet intended for drilling. Thus, drilling characteristics of acrylic-based composite materials with ceramic additives have not yet been quantitatively studied.

1.5. Research scopes and objectives

In this chapter, backgrounds and literatures focusing on biomodel, bone, and drilling are studied, including the current limitations and challenges in the development of bone biomodels. After a vast literature review, the research background can be summarized as follows:

1. Bone biomodels are useful particularly in surgical training and for mechanical tests of medical devices,
2. Polyurethane foam from Sawbones® is one of the standard bone biomodels for cancellous bone defined in a test standard, while no biomodels are referred for cortical bone,
3. Bone drilling is one of the fundamental surgical steps in dentistry or orthopedics, but the replication of bone drilling has been out of research scope,
4. Thus, no quantitative evaluation items are currently available for the development of bone biomodels, except for perceptual feedback of surgeons.

Therefore, there have been many trials and errors for the development of bone biomodels. This study will address this situation by quantitatively studying drilling characteristics of bone biomodels. As stated above, contrary to a wide range of options possible for materials and machining conditions, there are only a limited number of previous studies related to drilling characteristics of bone biomodels available, resulting in the lack of understanding in drilling properties of bone biomodels. This study chooses to perform drilling tests under surgical machining conditions, focusing on acrylic composite materials with ceramic additives as well as bones and Sawbones® test materials. Drilling characteristics are dependent on various dominants. This study focuses on mechanical properties of

work materials, acrylic composite materials. The authors aim to control drilling characteristics by altering the mechanical properties that shall be controlled in response to the material composition. Through controlling the material properties, the objectives of this study are as follows:

1. Apply engineering standpoints into surgical drilling of bone biomodels, by quantitatively measuring drilling properties such as thrust force, torque, and temperature rise during drilling.
2. Understand the drilling characteristics of acrylic resin and acrylic composite materials under surgical drilling conditions toward the use application as bone biomodels.
3. Elucidate the effects of additives on mechanical and drilling properties of the matrix by controlling the composition of composite materials.
4. Elucidate also the effects of drilling properties on tactile feedback of surgeons.
5. Obtain the future direction of the development of bone biomodels through understanding of the relationships between material compositions, mechanical and drilling properties, and perceptual properties during drilling.

1.6. Organization of the thesis

In consideration of research motivations and objectives as stated above, the contents of this thesis are outlined as follows:

Chapter 1: backgrounds and literature reviews on this study focusing on biomodel, bone, and drilling are summarized, including the use application of bone biomodels, the current knowledge of drilling of natural bone and bone biomodels. The current limitations and challenges in the development of bone biomodels led to the research objectives.

Chapter 2: drilling tests of natural bone and Sawbones® test materials are preliminarily performed to understand the discrepancy of drilling characteristics and the current limitations of bone biomodels. Machining parameters are selected to reproduce realistic surgical drilling.

Chapter 3: drilling of acrylic resin are studied as a matrix toward fabrication of acrylic composite materials. The effects of cutting parameters and temperature elevation during drilling are investigated.

Chapter 4: Acrylic composite materials are fabricated using ceramic additives, and then their drilling properties are studied for the replication of drilling of bone.

Chapter 5: The relationship between drilling response and mechanical properties of work

materials, such as hardness, stiffness and viscoelasticity were examined through several mechanical tests. Additionally, the effect of additives on mechanical properties is studied.

Chapter 6: The relationship between drilling properties and tactile feedback of surgeons is studied to elucidate the dominants affecting tactile sense during drilling.

Chapter 7: Concluding remarks of this study from the obtained results and an outlook for the prospectus research works toward the development of future bone biomodels are described.

Chapter 2: Characterization of drilling in bone and Sawbones® test materials

This chapter presents the experimental and analytical methods for drilling tests under constant thrust force and constant feed rate using natural bone and Sawbones® test materials. Characterization of drilling includes measurements of drilling properties such as thrust force, torque, and temperature rise during drilling, and observation of cutting chips generated during drilling. The difference of drilling behavior between natural bone and Sawbones® test materials is discussed with taking into account the effect of rotation speed, feed rate, and thrust force.

2.1. Introduction

There are a lot of literature works available concerning drilling of bone, but drilling properties reported in their experimental results are not directly comparable due to the wide options possible for the material properties of bone and machining conditions. This chapter presents the characterization of drilling behavior in natural bone and Sawbones® test materials, which is intended to obtain the target values of drilling properties of natural bones, and understand the discrepancy of drilling behavior between natural and synthetic bones toward development of bone biomodel. It also introduces the test rig for drilling testing, where drilling is performed in consideration of machining conditions in surgical operations. The effects of machining parameters such as applied thrust force, rotation speed, and feed rate are taken into account. After drilling tests, cutting chips were observed using optical microscope and scanning electron microscope (SEM), in order to characterize the fracture behavior in material removal during drilling.

2.2. Test materials

2.2.1. Bone

Natural bones were obtained for this study. As stated at the section 2.3 in chapter 1, natural bone is known to show a large variance in material properties due to animal species, anatomic position, and dry condition, as well as conservation history. In terms of bone mineral density, which is tied to mechanical properties of bone [74,198], Aerssens *et al.* reported that canine and porcine bone shows similarities to human bone among a variety of animal bones [34,35]. Then, considering the similarity in bone mineral density, canine and porcine bone were provided by Prof. Viguier (VetAgro Sup, University of Lyon, France). The obtained anatomical position was mandibular part. The mandibular bases were taken out, and periosteum on the surface was removed to expose bone tissue. The bone specimen was then kept in 99.9% of ethanol for 24 hours to reduce the risk of infection. The authors estimated that the storage in ethanol has no significant effect on mechanical response in drilling as it had been reported that the storage in ethanol did not change the elastic properties of trabecular bone [199]. Likewise, porcine femoral bone was obtained from local butcher. Bone shaft was extracted and skins and bone marrow inside the shaft were removed, and subsequently conserved in ethanol.

In order to firmly fix the bone specimens for drilling tests, a flat surface was required for each

sample. Considering the complicated geometry of bone samples, the upper side of extracted mandibular bases that included teeth, were embedded in epoxy resin in a plastic box with a flat bottom surface, so that the mandibular bone embedded in epoxy resin can be fixed on the work stage, and the bottom side of mandibular bases can be drilled. Femoral bone specimens are fixed on a work stage with a clay.

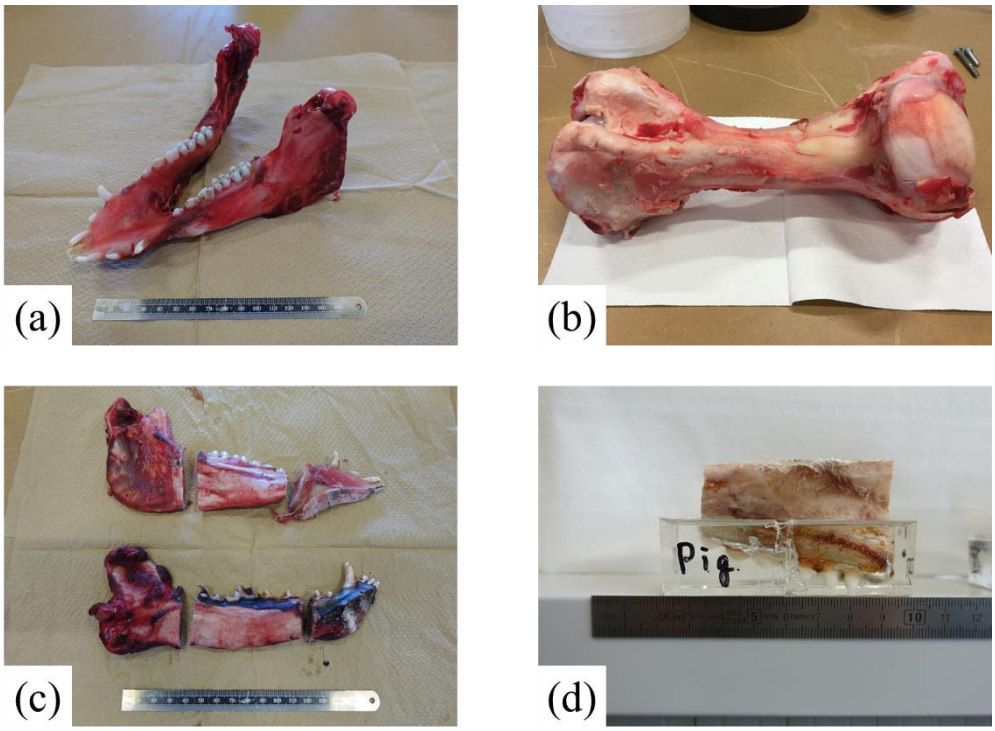

Fig. 2-1 Bone specimens; (a) obtained mandibular bone, (b) obtained femoral bone, (c) cutting of mandibular bases, (d) mandibular bases embedded in epoxy resin for drilling tests

2.2.2. Sawbones® test materials

Sawbones® test materials were obtained to measure drilling properties of conventional bone biomodels. Three types of conventional bone biomodels were prepared in this study. One is a cortical bone model (Composite sheets #3401-06, Pacific Research Laboratories, Inc., Vashon, WA, USA [48]) (called as Saw-EP below) made of epoxy resin and glass fiber (Fig. 2-2 (a)). The two are cancellous bone models (Solid Rigid Polyurethane Foam Block 20 pcf #1522-03, and 50 pcf #1522-27 [48]) (called as Saw-PU20 and Saw-PU50 below) made of polyurethane foam with different values of density (Fig. 2-2 (b)). Sawbones® test materials were processed into cubic pieces from the bulk of products for drilling tests.

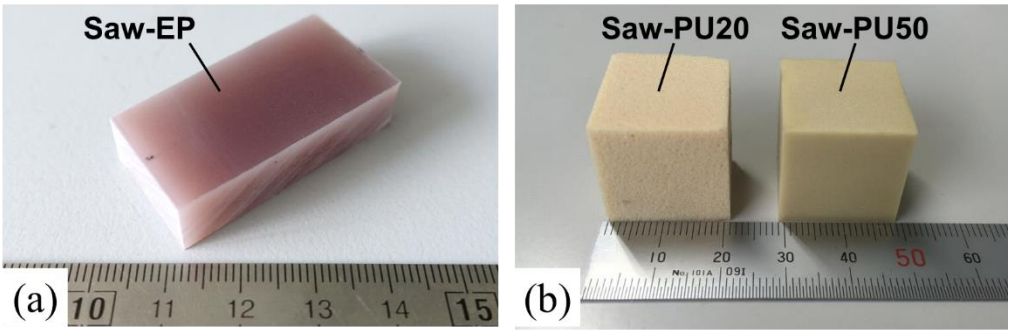

Fig. 2-2 Sawbones® test materials: (a) Saw-EP, and (b) Saw-PU20 and Saw-PU50

2.2.3. Comparison of general properties

Table 2-1 lists the general properties such as tensile strength and elastic modulus for bone and Sawbones® test materials. Saw-PU20 and Saw-PU50 replicates the properties of cancellous bone, showing relatively lower stiffness compared to both Saw-EP and bones. Saw-EP displays its stiffness within the values exhibited by bones. However, even though mechanical properties such as tensile strengths and elastic modulus are equivalent, drilling properties such as thrust force and torque reported by the literature are different [53]. Therefore, it can be possible that not only the stiffness but also other mechanical properties are important to determine the drilling properties.

Table 2-1 Comparison of general properties between animal bone and Sawbones® test materials, referred from [48][a], [75][b], [90][c], [32][d], [91][e]

Material	Tensile strength [MPa]		Elastic modulus [GPa]	
	Axial (longitudinal)	Radial (traverse)	Axial (longitudinal)	Radial (traverse)
Sawbones 1522-03 (Saw-PU20)	5.6[a]		0.284[a]	
Sawbones 1522-27 (Saw-PU50)	27[a]		1.5[a]	
Sawbones 3401-06 (Saw-EP)	106[a]	93[a]	16[a]	10[a]
Canine cortical bone	108.3 ± 20.5[b] (ultimate)		13.86 ± 1.17[b]	
	251.0 ± 49.1[c] (ultimate)		15.6 ± 2.6[c]	
Porcine cortical bone	88 ± 1.5[d]		14.9[d]	
	194.5 ± 14.45[e]		17.4 ± 1.11[e]	

2.3. Drilling test methods

Drilling tests carried out in this study includes both drilling under constant thrust force and under constant feed rate in order to obtain the target properties presented by thrust force, torque, and feed rate. Drilling by surgeons is supposed to be performed manually under a quasi-constant axial thrust force [152]. However, previous works focusing on constant thrust force drilling for a comparison of natural bone and Sawbones® test materials cannot be found. Thus, this study provides the information of constant thrust force drilling in Sawbones® test materials under surgical machining conditions.

On the other hand, not a few literatures can be found about drilling of bone under constant feed rate in search for reference values of drilling properties. However, a vast number of combinations of machining conditions as well as tested bone types prevent the present study from directly referring to reported drilling properties. For the purpose of making a comparison of drilling properties of natural bones, Sawbones® test materials, and composite materials developed in this study, drilling tests under constant feed rate were also performed in advance of fabrication of composite materials.

2.3.1. Experimental apparatus and methods

- **Drilling under constant thrust force**

Drilling tests were performed on a test rig, displayed in Fig. 2-3, developed in Laboratoire de Tribologie et Dynamique des Systèmes (LTDS), Ecole Centrale de Lyon, based on a spindle Electrobroche SD 5084, Precise, France. A drill bit was fixed to a chuck of the spindle, whose rotation was numerically operated by a spindle control system. Work pieces were pasted on a work table with double faced adhesive tape for mandibular bone samples and Sawbones® test materials, and with clay for femoral bone samples. The height of the work table was controlled by deadweights attached to a double pulley system, and a stopper fixed on a nearby bar. The height of the work table was adjustable in response to the height of deadweights. The axial thrust force was applied to the drill bit when the work piece contacted the drill bit under the applied constant load. In advance of each drilling test, the drill bit was hold on the surface of work materials having a space of a piece of filter paper, and the penetration of the drill bit was finished when the working table reached the stopper. The drilling displacement was controlled by a spacer that was put between the working table and the stopper. The length of the spacer was corresponding to the desired penetration depth. When the spacer was removed,

the work table moved up along the decrease in height of the deadweights, and subsequently drilling took place in the contact between the drill bit and the work specimens.

The test rig also included a strain gauge, a displacement sensor, and an infrared camera to obtain the measurements during drilling. Torque was measured using a strain gauge that was connected to the working table through an arm. The strain gauge transfers the measurements through the amplifier which can be acquired in the acquisition system based on LabVIEW software. A magnetic displacement sensor was mounted on the bar, in order to measure the penetration displacement of the drill bit. Having the constant drilling distance, the drilling feed rate can be calculated for each drilling test. Thermal images during drilling were taken using an infrared camera (FLIR SC7000), which observes perpendicularly to work pieces. In addition to acquisition of the drilling properties, cutting chips generated during drilling were collected after the drilling tests toward the morphological observation.

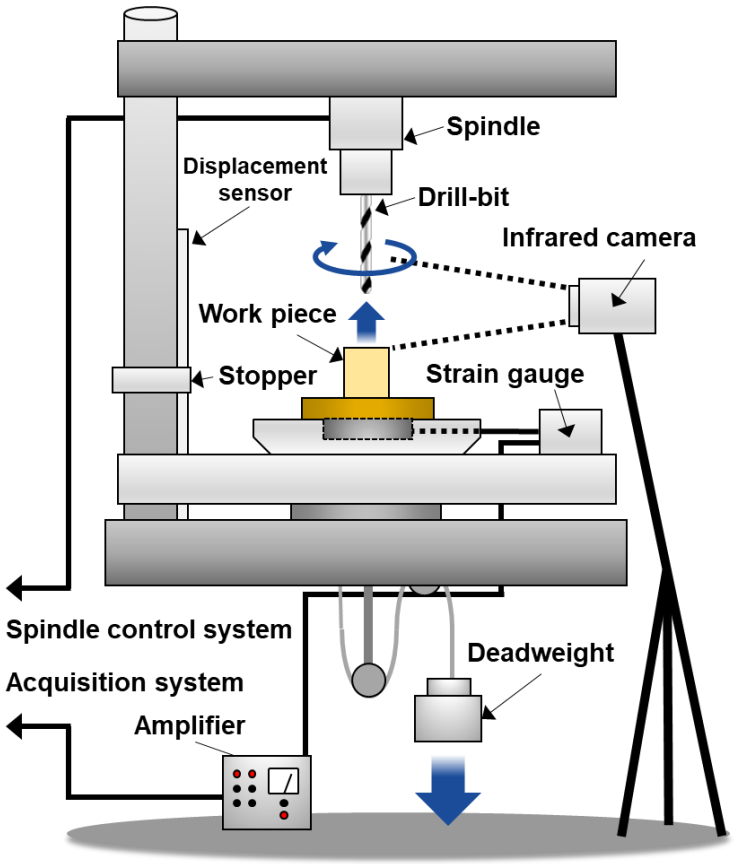

Fig. 2-3 Experimental apparatus of drilling test rig

- **Drilling under constant feed rate**

Drilling tests were performed using a CNC tapping center (Tapping center BROHTER TC-22A, Brother Industries, Ltd.) for drilling under constant feed rate. Fig. 2-4 shows an example of global view of experimental set-up. As depicted in Fig. 2-5, the tapping center was equipped with a working area including a spindle and a dynamometer (Kistler Type 9125A). The dynamometer was mounted on the spindle for measurement of drilling haptics. Thermal images were taken with an infrared camera (Infrared thermography FSV-2000, Apiste Corporation) during drilling. Specimens were clamped on a working table.

Under constant feed rate drilling context, drill bit was lowered toward work specimens automatically by the CNC tapping center at the specific feed rate. Axial thrust force and torque required for drilling were recorded. After reaching a desired displacement, the drill bit was immediately extracted from work piece meaning the end of drilling. Cutting chips on the drill bit was wiped after every 1 hole of drilling test. More than 3 holes were drilled for each specimen.

2.3.2. Test measurements

Between two types of loading methods available for drilling, different measurements can be obtained. In the characterization of drilling behavior, this study focuses on cutting forces (thrust force and torque), temperature rise, and feed rate for drilling properties as key factors.

In case of drilling tests under constant thrust force, torque, temperature rise, and feed rate can be obtained as drilling properties, where constant thrust force is applied as one of the machining parameters. Drilling feed rate varies depending on work materials under same machining conditions, which can be calculated by drilling time required for drilling until the specific displacement.

In case of drilling tests under constant feed rate, instead of thrust force as one of the parameters in machining conditions, the feed rate is set constant meaning that the drilling time required to penetrate the specific distance is corresponding regardless of work materials.

Fig. 2-4 CNC tapping center used for constant feed rate drilling

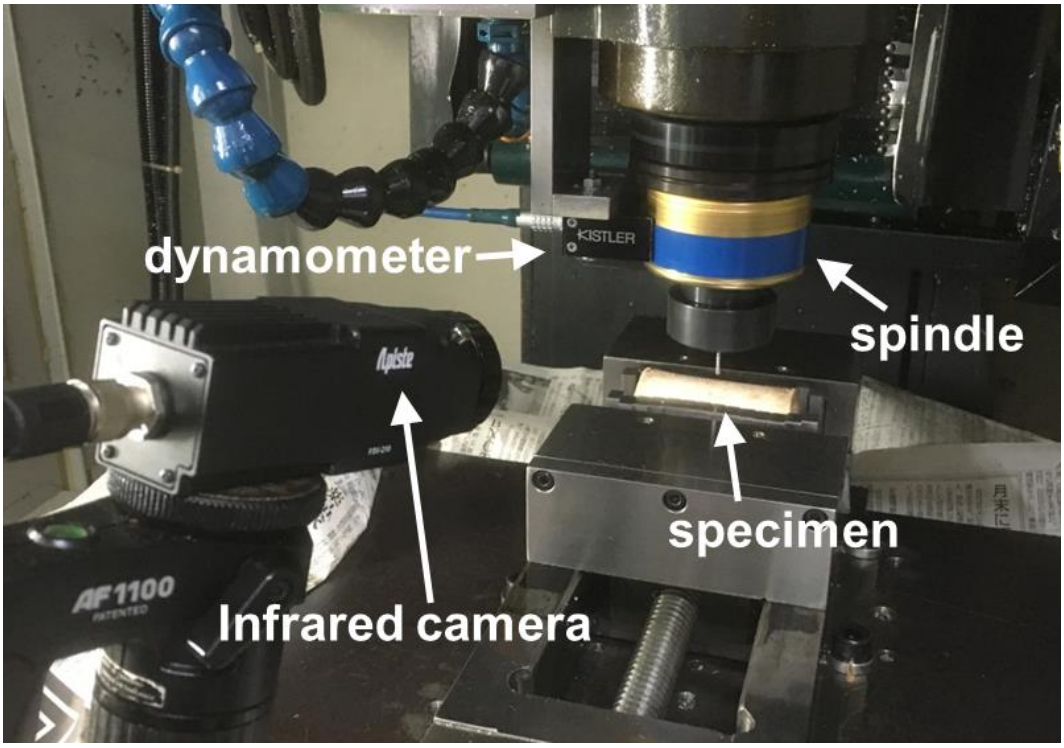

Fig. 2-5 Working area of the tapping center

2.3.3. Test conditions

Variable parameters affecting drilling tests are summarized in this section. After reviewing the parameters, test conditions were determined to reproduce surgical drilling under constant thrust force (Table 2-2) and under constant feed rate (Table 2-3).

Table 2-2 Machining conditions for drilling tests under constant thrust force. ○ indicates the used combinations of machining parameters

Drill bit		Twist drill, φ2 mm, point angle 80°, helix angle of 12°		
Environment		Dry conditions (no irrigation)		
Drilling depth [mm]		5		
		Rotation speed [rpm]		
		700	1000	1500
Thrust force [N]	15	—	○	—
	20	○	○	○
	25	—	○	—

Table 2-3 Machining conditions for drilling tests under constant feed rate. ○ indicates the used combinations of machining parameters

Drill bit		Twist drill, φ2 mm point angle 80°, helix angle 12°		
Environment		Dry conditions (no irrigation)		
Drilling depth [mm]		5		
		Spindle speed [rpm]		
		700	1000	1500
Feed rate [mm/rev]	0.030	—	○	—
	0.060	○	○	○
	0.100	—	○	—

- **Cutting tools**

A large variety of cutting tools available for drilling tests. The variety is coming from the wide options in tool geometry including point angle, helix angle, and number of flutes. This study used surgical twist drill (Nobel Biocare Japan Co., Ltd) (Fig. 2-6). The drill bit was made of the type 316L stainless steel with a diameter of 2 mm, a point angle of 80° and a helix angle of 12°. The tips of the prospective drill bits were scrutinized in advance of the drilling tests to reject inferior products with shape defects, tears, or cracks. The drill bit is normally used for material removal by creating a hole of the required depth to insert an implant device, after determining of the drilling position. The same drill bits were repeatedly used for the same machining conditions and work specimens. When machining conditions or work specimens were changed, a fresh drill bit was used.

Fig. 2-6 Twist drill bit used for a series of drill tests

- **Rotation speed**

The rotation speed represents the number of rotation of the spindle per minute. The developed test rig for constant thrust force drilling is capable to provide as much as 20,000 rpm for rotation speed of the spindle. According to the literatures, in the majority of the research cases the rotation speed less than 3,000 rpm was applied [169] although the application example of even 20,000 rpm for drilling of bone can be found [200]. For the clinical operation, the rotation speed less than 1,500 rpm is recommended by the surgical drill provider [201]. Then, this study adopted 700, 1,000, and 1,500 rpm of rotation speed for a series of drilling tests.

- **Thrust force**

According to the bibliography, thrust force from 1.9 N to 120 N were applied in previous studies, where less than 25 N for dentistry and between 20 N and 120 N for orthopedics [137,152,158,202]. In this study, thrust force of 15, 20, and 25 N was adopted under constant thrust force drilling. Under constant feed rate context, thrust force was obtained as a resistance force of work specimens against penetration of drill bit depending on materials under equivalent machining conditions.

- **Feed rate**

Under constant thrust force drilling, the feed rate depends on the applied thrust force. Regardless of work specimens, the much applied thrust force is, the much the feed rate is. The average drilling feed rate can be calculated in response to the drilling time required to reach the specific depth. Under constant feed rate drilling, the values of feed rate vary among researchers [170], where the feed rate at 1 mm/s seems realistic as suggested by orthopedic surgeons according to [180].

- **Penetration depth**

Considering the length of screws or prosthesis required for insertion, usually less than 10 mm of drilling depth was applied in the clinical circumstances. In this study, the penetration depth was determined as 5 mm. This is because the actual thickness of canine and porcine cortical bone was often 3 to 4 mm, and 5 mm-depth was considered enough to obtain cutting forces with the drill tip fully engaged in penetration.

- **Sampling rate**

The sampling rate indicates the frequency of the data acquisition. For any sort of experiments, sampling rate has to be determined to catch the global picture of the phenomena within the acceptable data capacity. In consideration of the rotation of the drill bit, 200 Hz was selected for the sampling rate of cutting forces and displacement. In case of 1,000 rpm of the rotation speed, which was estimated to accumulate the sufficient number of data amounts (12 times of data acquisition per rotation of the drill bit). On the other hand, thermal images were taken at the maximum sampling rate of infrared cameras respectively, 10 Hz for FLIR SC7000 and 5 Hz for FSV-2000.

- **Number of drill tests**

Previous studied often performed at least three times of drilling for each sample. In consideration of individual and location variance of material properties especially for bone samples, at least five times of measurements were performed, while three times for Sawbones® test materials.

- **Test environment**

The realistic surgery often accompanies the irrigation in drilling of bone. Besides, natural bone is always stored under wet conditions in mother bodies. Therefore, the ideal conditions for performing drilling of bone in surgical training or mechanical tests of medical devices is under wet conditions. However, it is not always easy for researchers and amateur doctors to prepare test or training system with the presence of liquid. This study preliminary concentrates on drilling of bone under dry conditions.

2.4. Analysis methods

2.4.1. Processing of acquired data during drilling tests

- **Drilling under constant thrust force**

Torque and displacement were acquired using LabVIEW software. A moving average filter was applied to smooth noise effects on the obtained data.

MATLAB R2018a was used to read the thermal images. The programming codes included several steps; definition of the spatial resolution, selection of a zone of interest, and illustration of the temperature fields. As depicted in Fig. 2-7, a zone of interest (ZOI) was selected to record the maximum temperature during drilling, which covers both the drill-bit and the specimen. Since the working stage moves upward as the drill bit penetrates the specimen, a cylindrical marker was put aside the stage for the programming of position tracking. ΔT is the temperature variation defined by $\Delta T=T-T_0$ (where T is the maximum temperature measured in the ZOI and T_0 the equilibrium temperature at the beginning of the tests). To analyze the drilling tests, torque, displacement and temperature variation were plotted as functions of time.

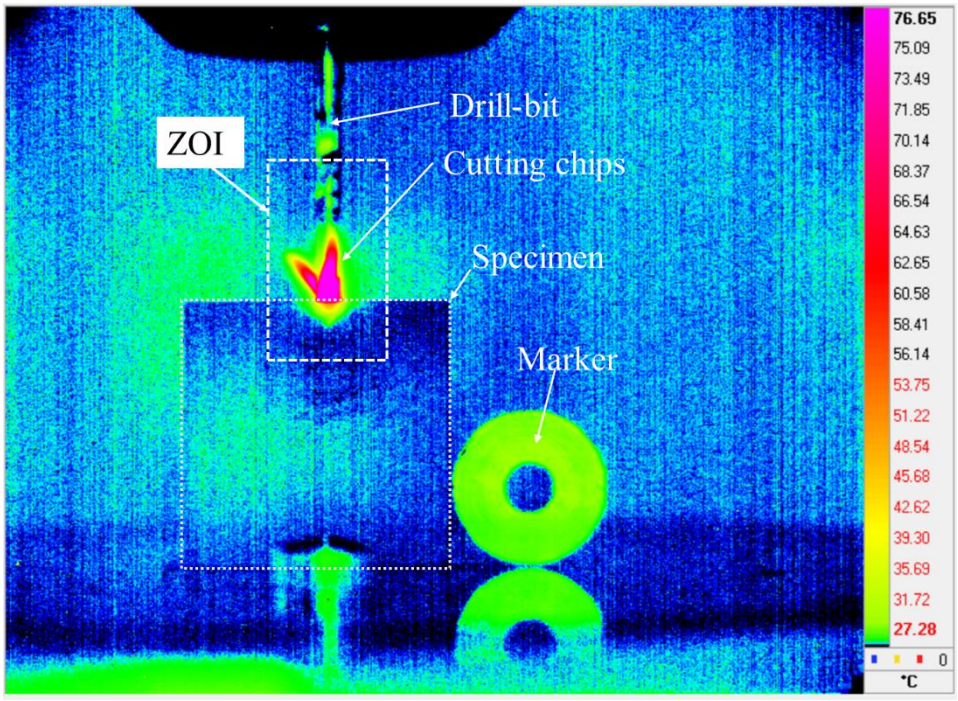

Fig. 2-7 An example of thermal images taken from drilling tests. ZOI is shown. The color is related to the temperature as indicated by the bar on the right axis.

- **Drilling under constant feed rate**

The cutting forces were acquired using the dynamometer as a function of time. A moving filter was also applied to smooth the obtained thrust force and torque. A series of recorded images were analyzed using a software (FSV-S2000, Apiste Corporation) with selecting a zone of interest including the drill bit and work specimen in the manner shown in Fig. 2-8. Maximum temperature in the selected zone was read to obtain ΔT as is similarly defined under constant thrust force drilling.

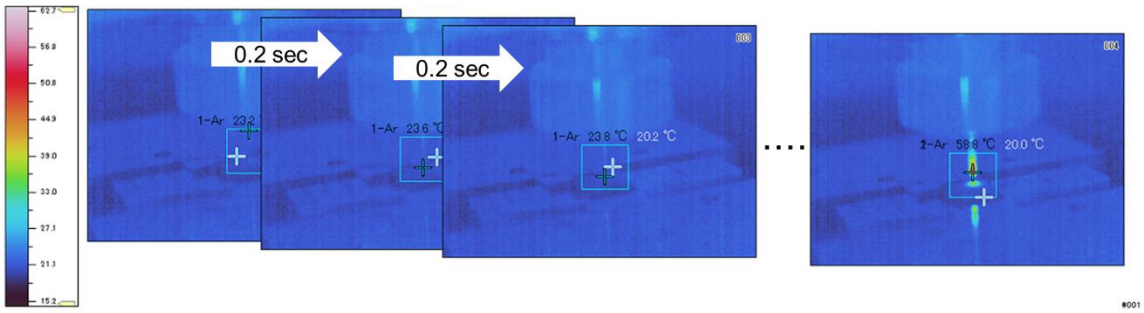

Fig. 2-8 Analysis procedure of obtained thermal images using the infrared camera

2.4.2. Observation by optical microscope

Both geometry of cutting chips and wear of drill bits were observed using the optical digital microscope (Keyence VHX-6000). Since chip formation was a non-negligible factor in understanding the drilling characteristics, cutting chips were collected after the drilling tests and observed in macro scale to precisely identify their morphology. There are various types of cutting chips possible to generate depending on the machining conditions, work materials, and cutting tool. Similarly, the geometry of drill bits before and after drilling tests was observed to take into account the degree of frictional damages depending on work specimens focusing on cutting and chisel edges, and rake face.

2.4.3. Observation by Scanning Electron Microscopy (SEM)

The observation of the cutting chips in micro scale was also performed, using SEMs (MIRA3, Tescan Orsay Holding a.s. and XL30 ESEM-FEG, Philips). For non-conducting materials such as bone and polymeric materials, gold/palladium alloy was sputtered to form a thin conductive layer to be prepared for observation with the SEM.

2.5. Results and discussions

2.5.1. Drilling properties

- **Drilling under constant thrust force**

❖ Comparison of representative curves between Sawbones® test material and porcine bone

Fig. 2-9(a) represents the typical evolution of torque, ΔT, and displacement as a function of time when drilling in Saw-PU50 under 20 N and 1,000 rpm. Drilling in Saw-PU50 takes about 2 seconds for 5-mm depth. This time length before the end of penetration is hereafter called as drilling time having different values for every work material. Displacement stays constantly at 5 mm after reaching the end of penetration, where no more penetration but the spindle still active for rotation. Torque increases along the penetration of the drill bit and reaches its maximum value slightly before the maximum depth at 5 mm, and keeps its value until the end of penetration. After the penetration, torque continuously decreases with a specific gradient.

ΔT increases drastically at the beginning of drilling firstly until about 50℃ and then increases again until about 120℃ around the end of drilling. Taking a look at thermal images taken during drilling tests as shown in Fig. 2-10(a), it turns out that maximum temperature was obtained from cutting chips evacuating through the drill bit, not from the bulk of work specimen. Considering possible thermal sources during drilling, it can be illustrated as shown in Fig. 2-11, indicating plastic deformation of work material due to creation of cutting chips, deformation of cutting chips evacuating through the flute of drill bit also having friction due to the contact with the flute and borehole wall, where drill bit similarly has friction with borehole wall both at the lateral and bottom surfaces. Along the progress in penetration of drill bit, the effects of deformation of cutting chips due to rotational motion, and friction among cutting chips, the flute of drill bit, and borehole wall of work material can become large. This effect is thought to be seen in the second peak of ΔT, as the cutting chips evacuating at 2 seconds after the beginning of drilling shows the maximum temperature possibly because the cutting chips travelled longer distance with exposed to deformation and friction for longer time than the firstly emerging cutting chips.

Fig. 2-9(b) illustrates the typical evolution of drilling properties in porcine mandible specimen under the same machining conditions. Note that the time scale is different from Fig. 2-9(a), in order to clarify the details of each evolution. Drilling takes about 10 seconds to reach 5 mm with increase in torque and temperature. There is a sudden increase in torque when the drill bit penetrates through the

cortical thickness at around 3 mm. After the penetration of cortical bone, the drill bit progressed through a hollow cavity without any material removal. After the peak attributed to the penetration, torque decreases to zero immediately, having the only contact between drill bit and work material for the cortical thickness.

ΔT increases drastically at the beginning, and then keeps the maximum value until the end of penetration. After the end of penetration, temperature decreases gradually. The increase in temperature is likewise considered to be associated to plastic deformation and friction during drilling. Contrary to drilling in Saw-PU50, discontinuous cutting chips were generated in drilling in porcine mandible, having the maximum ΔT around 50°C (Fig. 2-10(b)). The magnitude of temperature rise is smaller in drilling in porcine bone rather than in Saw-PU50. Several reasons can be described. Firstly, considering the drilling feed rate, drilling in Saw-PU50 is much faster, implying that the volume of material removal per unit of time is larger in Saw-PU50 rather than in bone specimen. Assuming that the degree of ΔT is related to the volume of materials removed by plastic deformation, the more the material removal occurs, the higher the ΔT can be. Secondly, the difference of thermal conductivity might be dominant. Supposing the thermal conductivity of porcine cortical bone to be 0.64 W/mK as well as that of bovine bone as stated at the section 4.3.2. in the chapter 1 [165], while approximately 0.034 W/mK for polyurethane foam [203], the bone specimens would show more than ten times higher in thermal conductivity, meaning less resistance against heat transfer. Thus, generated heat can more easily diffuse to the air in bone specimens, reducing the effect of heat accumulation in cutting chips. In this regard, the powdery shape of cutting chips in bone specimen may facilitate the heat diffusion rather than in continuous chips, due to the increase in contact of surface area with the air. Thirdly, the difference of frictional behavior in Saw-PU50 and bone specimen should be considered. Since a portion of thermal energy derives from the friction involving work materials, the degree of heat generation depends on the friction properties of work material.

Mentioning thermal effects on surrounding tissue near the borehole, the absolute temperature above 47°C is obtained for both specimens during drilling, which should be avoided taking into account the osteonecrosis. However, those high temperatures are obtained not on the surrounding tissue, but on the cutting chips according to thermal images. Although the surrounding tissue around the borehole is surely exposed to high temperature above 47°C due to the contact with evacuating cutting chips, it is still uncertain how much temperature the adjacent tissue reaches from the analyzation of thermal images taken by the infrared camera, because of the temperature gap between

measurable lateral surface of test specimens and inside the borehole wall.

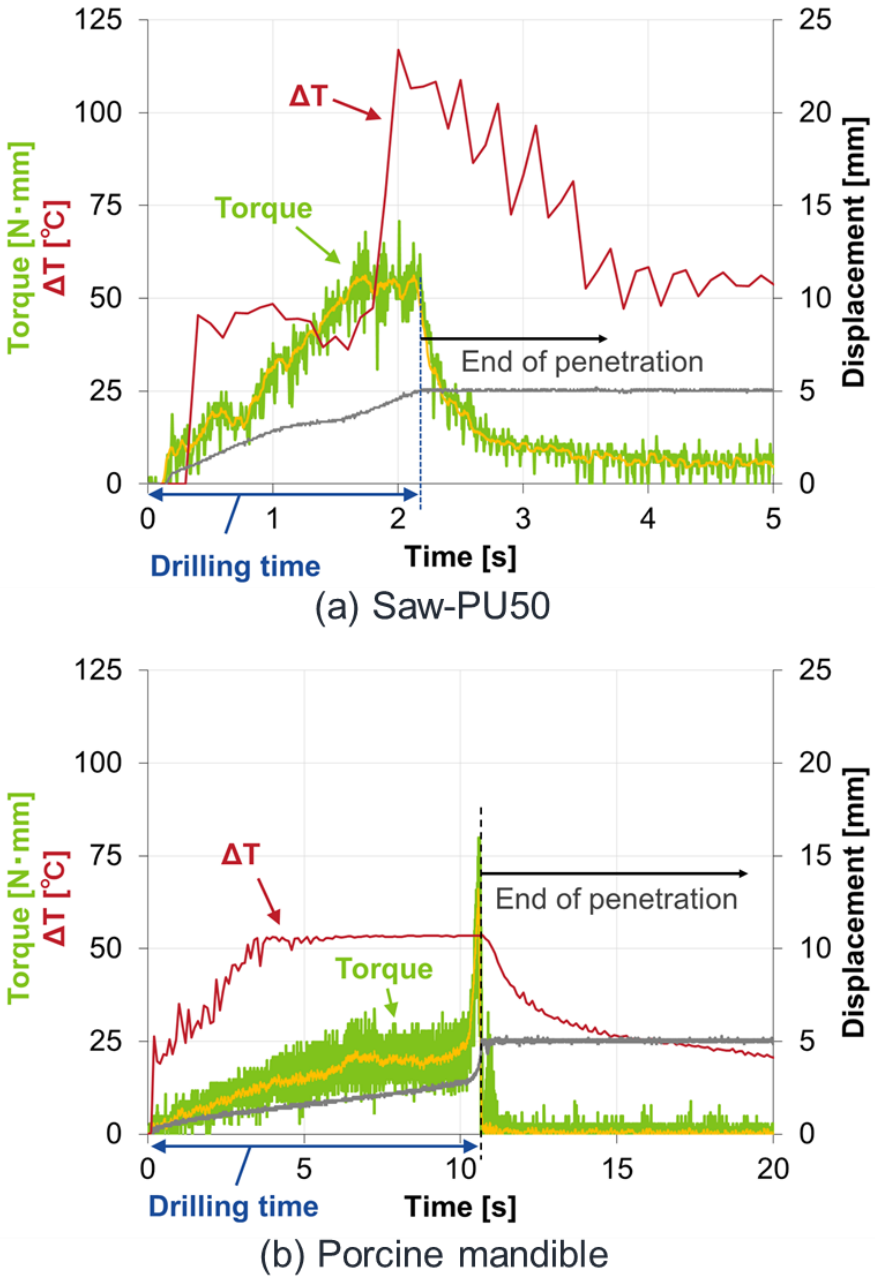

Fig. 2-9 Representative evolution of drilling properties in (a) Saw-PU50, and (b) Porcine

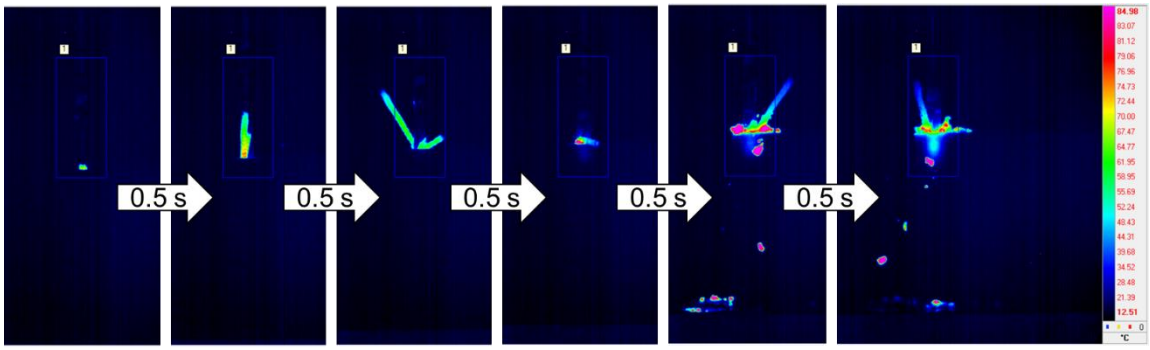

(a) Saw-PU50

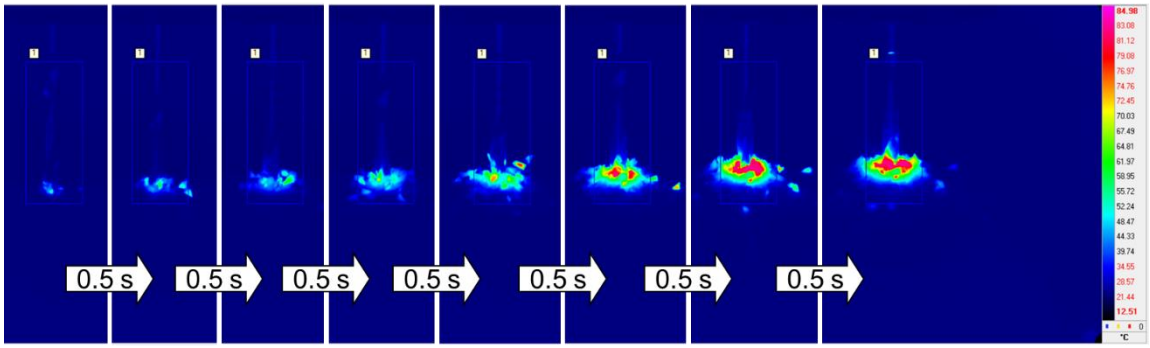

(b) Porcine mandible

Fig. 2-10 Thermal images for each 0.5 second from the beginning of drilling on (a) Saw-PU50, and (b) Porcine mandible. The maximum temperature seems to be extracted from cutting chips generated during drilling for both test specimens.

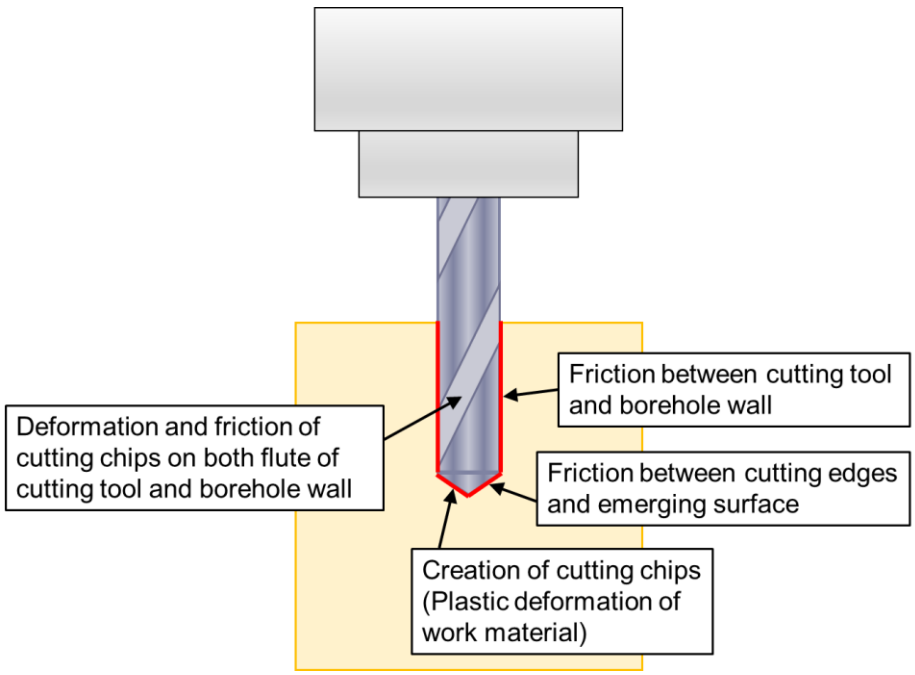

Fig. 2-11 Schematic image of possible thermal sources on drilling site during drilling

❖ Comparison of average values among test materials

Fig. 2-12 shows the comparison of typical evolution of drilling properties for all the six specimens including (a) Saw-PU20, (b) Saw-PU50, (c) Saw-EP, (d) Canine mandible, (e) Porcine mandible, and (f) Porcine femur. The machining conditions are 20 N for thrust force and 1,000 rpm for rotation speed. The trend that torque and ΔT increases along the progress of drilling can be seen for every material. The gradient of decrease in torque after the end of penetration seems to depend on materials; torque gradually decreases in Saw-PU50 while sharply decreases in mandibular bone specimens. The stress relaxation of polymer materials due to the viscoelasticity can be considered to have an effect on the gentile decrease of the torque. Bone specimens show drilling time between 10 and 15 seconds, and Saw-EP shows the corresponding drilling time. Saw-PU20 and Saw-PU50 show quite shorter drilling time compared to other specimens, while largest maximum temperature was obtained in Saw-PU50 among the tested specimens.

To characterize the drilling properties depending on materials, the maximum values of torque, drilling time, and ΔT was averaged. Fig. 2-13 summarizes the average values of drilling time, maximum torque, and ΔT as a function of rotation speed and thrust force focusing on Saw-PU20, Saw-PU50, Saw-EP, and Porcine mandible. The effects of rotation speed and thrust force on drilling properties among four materials will be described. Note that the actual thickness where drilling was performed in bone specimens is less than 5 mm contrary to the fixed drilling depth of 5 mm.

❖ The effect of rotation speed

In Saw-PU20 and Saw-PU50, torque and drilling time were crucially lower compared to cortical model and bone specimens, while having low ΔT in Saw-PU20 and high ΔT in Saw-PU50. Although the usage of these polyurethane foam is commonly suggested as an alternative test material of bone specimen in JIS [41,43], it is implied that drilling properties can be different.

As for the cortical bone model from Sawbones, drilling time and torque often show corresponding values under 1,000-rpm and 1,500-rpm rotation speed. Observed temperature also shows its similarity in maximum values. However, it takes drastically longer drilling time under the machining conditions of 20-N/700-rpm, with the lowest rotation speed. By taking a look at the evolution of drilling (Fig. 2-14(h)), it can be observed that the penetration of drilling takes time at the initial phase, with little feed rate for penetration. Under the machining conditions of 20-N/700-rpm, the penetration stagnates at the surface, almost equal to displacement of zero. From this trend, there is a possibility of idle running on the surface of the Saw-EP. This phenomenon cannot be found in bone

specimens.

Bone specimens show almost similar values of drilling properties regardless of the rotation speed applied in this experiment.

❖ The effect of thrust force

There is an effect of thrust force on four specimens in terms of torque. This trend can be due to the increased force converted for material removal along the increase in thrust force. The increased force in material removal results in much materials can be removed per rotation, therefore making drilling time shorter, maximum torque larger. Temperature rise is less affected by the increase in thrust force.

Comparing Saw-EP and bone specimens, the closer drilling properties was observed under thrust force of 20 and 25 N. However, under 15-N/1,000-rpm, which is the lowest thrust force, drilling takes longer time than that of bone specimen. This case also can be resulting from the stagnation of drilling at the surface layer of the material (Fig. 2-15(h)).

As a result, Saw-EP, the cortical bone biomodel from Sawbones, showed the corresponding values of drilling properties such as maximum torque, drilling time, and ΔT. However, the discrepancy still exists under certain machining conditions such as 20-N/700-rpm and 15-N/1,000-rpm, which are with the lowest rotation speed or the lowest thrust force applied in this study. Considering the mechanical properties as presented at the Table 2-1, Saw-EP shows the almost corresponding tensile strength and elastic modulus. Drilling tests showed that the replication of mechanical properties such as strength and elasticity cannot always reproduce the drilling properties. Since Saw-EP especially seemed to show the stagnation of drilling penetration at the surface layer that cannot be observed for bone, the surface conditions was possibly different between Saw-EP and bone specimens, which should be further taken into account for the replication of bone.

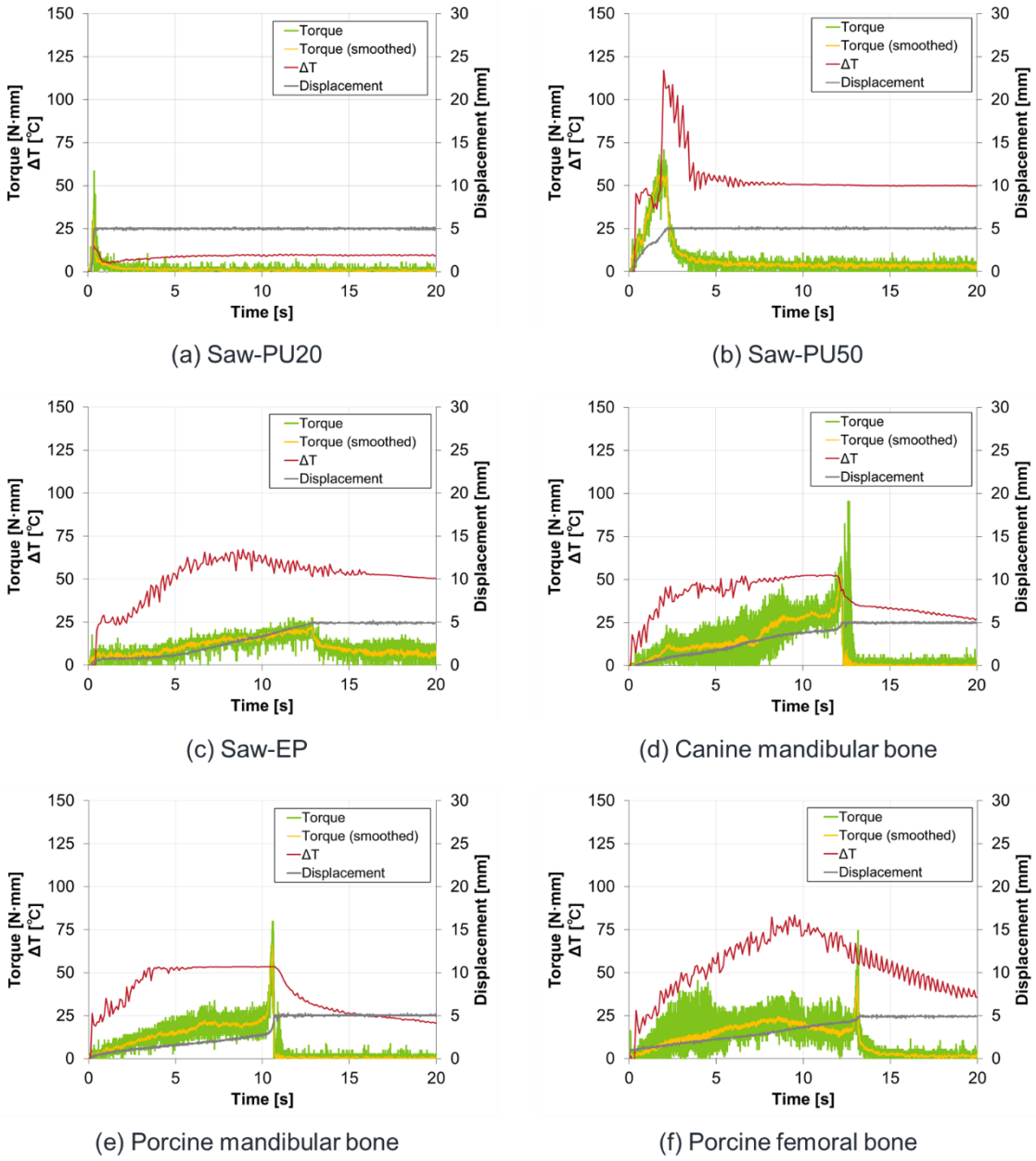

Fig. 2-12 Drilling properties as a function of time obtained from drilling tests under the machining conditions of 20-N thrust force and 1,000-rpm rotation speed.

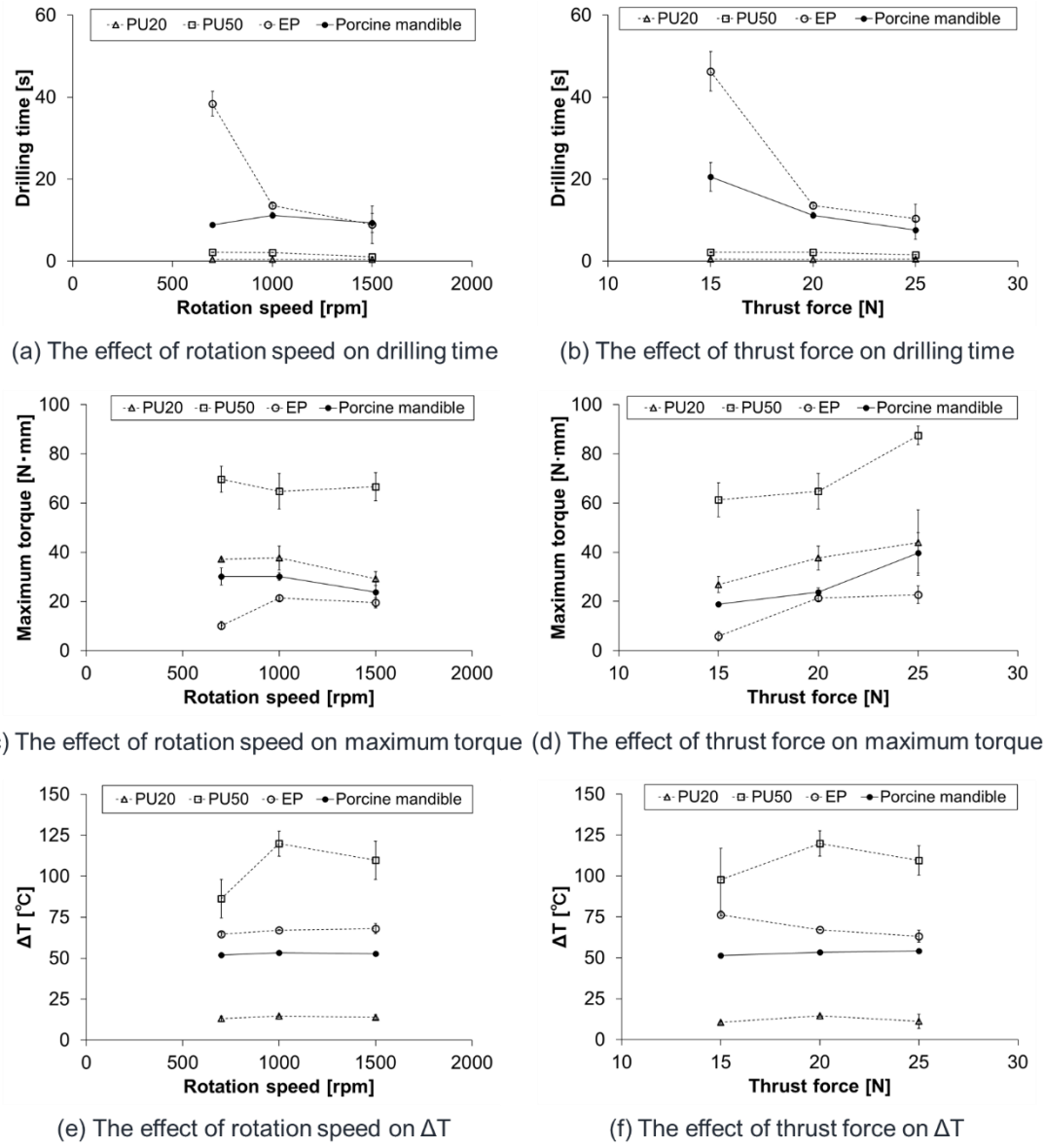

(a) The effect of rotation speed on drilling time

(b) The effect of thrust force on drilling time

(c) The effect of rotation speed on maximum torque

(d) The effect of thrust force on maximum torque

(e) The effect of rotation speed on ΔT

(f) The effect of thrust force on ΔT

Fig. 2-13 Average values of drilling properties such as drilling time, maximum torque, and ΔT as a function of rotation speed for (a), (c), and (e), and thrust force for (b), (d), and (f)

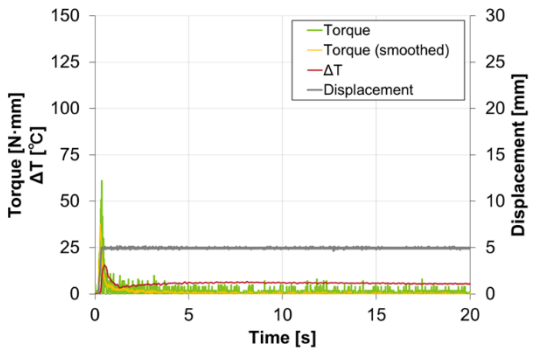

(a) Saw-PU20, 20 N, 700 rpm

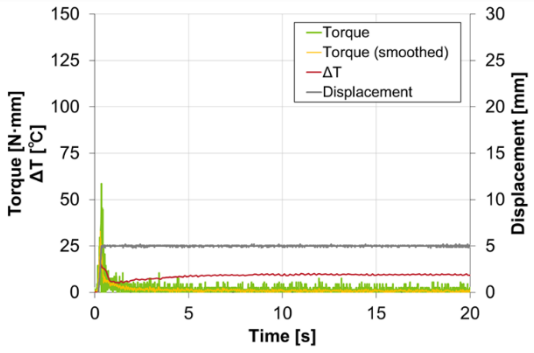

(b) Saw-PU20, 20 N, 1000 rpm

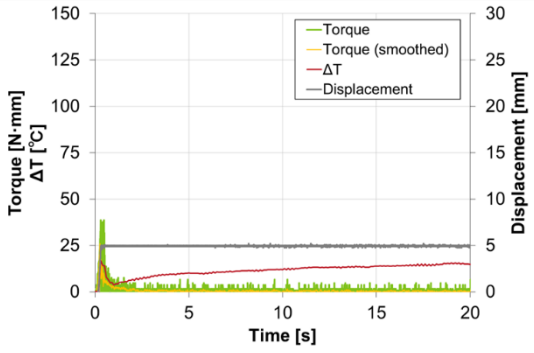

(c) Saw-PU20, 20 N, 1500 rpm

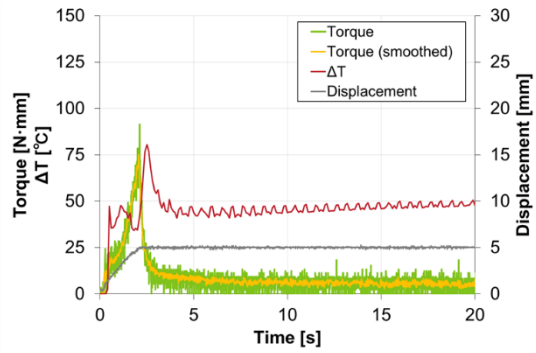

(d) Saw-PU50, 20 N, 700 rpm

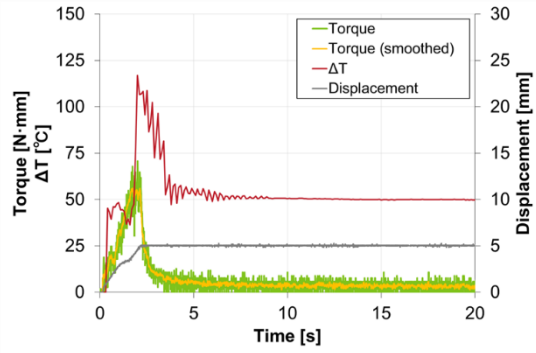

(e) Saw-PU50, 20 N, 1000 rpm

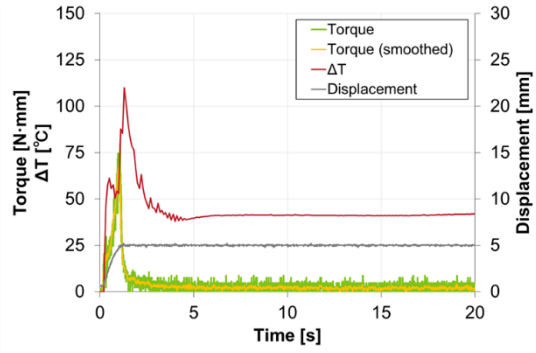

(f) Saw-PU50, 20 N, 1500 rpm

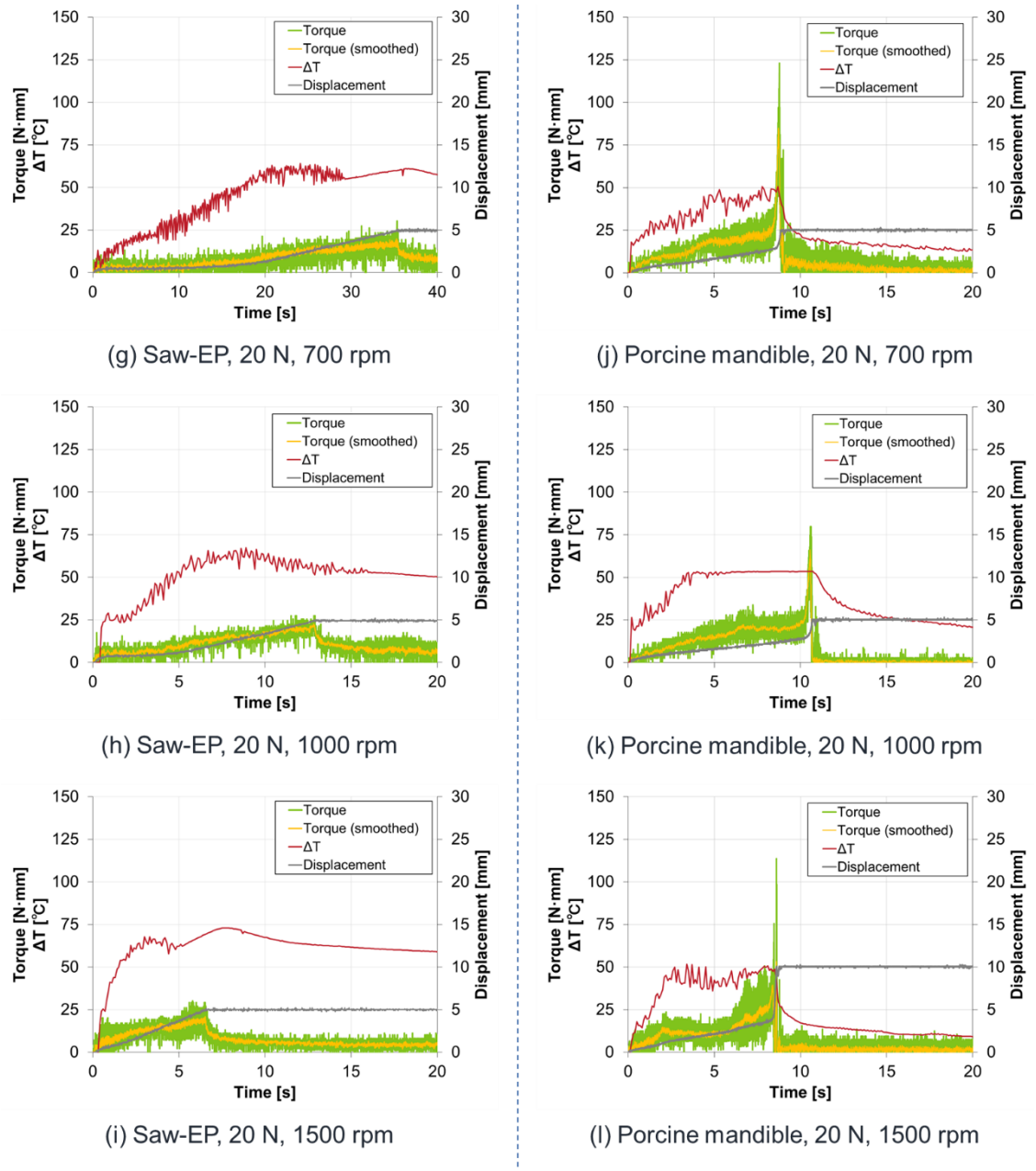

Fig. 2-14 Typical evolution of drilling properties for four materials under the machining conditions of 20 N in thrust force, and 700, 1000, 15000 rpm in rotation speed

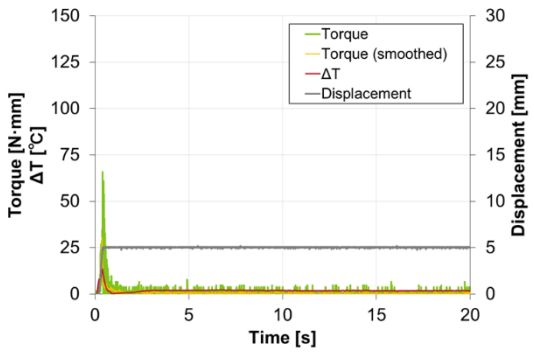

(a) Saw-PU20, 15 N, 1000 rpm

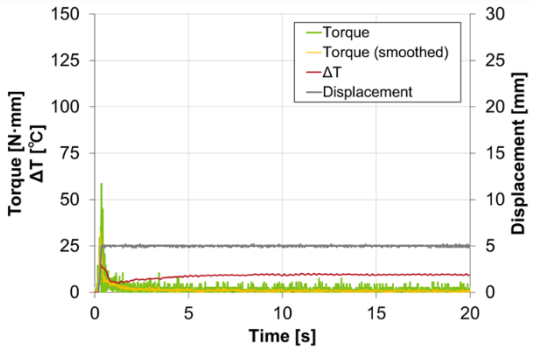

(b) Saw-PU20, 20 N, 1000 rpm

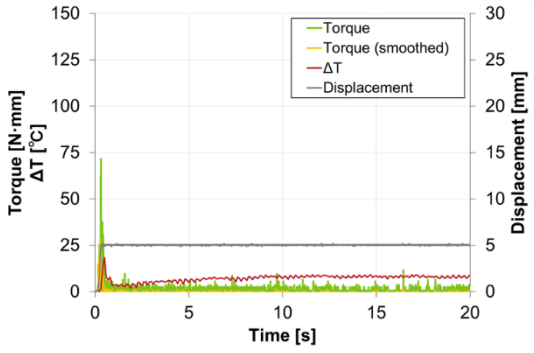

(c) Saw-PU20, 25 N, 1000 rpm

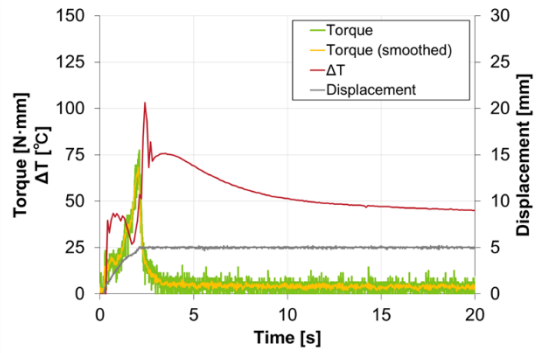

(d) Saw-PU50, 15 N, 1000 rpm

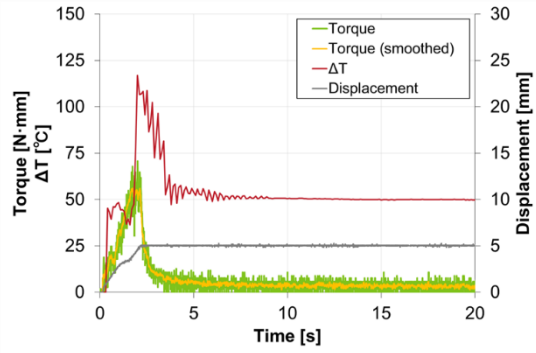

(e) Saw-PU50, 20 N, 1000 rpm

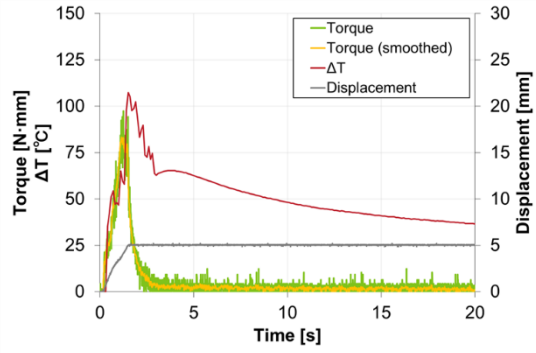

(f) Saw-PU50, 25 N, 1000 rpm

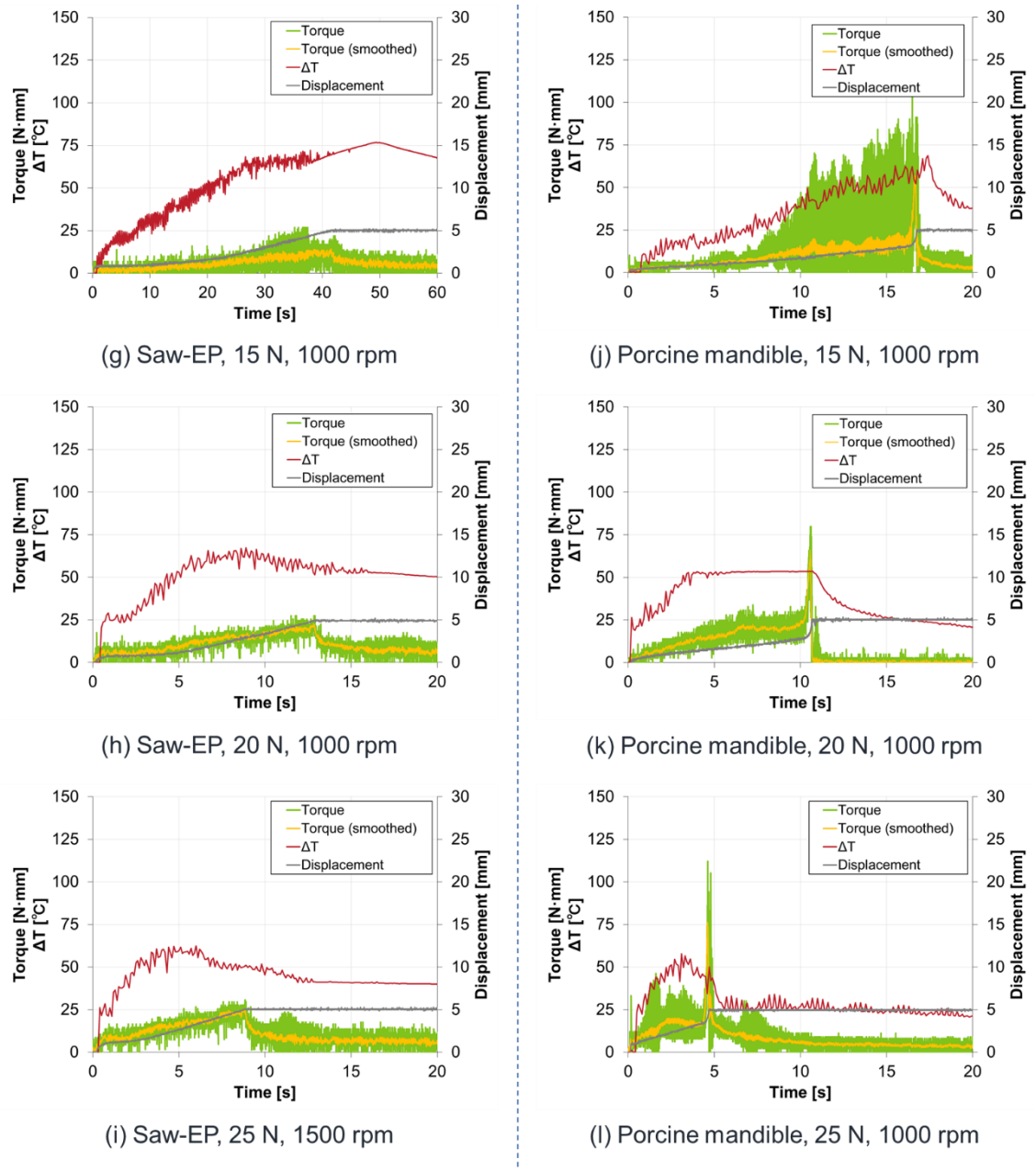

Fig. 2-15 Typical evolution of drilling properties for four materials under the machining conditions of 1000 rpm in rotation speed and 15, 20, and 25 N in thrust force

- **Drilling under constant feed rate**

❖ Comparison of representative curves between Sawbones® test material and porcine bone

Fig. 2-16 shows typical evolution of drilling properties such as thrust force, torque, and ΔT during drilling under the machining conditions of 1,000-rpm rotation speed and 0.060-mm/rev feed rate for porcine mandibular and femoral bone, and Sawbones® test materials. Drilling properties are obtained as a function of displacement of the drill bit. Moving filter is applied to smooth the profile of thrust force and torque. According to the Fig. 2-16, thrust force globally increases at the beginning of the penetration and then stays around the maximum values, while torque and temperature are gradually increasing until the end of penetration at the 5-mm depth where the extraction of the drill bit occurs. ΔT increases in response to the increase of torque as stated in previous works [53]

Fig. 2-17 shows an averaged evolution of thrust force until 3-mm depth. As for the comparison among bones and Sawbones® test materials, the scale of maximum values of thrust force ranks Saw-EP, porcine femoral bone, porcine mandible bone, Saw-PU50, followed by Saw-PU20. According to this ranking, Saw-EP shows slightly higher thrust force in comparison of natural bones, while Saw-PU20 and 50 show quite lower values. Lughmani *et al.* performed drilling tests with bovine femoral shaft with average cortical thickness of 7 to 9 mm and measured both thrust force and torque for establishing numerical model for predicting drilling forces in bone drilling [176]. They reported that the measured force varies between 25 to 75 N, while torque 120 to 160 N· mm, under the spindle speed of 800 to 1500 rpm and constant feed rate of 0.05 to 0.1875 mm/rev. They also summarized previous studies about drilling of bone from various anatomical positions and animal species, and concluded that thrust force varied up to from 0 N up to 70 N and torque 0 N· mm up to 380 N· mm [176]. The difference between the experimental measurements comes from the different applied drilling conditions depending on researchers, such as the geometry of the drill, rotation speed, feed rate and bone type. The obtained results for drilling porcine mandible bone and femoral bone in this study are within the reported range, corresponding to the relatively lower data.

The effects of machining conditions such as rotation speed and feed rate are seen in Fig. 2-18 and Fig. 2-19 respectively. Globally, there is a trend that both thrust force and torque decrease along the increase in rotation speed, and increase along the increase in feed rate, while it seems that both rotation speed and feed rate have less impacts on temperature elevation within the machining conditions applied in this range. These trend is in good agreements with literatures [133,176].

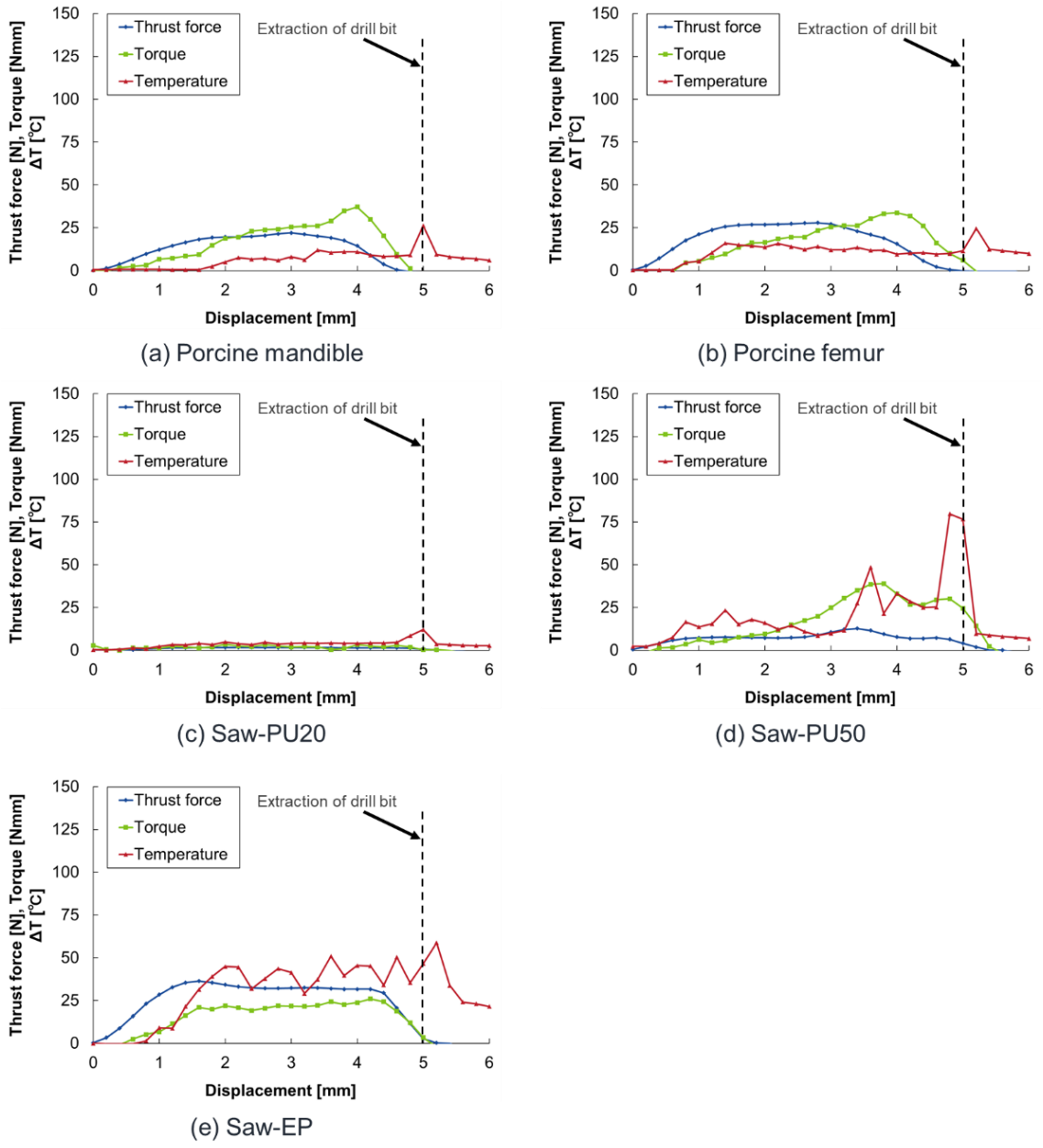

Fig. 2-16 Typical evolution of drilling properties under constant feed rate drilling for porcine bone and Sawbones® test materials

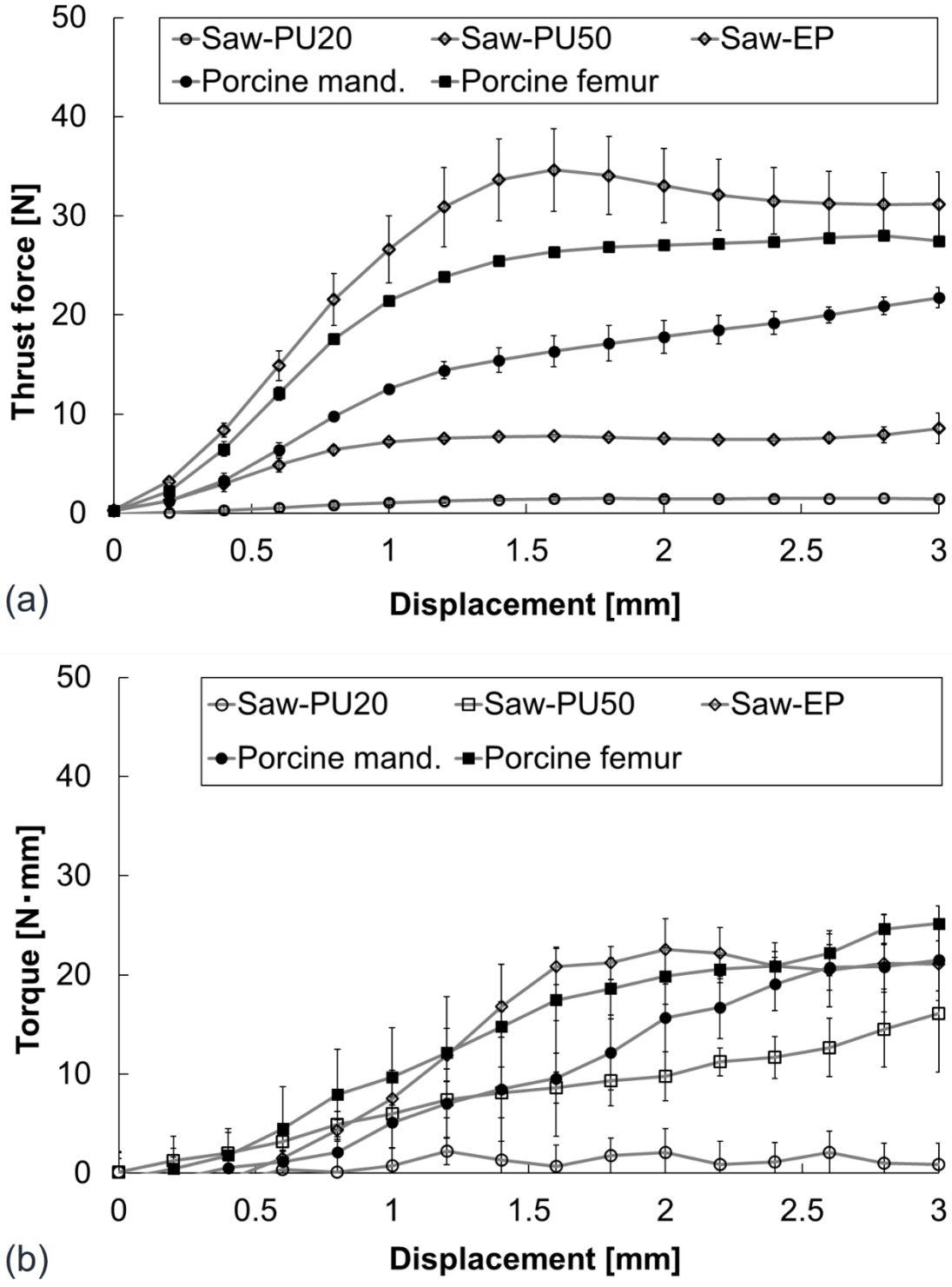

Fig. 2-17 Averaged evolution of (a) thrust force and (b) torque for bone specimens and Sawbones® test materials

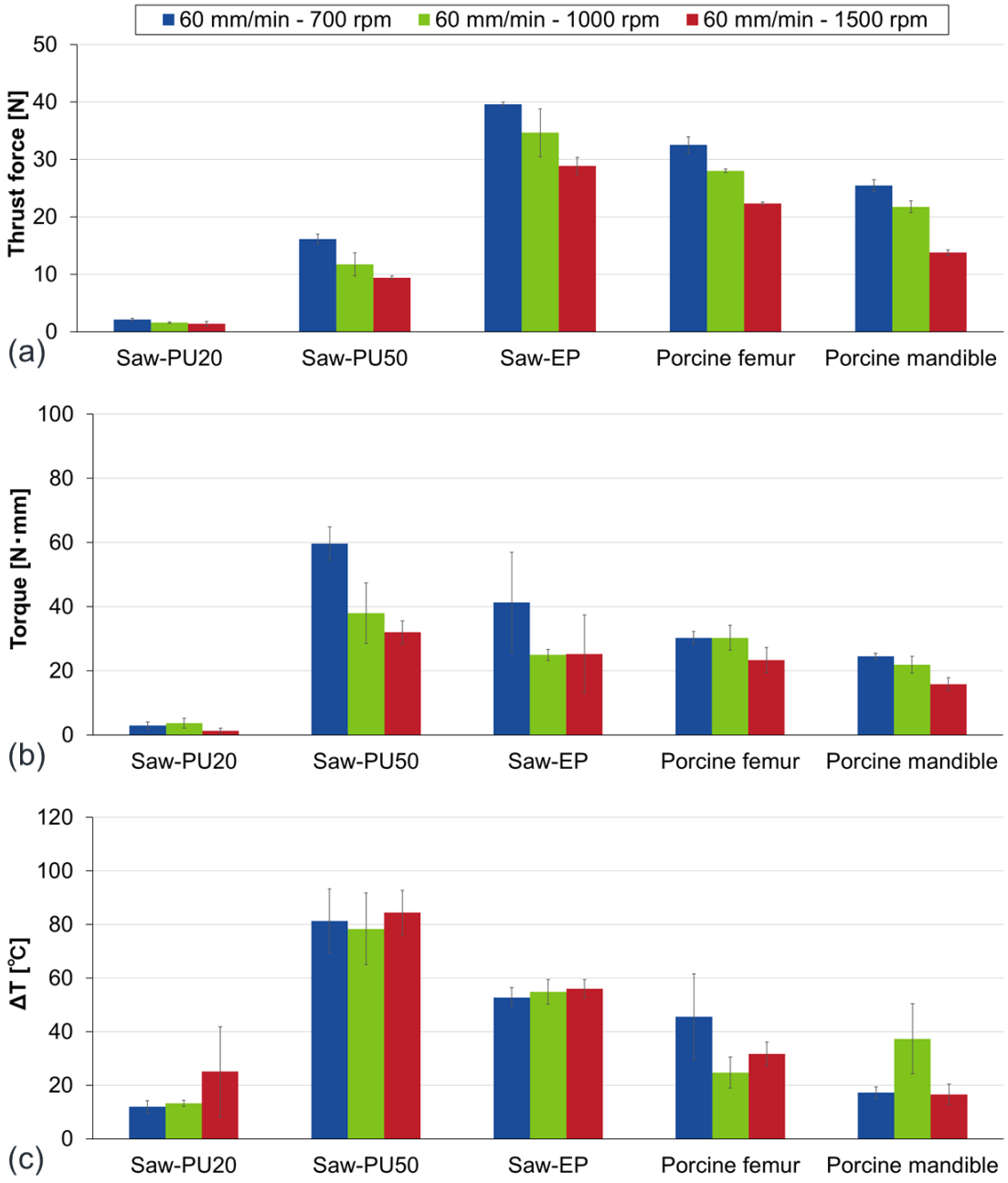

Fig. 2-18 Comparison of (a) Thrust force; (b) Torque; and (c) Temperature elevation (ΔT) as a function of test specimens under machining conditions with various rotation speed.

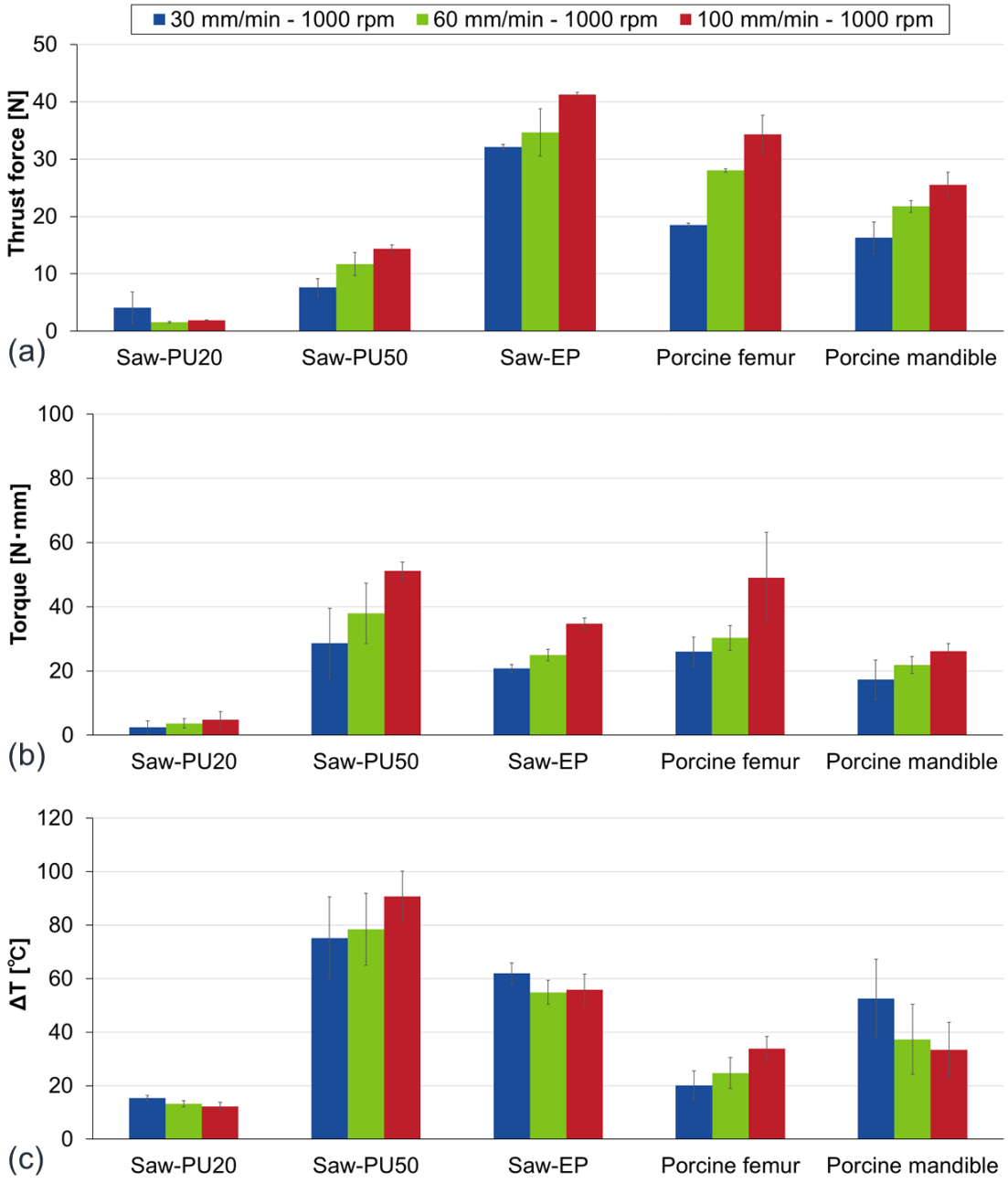

Fig. 2-19 Comparison of (a) Thrust force; (b) Torque; and (c) Temperature elevation (ΔT) as a function of test specimens under machining conditions with various feed rate.

2.5.2. Observation of cutting chips

Cutting chips generated during drilling tests were observed using optical microscope. The morphology of cutting chips was compared among tested specimens. Fig. 2-20 shows the optical images of cutting chips collected after drilling tests performed under the machining conditions of 20-N thrust force and 1,000-rpm rotation speed. Each material shows the specific morphology.

Generally, cutting chips can be classified into four types; flow type, shear type, tear type, and crack type [110,204], where chips in flow type can be also categorized as a continuous chips, and shear type, tear type and crack type roughly as discontinuous (or segmental) chips [205].

Cutting chips from bone specimens are shows in Fig. 2-20(a) and (b). Canine mandible generated discontinuous shear-typed chips, where chips were torn per rotation, while porcine mandible generated continuous flow-typed chips at the beginning of drilling. From the standpoint of the cutting theory, the generation of cutting chips is related to shear strength and fracture toughness of the work materials [205]. As Fig. 2-21 illustrates the relationship between cutting forces, shear force is applied to cutting chips by cutting tools along the rake surface, and fracture toughness is related to the resistant force of the cutting chips against the cutting tools. In order to slide on the rake surface without fracturing, the work material has to show sufficient resistant force, fracture toughness in other words. The difference of chip formation is, therefore, meaning the difference in resistant force of work materials between canine and porcine mandible under the same machining conditions. In order to obtain the similar typed cutting chips, it is possibly necessary for the work materials to have the equivalent mechanical properties that are dominant for chip formation.

Regarding Saw-EP, both continuous and discontinuous chips are obtained. It implies that continuous chips were generated at the beginning of drilling, and then the morphology shifted into discontinuous chips. The morphology transition is considered to happen due to the temperature elevation during drilling. As stated above, the chip formation pertains to fracture toughness of the work material. Since polymeric materials show temperature dependency in their mechanical properties, there is a possibility that Saw-EP showed the relatively ductile behavior at the beginning of drilling at room temperature, but gradually altered to show feeble toughness along the increase in temperature in the work material itself and the drill bit, consequently inducing shear-typed chips.

Apparently, continuous chips are observed in (b), (c), and (d) having the helical geometry, but the detailed geometry such as the whole length, diameter, and pitch of the chips are different respectively. These variances can be an outcome of mechanical properties related to chip formation.

Fig. 2-20(d)~(f) shows the cutting chips from polyurethane foam with different density. When drilling porous material, cutting chips easily get separated to small segments because of the presence of hollow spaces in the work material. The decrease in the size of generated segments are obvious along the decrease in density.

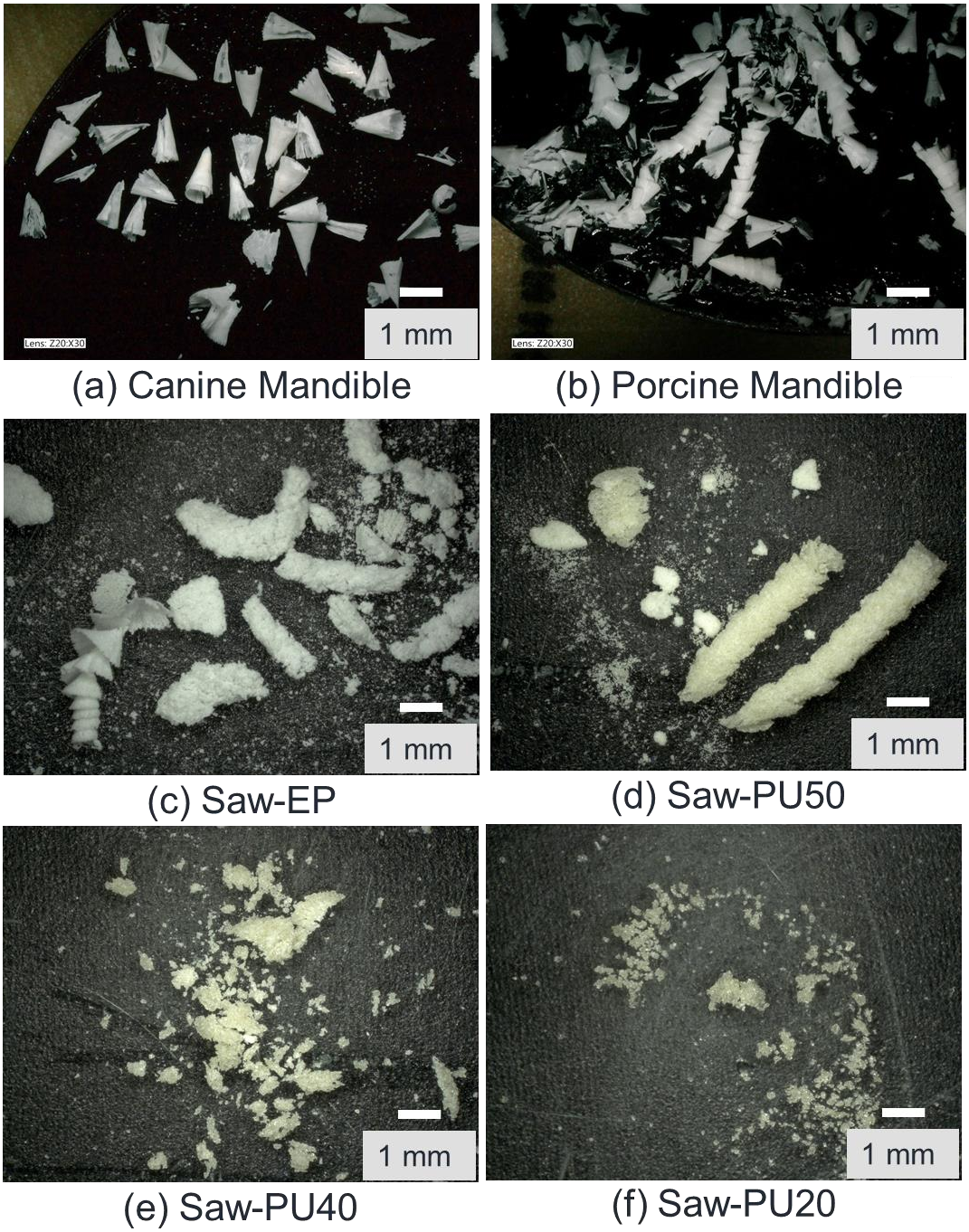

Fig. 2-20 Optical images of cutting chips generated during drilling tests under machining conditions of 20-N thrust force and 1,000-rpm rotation speed.

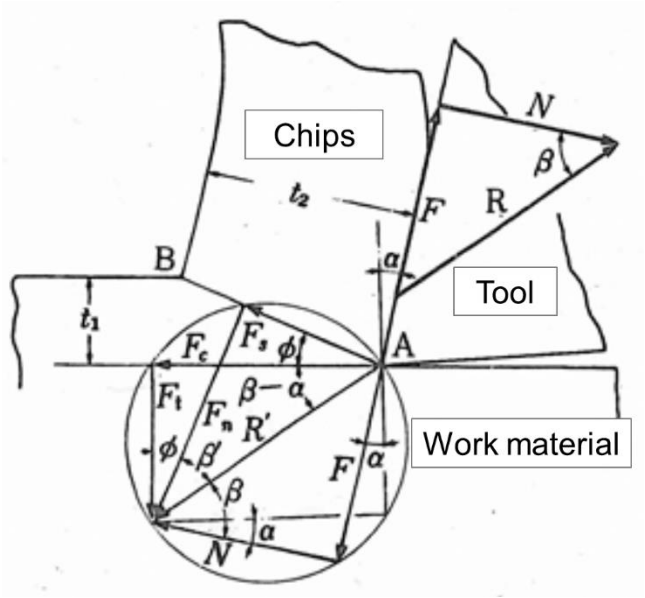

Fig. 2-21 Relationship among cutting forces [205]

2.6. Conclusions

In this chapter, in order to obtain the target drilling properties of natural bone, and also to understand the limitation of conventional bone biomodels, drilling tests were performed under both constant thrust force and feed rate with taking into account the realistic machining conditions applied in surgical operations. Drilling is characterized by properties such as thrust force, torque, drilling time, and temperature elevation during drilling. Cutting chips generated during drilling were also observed. The experiments brought findings as follows.

- The cortical bone biomodel from Sawbones generally exhibits the corresponding drilling properties of mandible bone in terms of torque, drilling time, and temperature rise during drilling under surgical machining conditions except 20-N/700-rpm and 15-N/1,000-rpm thrust force/rotation speed. The surface conditions of cortical bone biomodel can impact drilling under the such feeble machining conditions.
- Under constant feed rate drilling, Saw-EP shows relatively higher thrust force rather than natural bones. The difference in thrust force during drilling may impact tactile feedback.
- Temperature elevation during drilling can induce the embrittlement of generating cutting chips, thus the morphology of cutting chips altering from continuous to discontinuous chips. This effect was observed especially in the Sawbones cortical bone biomodel.

- The variance in drilling properties and morphology of cutting chips was observed among bone specimens. Since bone shows a range of drilling properties, the target properties shall be determined considering the anatomical location, animal species, and mineral contents and so on. There is only one type of conventional cortical bone biomodel, possibly not covering all the conditions of cortical bone. Therefore, improved fabrication method of bone biomodels that can replicate a wide range of drilling characteristics is required.
- From the point of cutting theory, shear strength and fracture toughness are the dominants that can determine chip formation. Toward the replication of drilling in bone, not only the stiffness such as tensile strength and elasticity, but also shear strength and toughness shall be taken into account. These mechanical parameters can be one of the properties to obtain the direction of further development of bone biomodels.

Chapter 3: Characterization of drilling in acrylic resin as a matrix of composite materials

This chapter presents the characterization of drilling in acrylic resin in advance of the fabrication of acrylic composite materials. Since acrylic resin can show unique drilling behavior attributed to its thermoplastic characteristics, drilling properties are discussed considering the morphology of cutting chips, and dynamic mechanical analysis (DMA) measurement results.

3.1. Introduction

In the chapter 2, drilling of bone and Sawbones® test materials was studied. As a result, in order to cover a wide range of drilling properties of natural bone, the methodology that controls material properties related to drilling was considered necessary. To develop this method, this study focuses on the fabrication of composite materials whose drilling properties can be controlled through the modification of mechanical properties based on the material composition. Then, in advance of the fabrication of composite materials, this chapter describes the characterization of drilling in acrylic resin as a matrix of the composite materials. Drilling tests, observation of cutting chips, and dynamic mechanical analysis (DMA) measurements are detailed.

3.2. PMMA as a matrix of composite materials

3.2.1. PMMA

Poly(methyl methacrylate) (PMMA), often called acrylic resin, is one of thermoplastic and non-crystalline polymer materials. Having its transparency and relatively high strength and impact resistance among polymers, a variety of applications of PMMA is known in industry; articles for daily use, walls at aquariums, and cockpit windows of aircrafts.

PMMA is also applied in medical fields especially for the replacement of human hard tissue. As early as 1950s, Sir John Charnley introduced a self-curing PMMA as an anchorage of femoral head prosthesis [206], which was the first example of the application of PMMA in orthopedic surgery. The usage of PMMA as bone cement continues up to the moment for the fixation of artificial joint (Fig. 3-1 (a)), and is also expanded to other specialties such as dentistry for artificial dentures (Fig. 3-1 (b)). In addition, as stated in the chapter 1, PMMA is recently getting attentions for the usage of bone biomodels thanks to their similarity to bone in tactile feedback during drilling [65,109,186].

Fig. 3-1 Usage examples of PMMA in medical fields: (a) bone cement, (b) acrylic dental resin

3.2.2. Fabrication methods

PMMA can be formed by radical polymerization, and consists of repeating unit of $C_5H_8O_2$, as shown in Fig. 3-2. There are several polymerization methods available such as heat polymerization, ultraviolet (UV) photo polymerization, and self-polymerization.

Acrylic resin is often composed of monomer liquid and polymer powder. The main component of the liquid is methyl methacrylate (MMA), while co-polymers of MMA for the powder. The powders are in the shape of small beads fabricated in suspension polymerization (or called pearl polymerization). During each polymerization procedure, MMA starts polymerization stimulated by heat, UV ray, or polymerization initiator respectively. Here, the monomer liquid often includes hydroquinone as polymerization inhibitor for protection, as well as ethylene glycol dimethacrylate as cross-linking agent for prevention of bubbles. The polymer powder may contain benzoyl peroxide as polymerization initiator, often including colorant for the replication of good appearance in artificial dentures.

PMMA was fabricated by self-polymerization, so-called quick polymerization method in this study, because of no requirements of production equipment. The prepared acrylic resin was composed of a co-polymer powder component (Miky blue, Nissin Dental Products Inc.) and a monomer liquid component (Miky liquid, Nissin Dental Products Inc.), where the liquid included benzoyl peroxide as a polymerization initiator. The polymerization reaction began to form solid acrylic blocks after adequate time when the powder and the liquid were mixed.

The entire fabrication procedure of the acrylic specimens is as follows. In advance, the polymer powder and the monomer liquid were weighed in a silicone cup and polypropylene (PP) tube,

respectively, in the amounts required to obtain the desired geometry of the acrylic specimen. Firstly, the polymer powder was added to the monomer liquid in the PP tube, and the mixture of the powder and the liquid was manually stirred with a spatula for 30 seconds. The polymer and the monomer were consistently mixed with a ratio of 1:1 (weight percentage). Secondly, the acrylic mixture was put in a freezer at −20°C for more than 24 hours to complete polymerization. After polymerization, the mixture was taken out of the freezer as a solid block. Finally, specimens were cut into a specific shape for a series of tests, a cubic shape with 20-mm sides for drilling tests, and a rectangular shape with dimensions of 30 × 10 × 3 mm (length × width × thickness) for DMA measurements.

Note that polymerization reaction accompanied the heat generation. In order to inhibit bubble generation inside the acrylic specimens because of the temperature rise during polymerization, the mixture was cooled down throughout the fabrication procedure. Beforehand, the powder and liquid were stored in the freezer, and the mixture in the PP tube after the mixing step was immersed in ice water within the freezer during polymerization.

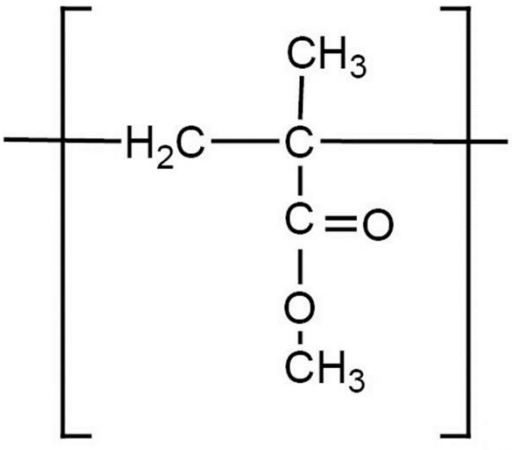

Fig. 3-2 Repeating unit of PMMA

3.3. Experimental methods

3.3.1. Drilling tests

Drilling tests were performed using the same test rig presented in the chapter 2. The same machining conditions for the drilling in bone and Sawbones® test materials were applied as listed in Table 2-2 in the chapter 2. Maximum drilling depth was set at 5 mm, which was almost equivalent to the thickness of human cortical bone. Drilling tests were performed at room temperature without any

presence of liquid. Three drilling holes were created with a new drill bit under each machining condition. Cutting chips were collected and observed using optical microscope. The obtained evolution of torque and displacement were plotted. Thermal images were taken using the infrared camera, and temperature distribution was obtained through the thermal image analysis.

3.3.2. Dynamic Mechanical Analysis (DMA) measurements

Drilling phenomena usually accompany temperature elevation, which can subsequently affect the mechanical properties locally at the drilling site. This thermal effect can be dominant especially in case of drilling in thermoplastic materials. However, it is currently unclear how this temperature increase impacts drilling. Therefore, DMA measurements were performed to take into account the effects of temperature elevation during drilling.

The dynamic viscoelastic behavior of the acrylic resin was measured using a 50-N 0.1-dB Metravib testing machine. Knowing the sample geometry, a complex tensile modulus (E*) was obtained based on the equation $E^* = E' + iE''$, where E' is the storage modulus and E'' the loss modulus. The loss factor (tan δ) is the ratio of the loss modulus to storage modulus, as described by $\tan \delta = E''/E'$. A dynamic periodic sinusoidal strain was applied to the specimens within a temperature range of 25℃-200℃ at a heating rate of 1 ℃/min. The changes in the storage modulus (E') and loss factor were plotted under a tension/compression loading cycle with a measurement frequency of 1 Hz.

Acrylic resin was polymerized and processed in accordance with the fabrication methods described at the section 3.2.2. Both short sides of the specimens were firmly clamped at the jig on the testing machine.

3.4. Results and Discussion

3.4.1. Characterization of cutting chips

Fig. 3-3(a) presents a global image of the cutting chips obtained throughout the entire drilling process. As exhibited in Fig. 3-3(b)–(d), the morphological characteristics of the chips can be classified into three sections: cylindrical helix, waved, and rounded nubby chips, respectively. The drilling behavior of acrylic resin can, therefore, be divided into three phases according to the classification of

chip generation. Although there is a difference in distance between borders, three-phase morphological transitions were consistently observed for other cutting chips obtained from a series of drilling tests.

Fig. 3-3(b) pictures the tips of cutting chips generated in the first phase of drilling, where cylindrical helix chips, defined in [204], are formed. The figure indicates that drilling was performed with an efficient clearance of cutting chips under industrially favorable machining conditions. There is an increase in the diameter of chips' tips, and then a constant diameter and length between pitches can be observed. The border between the first phase and the second phase roughly corresponds to drilling until N_{rot} equals about 33 rotations of the drill-bit. Assuming that one rotation on the chips corresponds to one rotation of the drill-bit, the cutting chips observed during the first phase are likely generated up until 2 seconds, as calculated based on the spindle speed (16.7 rev/s).

In the second phase, continuously waved chips with irregular length between pitches were formed, as can be observed in Fig. 3-3(c). This phenomenon can be caused by defective chip evacuation. As the drill bit progresses, the constraint force of the drilled walls becomes increasingly dominant, which means that the deeper the drill-bit progresses, the more force is required to evacuate the chips. Since the thrust force of the drilling system was kept constant, it is possible that the evacuation stagnated causing the chips to be folded in layers, which make them appear waved.

Subsequently in the third phase, the chips' shape assumes a rounded and nubby form, as observed using the optical microscope seen in Fig. 3-3(d). The rounded nubby characteristics of the chips likely result from thermal deformation due to melting of the acrylic resin. It is possible that the waved chips formed in the second phase receive compressive force from subsequently emerging chips, which apply vertical force and increase the contact area to the surrounding surfaces of both the drill bit and the drilled wall of the acrylic specimen. During the tests, when the chips receive locally high pressure and are continuously exposed to severe friction at the spindle speed of 1,000 rpm, there is a chance that the temperature around the chips rises drastically due to friction heat, exceeding the glass transition temperature (T_g) of acrylic resin, which is reported between 85 and 165°C according to existing literature [207].

The border between the second and third phase cannot be fixed simply by assessing the number of rotations because of the inconsistency of one rotation between a drill-bit and the chips caused by the defective evacuation. However, it is assumed that temperature rise during drilling is associated with the morphological transition of the chips from the second phase to the third phase. Furthermore,

since the viscoelastic properties of acrylic resin are dependent on temperature, the change of mechanical properties can also influence the evolution of drilling properties.

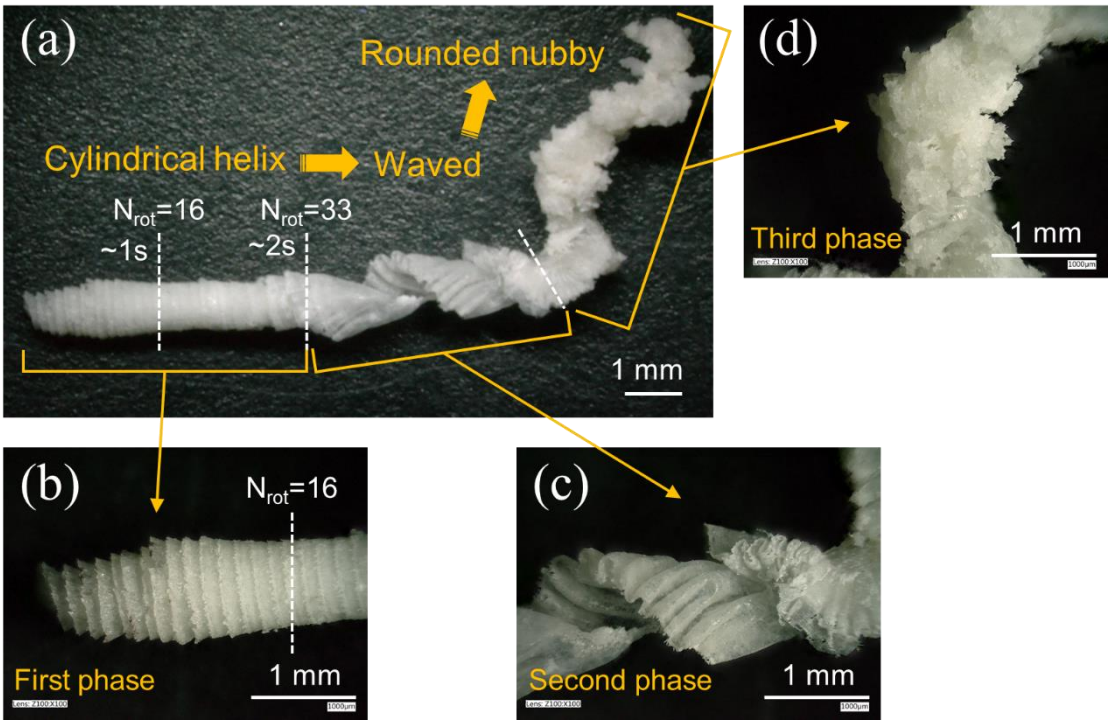

Fig. 3-3 Cutting chips obtained from the drilling tests under machining conditions of 1,000-rpm spindle speed and 20-N thrust force. (a) The entire appearance, (b) the tip of the cylindrical helix chips generated through the first phase, (c) a part of the waved chips generated in the second phase, and (d) a part of the rounded nubby chips generated in the third phase.

3.4.2. Drilling properties related to chip formation

Fig. 3-4 demonstrates the representative evolution of drilling properties (torque, displacement, and ΔT) in the acrylic specimen under machining conditions of 1,000-rpm spindle speed and 20-N thrust force. According to the cutting chip classification, drilling in the first phase occurs up until 2 seconds. The first phase can be further divided into three zones considering the evolution of torque, denoted as zone I, II, and III. Zone I indicates the beginning of penetration, with a sharp increase in drilling displacement, as the drill-bit cuts into the surface of the specimen with its the chisel edge. Zone II includes the continuous penetration of the drill-bit, where initial material removal is observed. A gradual rise in torque and displacement occurs, as well as a sharp increase in ΔT. The slow evolution of torque correlates with the chisel edge expanding in the cutting area. Zone III consists of steady

material removal by the fully engaged drill bit and smooth evacuation of cutting chips, which is also indicated by the torque saturation value of about 20 N・mm. ΔT gradually increases up to about 75℃ throughout the penetration. The increase in ΔT is likely correlated with the friction heat generated by the chips traveling through the flutes of the drill-bit. The deeper the drill bit penetrates, the longer the chips are exposed to friction between the drill-bit and the borehole wall, causing the maximum temperature to increase over time.

Drilling in the second and third phases respectively correspond to the early and late stages of zone IV, which occurs during drilling from 2 seconds to the end of about 3 seconds. In zone IV, a sharp increase in torque occurs, reaching the maximum value, followed by a slight decline. The maximum value of ΔT is almost 125℃, after torque peaks. The transition of the cutting chip shapes, as described in the section 3.4.1, manifests in zone IV, but the precise time of this transition is unclear because temperature measurements using the infrared camera cannot observe the interior of the borehole. Zone V compasses the end of drilling after the drill-bit reaches maximum displacement at 5 mm, where no more material is removed but the spindle still rotates. Since there is neither more plastic deformation due to material removal nor emerging chips traveling through the drill flutes, torque and ΔT gradually decrease with time. It is important to note that the penetration rate is constant from zone II to IV (linear evolution of displacement with time).

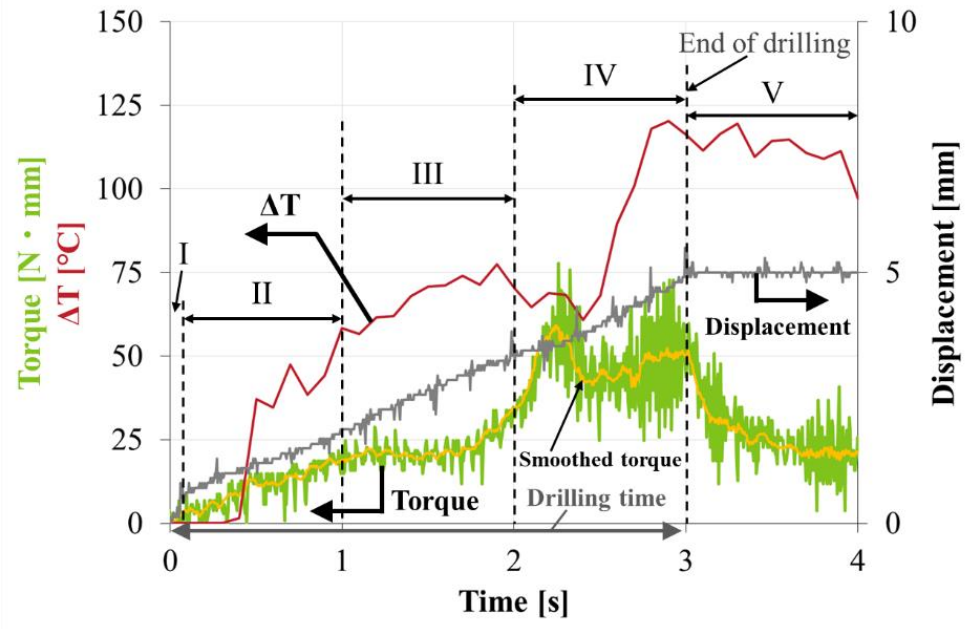

Fig. 3-4 Typical evolution of drilling properties for an acrylic specimen. Torque, ΔT, and displacement are plotted over time. Machining conditions are 1,000 rpm for spindle speed and 20 N for thrust force.

3.4.3. Effects of machining conditions on drilling properties

Fig. 3-5 presents the drilling properties under various machining conditions for an acrylic specimen, plotted with the average values of maximum torque, maximum ΔT, and drilling time. Particularly, Fig. 3-5(a) exhibits the effects of thrust force, and Fig. 3-5(b) indicates the effects of rotation speed. It can be observed that thrust force impacts maximum torque but not maximum temperature. The drilling time it takes to reach a depth of 5 mm decreases as thrust force increases from 15 N to 25 N. This result can be explained considering that the drill-bit removes a larger amount of material per revolution under larger thrust force. Consequently, as more material is removed and displaced, the maximum torque and thrust force both increase.

As shown in Fig. 3-5(b), in the case of various spindle speeds, maximum torque and drilling time decrease while maximum temperature slightly increases. Fig. 3-6 displays the number of rotations required for drilling of 5 mm under constant thrust force with different spindle speeds. As can be observed, the total number of rotations required for drilling increases as a function of rotation speed, which means that less material is removed per revolution as rotation speed increases. This phenomenon can be explained possibly by the viscous component of acrylic resin, which could enable a shorter length of penetration in a shorter time. The decrease in drilling time along with the increase in spindle speed can be explained by how the amount of material removed per unit of time increases even if less material is removed per revolution. As for the maximum torque, it is mathematically reasonable that torque decreases as distance per unit of time increases assuming the rotational force of the spindle is constant. The present results corroborate those obtained by Kobayashi about the relationship between torque and rotation speed in polyethylene [113]. For maximum temperature, one can assume that the increase in temperature is related to friction behavior intensifying on the cutting chips in the contact area between the drilled wall and the drill bit as spindle speed increases from 500 rpm to 1,500 rpm.

In the machining industry, the effect of spring back is known to take place during/after drilling. This phenomenon means that the borehole walls shrink slightly after the drill bit is removed from the material. Spring back behavior is dependent on time, and thus on the viscous component of work pieces. With increased spindle speed, drilling can be performed faster and therefore the drill bit receives less resistance from the borehole wall due to the spring back effect before reaching maximum displacement. This mechanical response can also result in a difference between the maximum values of torque.

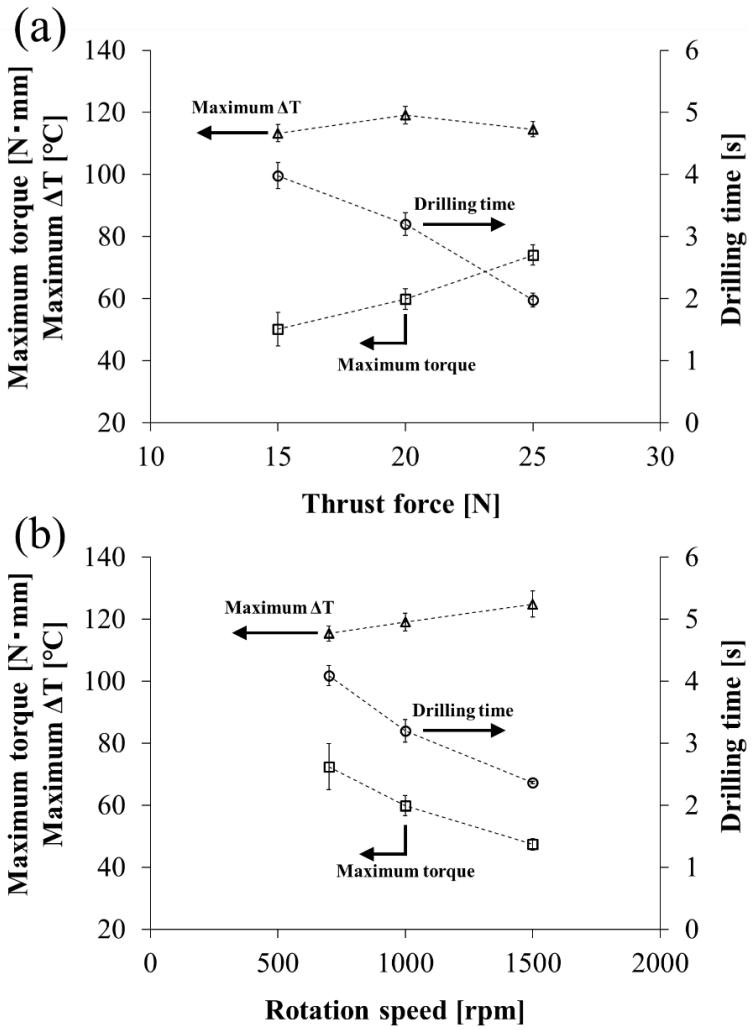

Fig. 3-5 Effects of machining conditions on drilling properties in an acrylic specimen**.** (a) the effect of thrust force, (b) the effect of rotation speed.

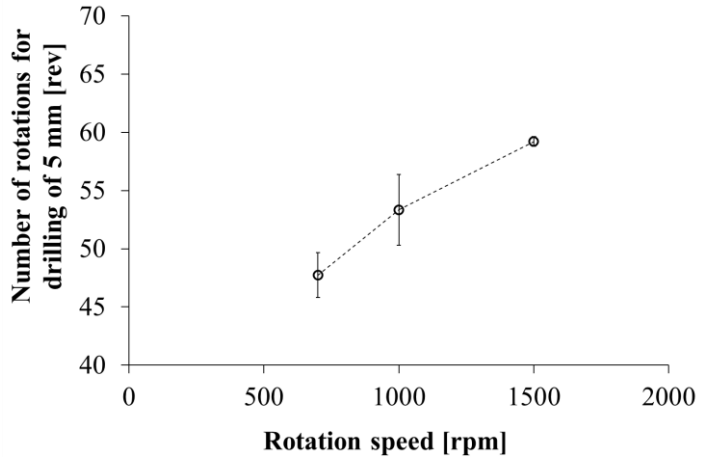

Fig. 3-6 The number of rotations for drilling tests under various rotation speeds.

3.4.4. Thermal effects on mechanical properties and drilling

Fig. 3-7 displays a plot of the storage modulus and tan δ of an acrylic specimen as a function of temperature at 1 Hz. The storage modulus decreases significantly as temperature rises, with only about one hundredth its value at 25℃ maintained at 100℃. Two peaks in tan δ can be observed: a low-temperature peak around 50℃ associated with β-relaxation and a high-temperature peak after reaching around 100℃ associated with α-relaxation. The β-relaxation of acrylic resin has been previously reported to result from the molecular rotation of the–$COOCH_3$ group connected to the main chain [208,209], while α-relaxation is caused by main chain motions [210]. The glass transition temperature (T_g) is known to be related to α-relaxation. The main chains between units of PMMA are delinked at T_g, and then the specimen softens and exhibits fluid characteristics. Above T_g, there is a chance that an acrylic specimen melts.

During drilling in the first phase, absolute temperature stays under 100℃ and morphological characteristics of melting cannot be observed. Melting of acrylic resin was first observed in the rounded nubby cutting chips, as depicted in Fig. 3-3(d), which are formed in the late phase of zone IV. This result indicates that cutting chips stagnated in the early phase of zone IV and were eventually exposed to temperatures above T_g, at which point the chips started melting and viscoelasticity decreased drastically. Based on this mechanism, the morphological transition of the chips at zone IV can be explained. A decrease of torque at zone IV in Fig. 3-4 is also considered to be affected by the temperature increase. As reported by Wiggins [167], there is a chance of a sudden increase in torque when drill flutes become clogged with cutting chips. In the case of drilling in acrylic resin especially, torque increases due to clogging, and then decreases slightly after the peak because of the decrease in viscoelasticity in the specimen, which in turn reduces the resistance force required for material removal by the chisel edge.

Considering the penetration rate of the drill-bit until a 5-mm depth is reached, the feed rate remains constant after the sharp increase at the zone I. This result implies that the decrease of viscoelasticity does not occur at the drilling site since the temperature may not reach a high enough value to facilitate the penetration process. Schmidt *et al.* reported that the majority of heat source generated in drilling process were transferred to cutting chips [160]. Therefore, temperature rise on the bottom surface where a new surface for material removal is created would be small, and then the effects on penetration behavior can be mitigated.

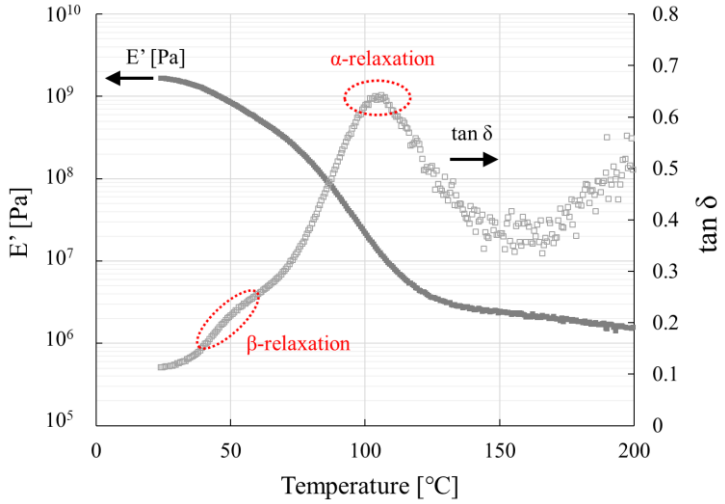

Fig. 3-7 Evolution of E' and tan δ as a function of temperature for an acrylic specimen.

3.5. Conclusions

In this chapter, drilling of acrylic resin was characterized with providing machining information about cutting chips and drilling properties (torque, displacement, and temperature rise) when drilling acrylic resin. The morphological characteristics of cutting chips and the evolution of drilling properties were analyzed considering the effects of temperature rise during drilling. The following conclusions can be drawn.

The drilling of acrylic resin can be classified into three phases based on the morphological characteristics of the cutting chips. In the first phase, cylindrical helix chips appear to be generated with smooth evacuation of the chips, which are not apparently affected by temperature rise. When cutting chips start to stagnate as a sign of defective evacuation, the second phase occurs, and waved chips are generated, which cause a drastic increase in torque. When the temperature of the chips reaches the glass transition temperature of about 100°C due to friction heat, the morphological characteristics shift to the third phase where melting is observed. At the transition border between phase two and three, there is a slight decrease in torque associated with the decrease in viscoelasticity of the acrylic resin.

Although the effects of mechanical changes due to temperature rise in acrylic resin on drilling behavior were observed while drilling, the temperature reached during drilling can vary depending on machining conditions, and possibly material composition when including additives. Therefore, it is necessary to consider the thermoplastic characteristics of acrylic resin as well as the machining environment toward developing bone biomodels made of acrylic resin.

Chapter 4: Fabrication of acrylic composite materials and their drilling properties

This chapter presents the development of acrylic composite materials especially including ceramic additives, followed by the drilling test results under constant feed rate and constant thrust force. Then, focusing on alumina cement as additive, the effects of additive amount on drilling properties are studied. The drilling properties of acrylic composite materials are also compared with those of bone and Sawbones® test materials.

4.1. Introduction

Bone biomodels are often made of polymeric and/or ceramic materials. Although acrylic composite materials have recently caught attentions for the usage of bone biomodels due to the possibility that those biomodels can reproduce the equivalent tactile feedback of bone during drilling [65,109,211], literatures on quantitative information of drilling in acrylic composite materials have not yet been available. Then, this study aims to provide the drilling characteristics of acrylic composite materials including ceramic additives. After studying the drilling of acrylic resin as the matrix in the chapter 3, ceramic additives were mixed to acrylic resin for fabrication of composite materials. In order to determine the effects of additives on drilling characteristics, drilling tests were carried out.

This chapter describes the ceramic additives used for the fabrication, and fabrication methods of composite materials, and subsequently performed drilling tests. Drilling tests included both constant load and constant feed rate drilling. After reviewing the effects of each ceramic material, the effect of additive amount was studied to control drilling characteristics of the composites.

4.2. Materials

4.2.1. Ceramic additives

Acrylic composite materials hold a potential to reproduce drilling haptics of bone. According to the patents for bone models for surgical training [186,211], the usage of ceramic powders are proposed as effective additives such as alumina (Al_2O_3), silicon dioxide (SiO_2), zirconia (ZrO_2), silicon carbide (SiC), titanium carbide (TiC), and hydroxyapatite (HAP), where hydroxyapatite is referred as the most preferable additive due to its presence in human bone. Another patent can be found for bone model, as Ohta *et al.* proposed the usage of wood flour as additive to acrylic resin [109]. However, Muramoto *et al.* found that the usage of organic powders such as wood flour, cellulose fibers, and cellulose nano-fibers into acrylic resin did not alter torque and drilling time under constant load drilling and concluded that other additives such as ceramic powders can be effective to control drilling properties [212]. Then, this study consequently adopted the usage of ceramic additives into acrylic resin.

Fig. 4-1(a)~(f) show the appearance of ceramic materials used for fabrication of composite materials at macro and micro scale. Six types of additives including alumina cement, silicon dioxide,

zirconia, hydroxyapatite, silicon carbide, and titanium carbide were selected among the ceramic materials presented in the patent [186].

(a) Alumina cement

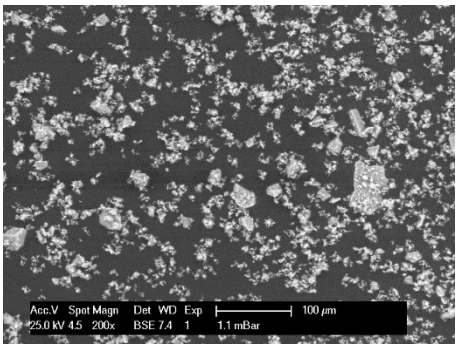

(b) Silicon dioxide

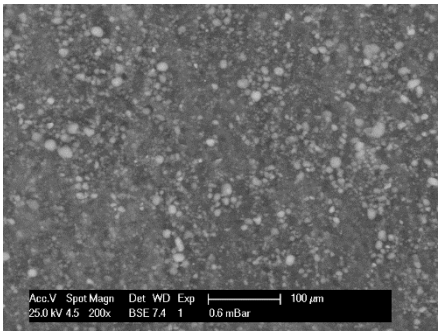

(c) Zirconia

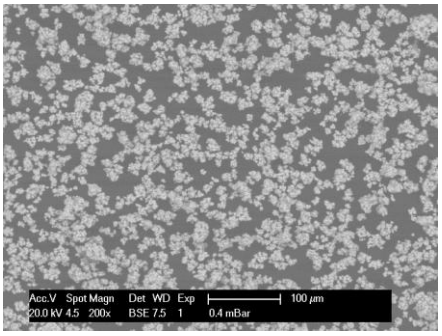

(d) Hydroxyapatite

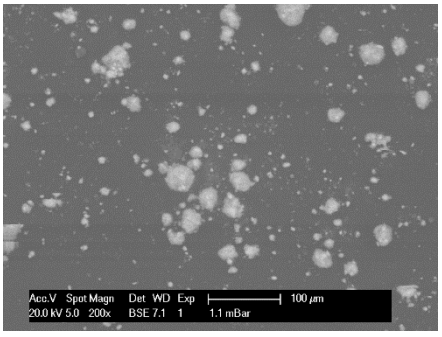

(e) silicon carbide

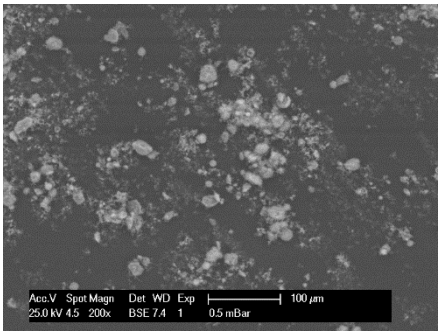

(f) titanium carbide

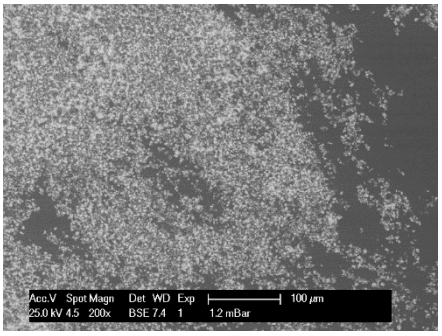

Fig. 4-1 Appearance of ceramic materials used for composite materials.

4.2.2. Fabrication of composite materials

Acrylic composite materials were produced using acrylic resin as a matrix and ceramic powders as additives (**Fig. 4-2**). Acrylic sample was fabricated by quick polymerization method when mixing polymer powder (Miky blue, Nissin Dental Products Inc.) and monomer liquid (Miky liquid, Nissin Dental Products Inc.) as presented in the chapter 3.

Ceramic additives were put together during the mixing process of polymer and monomer, in order to develop acrylic composite materials. The mixing ratio of the polymer and the monomer was constant at 1:1 of weight percentage in this study. **Table 4-1** shows a list of ceramic additives used for fabrication of composite materials, including the name of additive, major component, combination ratio against pure acrylic resin calculated from (additive)/(total weight), and its notation of composite materials. Combination ratio of SiO_2 was 5 wt% because of its water absorbability, while 20 wt% for other additives.

Acrylic composite materials as well as pure PMMA were fabricated along the following steps as depicted in **Fig. 4-3**. At first, polymer powder, monomer liquid, and each additive were weighed respectively at the required amounts. Then, the monomer liquid and the additive were manually mixed in a polypropylene tube, followed by the polymer powder. The mixture was mixed and kept in a freezer at -20°C. Both the polymer powder and the monomer liquid were kept beforehand in the freezer, and

mixing process took place immediately, in order to avoid an occurrence of bubbles inside the specimens as a result of prevention of rapid increase in temperature by delaying the polymerization reaction. In the completion of polymerization after more than 24 hours, the mixture was taken out of the container as a solid block. Acrylic blocks were then processed to have a flat surface ready for drilling tests.

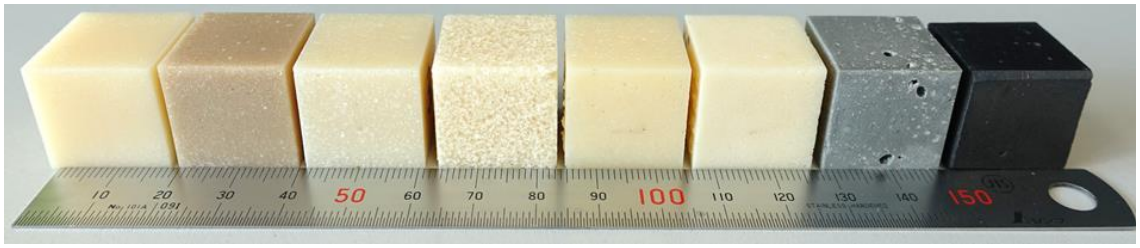

Fig. 4-2 Examples of acrylic composite materials fabricated in this study

Table 4-1 List of ceramic additives used for composite materials

Base material : Acrylic resin (PMMA)			
Name of additive	Major component	Combination ratio (Additive)/(Total weight)	Notation
Alumina cement	Al_2O_3 (54.8%) CaO (36.0%)	20 wt%	AC
Silicon dioxide	SiO_2	5 wt%	SiO2
Zirconia	ZrO_2	20 wt%	ZrO2
Silicon carbide	SiC	20 wt%	SiC
Titanium carbide	TiC	20 wt%	TiC
Hydroxyapatite	$Ca_{10}(PO_4)_6(OH)_2$	20 wt%	HAP

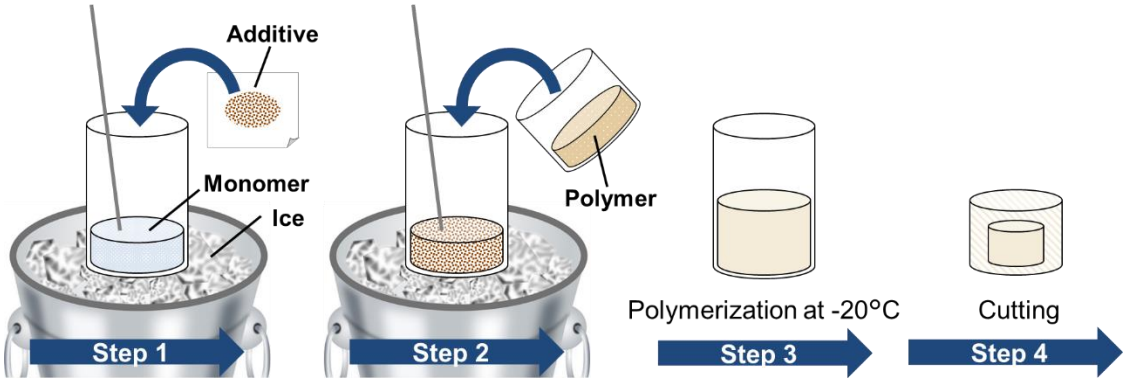

Fig. 4-3 Schematic images of fabrication procedure of acrylic composite materials

4.3. Experimental methods

4.3.1. Drilling under constant thrust force

Drilling tests under constant thrust force were performed using a drilling test rig presented at the section 2.3.1 in the chapter 2. The machining conditions listed in the table 2-2 was applied. Drilling properties of bone, Sawbones test materials, and acrylic resin were also plotted to review the obtained results. For each material, the drilling feed rate was calculated from the drilling time. Knowing the individual difference of the thickness, the average drilling feed rate was calculated by measuring the required time to drill until 3-mm thickness for bone specimens.

4.3.2. Drilling under constant feed rate

Drilling tests under constant feed rate were performed using a CNC tapping center (Tapping center BROHTER TC-22A, Brother Industries, Ltd.) as presented at the section 2.3.1 in the chapter 2. Thrust force and torque were recorded with a sampling rate of 1000 Hz. Machining conditions listed at the table 2-3 was applied for the drilling tests. All the test materials were presented for the comparison of drilling properties such as thrust force, torque , and temperature elevation.

4.4. Results and discussion

4.4.1. The effects of additives under constant load drilling

Fig. 4-4 shows the results of maximum torque as a function of drilling time for tested specimens. It is observed that maximum torque and drilling time can be altered respectively with the inclusion of additives in acrylic resin. SiC, TiC, and AC result in lower values of maximum torque and longer drilling time meaning that penetration of the drill bit progresses slower than in PMMA, while SiO2 scores higher values of torque and shorter drilling time meaning faster penetration. Natural bones and Saw-EP exhibit the equivalent values for maximum torque and drilling time. Since torque indicates the cutting force consumed for material removal, the close value in maximum torque implies the cutting force required for material removal by the chisel edge of the drill bit can be equivalent. Therefore, in order to develop a material that can reproduce the drilling characteristics of cortical bone, it is necessary for the materials to have the similar value in torque and drilling time. **Fig. 4-5** shows

the relationship between maximum torque and drilling feed rate. The feed rate was calculated from drilling time in order to normalize the effect of drilling thickness considering bone specimens. Similarly, it can be confirmed the effect of ceramic additives to control the drilling feed rate of PMMA closer to that of bone. As the inclusion of certain types of ceramic additives can lead the drilling characteristics closer to that of cortical bone, the effects of additive amounts were subsequently studied focusing on alumina cement.

Fig. 4-6 summarizes the results of drilling in AC10 to AC40 in addition to controls. As shown, the drilling time for the composite materials tend to slightly increase with additive amount. The effect becomes larger along the increase in additive amount up to 40 wt%. The higher the additive amount is, the less the materials are removed by the chisel edge to result in lower maximum torque and drilling time. When converting drilling time into drilling feed rate, the trend is also obvious as shown in **Fig. 4-7**. This trend shall be brought by the alternation of mechanical properties due to the presence of alumina cement. It is likely that ceramic additives such as alumina cement can increase the stiffness or other mechanical properties of the matrix related to drilling characteristics and the effects of alternation can increase with the elevation of additive amount.

Furthermore, in terms of maximum torque and drilling feed rate, the drilling characteristics in AC40 can be similar to that of cortical bones. Having the equivalent drilling feed rate, the amount of material removal per rotation can be regarded as equal. Besides, the similar value of torque indicates the equivalent cutting force are required for the material removal regardless of material type. It can be thus possible that the inclusion of ceramic additives such as alumina cement into acrylic resin, for example, makes the drilling characteristics of a matrix controlled depending on its additive amount, as similar as the result of canine or porcine mandible bone in terms of torque and drilling feed rate. For the imitation of drilling characteristics, mechanical properties related to the material removal around the tip of drill bit should be dominant. Focusing on the stiffness, mechanical properties such as hardness or elastic modulus is analyzed in the next chapter.

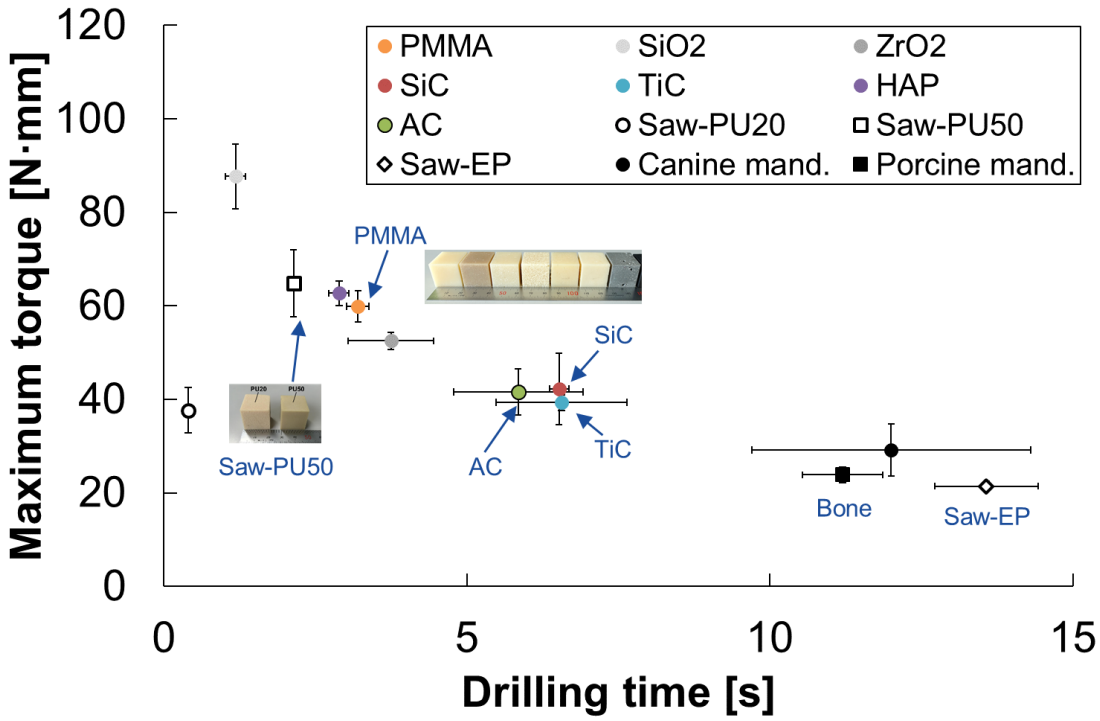

Fig. 4-4 Maximum torque as a function of drilling time: comparison of work materials

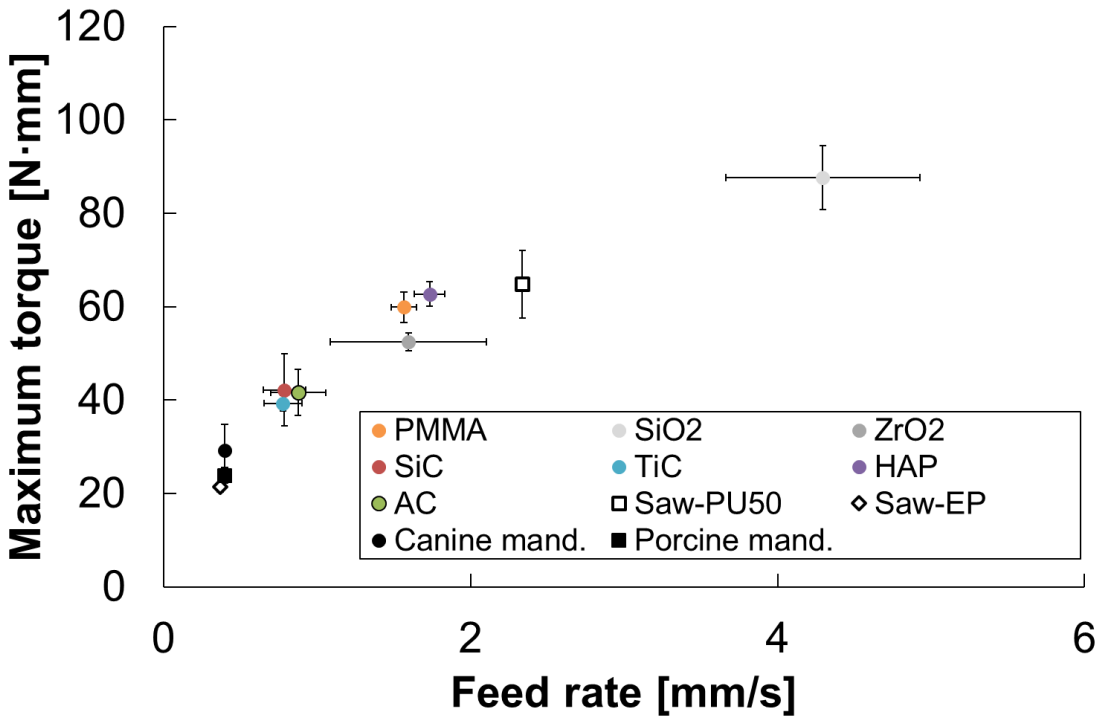

Fig. 4-5 Maximum torque as a function of drilling feed rate: comparison of work materials

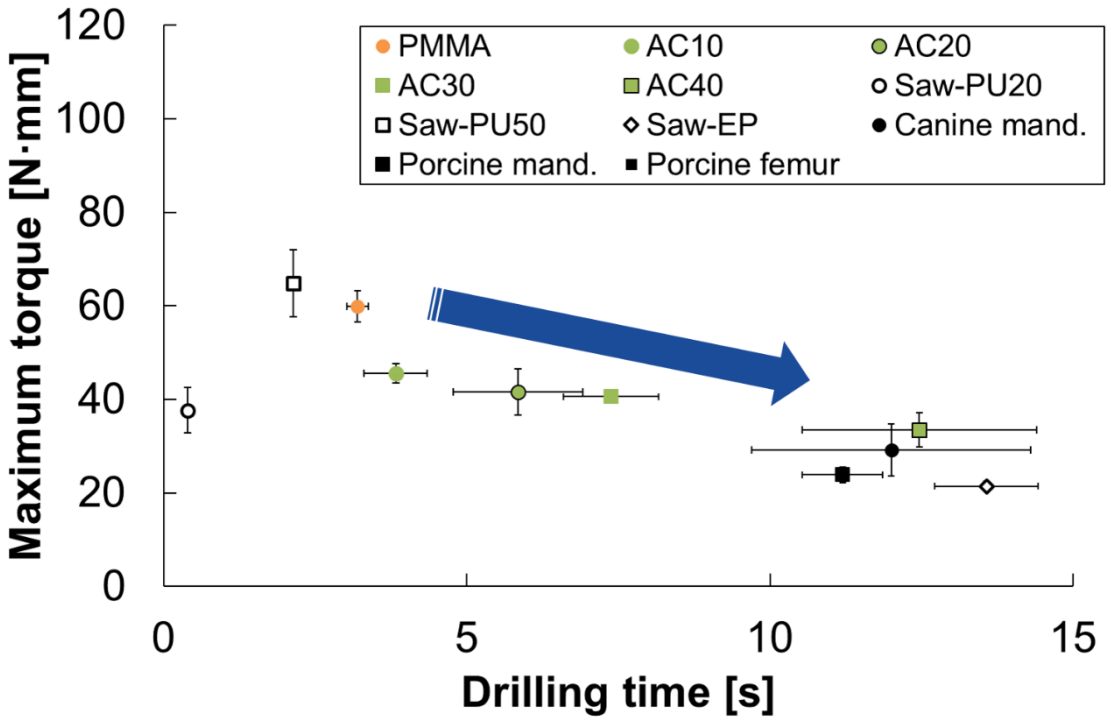

Fig. 4-6 Maximum torque as a function of drilling time: the effect of additive amount

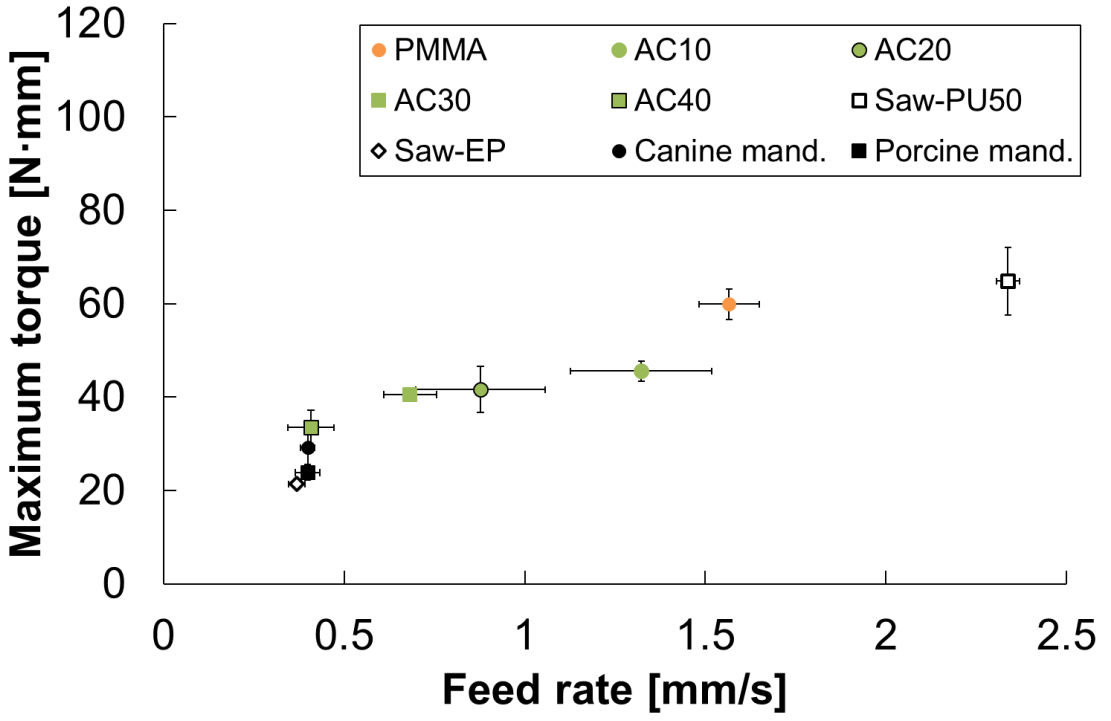

Fig. 4-7 Maximum torque as a function of drilling feed rate: the effect of additive amount

4.4.2. The effects of additives under constant feed rate drilling

Fig. 4-8 shows typical evolution of drilling properties such as thrust force, torque, and ΔT during drilling under the machining conditions of 1,000-rpm rotation speed and 0.060-mm/rev feed rate for all the materials. Drilling properties are obtained as a function of displacement of the drill bit. Moving filter is applied to smooth the profile of thrust force and torque. According to the Fig. 4-8, thrust force globally increases at the beginning of the penetration and then stays around the maximum values, while torque and temperature are gradually increasing until the end of penetration at the 5-mm depth where the extraction of the drill bit occurs. Temperature elevation is in response to the increase of torque as stated in previous works [53]

Fig. 4-9 shows a comparison of evolution of thrust force until 3-mm depth. When taking into account the results of acrylic specimens such as PMMA, AC20, and AC40, the three materials show thrust force between Saw-EP and Saw-PU covering the results of bone. These results imply that the drilling haptics until 3-mm depth can be similar between acrylic specimens and bone.

When focusing on the evolution of thrust force for Saw-EP, PMMA, AC20, and AC40, each curve shows a peak at the depth of around 1.6 mm and then thrust force gradually decreases. This trend is considered to pertain to thermal effect during drilling since polymeric materials such as epoxy and acrylic resin show feeble atomic forces between atoms along the increase of temperature. Although thermal images show low temperature at the depth of 1.6 mm, in fact, there is a temperature gap between on the surface where infrared camera can measure the temperature and on the drill tip inside the drilled hole. Even though the recorded temperature is still lower than the range of glass transition temperature especially for PMMA where thrust force starts to decrease, the effect of temperature on thrust force should not be ignored as concluded at the chapter 3.

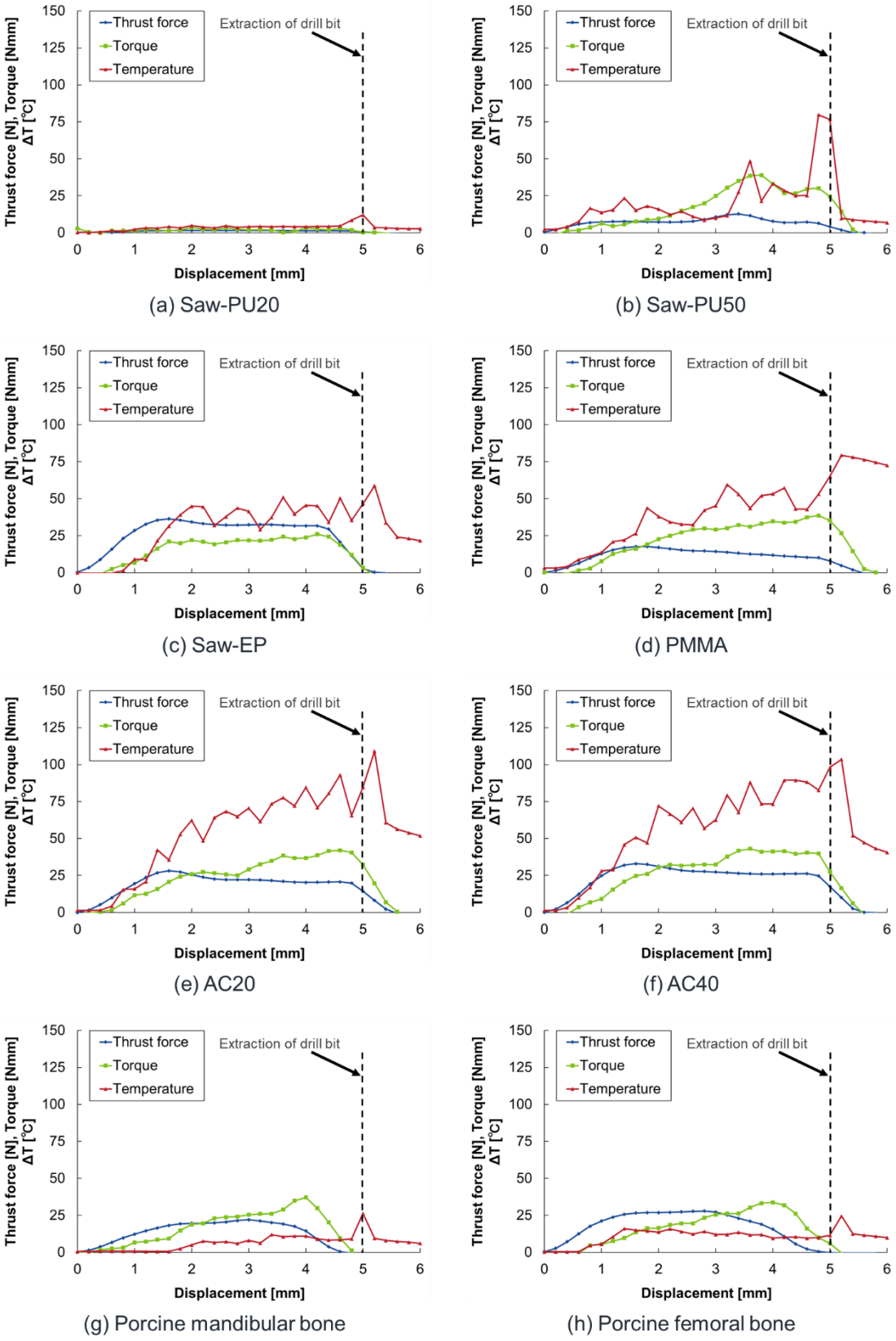

Fig. 4-8 Typical evolution of drilling properties under constant feed rate drilling for all materials

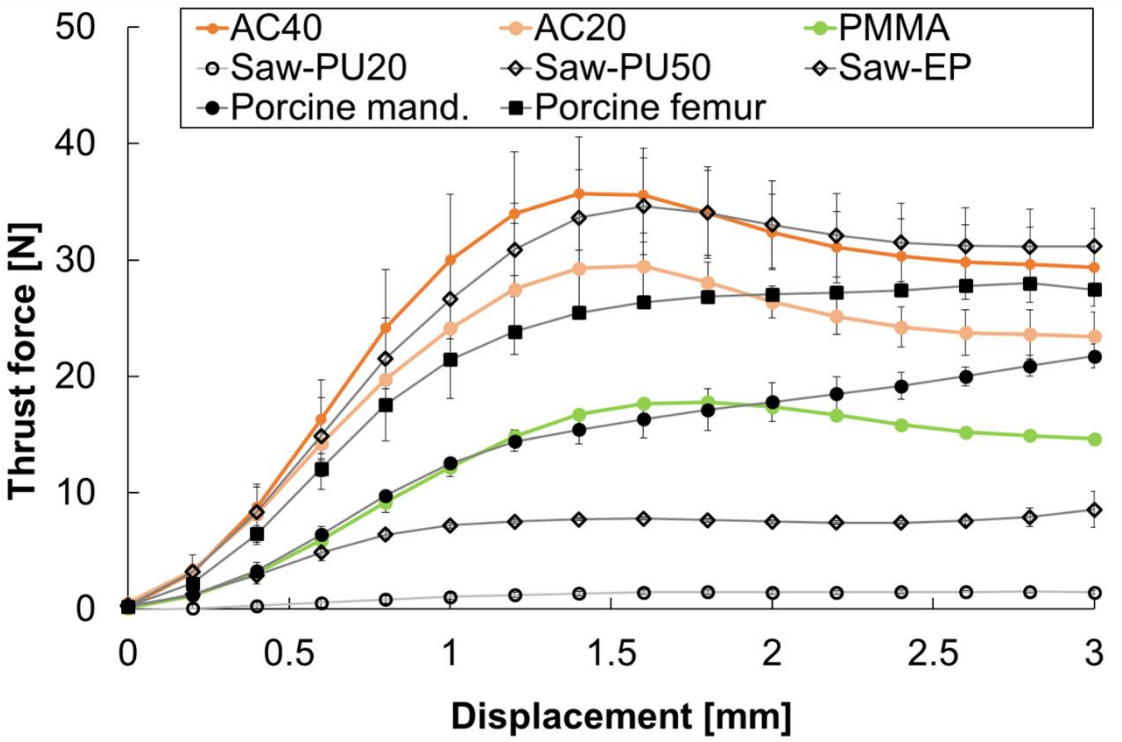

Fig. 4-9 Comparison of the evolution of thrust force

4.5. Conclusions

In this chapter, acrylic composite materials were successfully fabricated using acrylic resin as a matrix and ceramic materials as additives. The fabricated composite materials were studied focusing on their drilling properties under constant load and feed rate drilling. The effects of ceramic additives on drilling properties were quantitatively analyzed under both drilling conditions.

The drilling test results revealed that the inclusion of ceramic additives are effective to control drilling properties presented by thrust force, torque, and drilling feed rate. Focusing on the effects of additive amount especially for alumina cement, each drilling property alters gradually in response to the additive amount; the drilling feed rate becomes lower under constant load drilling, while the thrust force becomes larger under constant feed rate drilling along the increase in included amount of alumina cement in acrylic resin. Furthermore, acrylic composite material including 40 wt% of alumina cement shows the comparable torque and feed rate under machining conditions applied in this study. It implies that drilling characteristics of certain locations and species of natural bone can be reproducible by optimizing the suitable material composition.

The similarity in drilling properties as presented in the drilling feed rate or thrust force can be

attributed to the similarity in mechanical properties related to drilling. In order to elucidate the relationship between drilling properties and mechanical properties, sorts of mechanical tests are carried out in the next chapter.

Chapter 5: Relationship between drilling and mechanical properties

This chapter presents the mechanical test results including bending tests, Microindentation tests, DMA measurements, and fracture toughness tests, considering the mechanical properties related to drilling properties. Acrylic composite materials including acrylic resin are used as specimens to see the effects of additive on change of mechanical properties. Relationship between drilling and mechanical properties are discussed by combining the test results.

5.1. Introduction

The inclusion of ceramic additives in acrylic resin can alter the drilling properties measured in thrust force, torque, and drilling feed rate. These changes should be related to the mechanical properties dominant on drilling characteristics, but mechanical properties related to the modification of drilling properties have not yet been clear. In this chapter, mechanical tests using the pure acrylic resin and acrylic composite materials are performed to see the effects of additives on mechanical properties. Considering mechanical properties that can influence drilling behavior after the beginning of material removal, mechanical tests such as bending tests, fracture toughness tests, microindentation tests, and DMA tests were performed to determine each mechanical property.

5.2. Materials and methods

5.2.1. Specimens

Three categories of materials were prepared for a series of mechanical tests. The first category was composed of acrylic specimens; pure acrylic resin (PMMA), acrylic composite materials including 10 to 40 wt% of alumina cement (notated AC10 for 10 wt% of additives, AC20 for 20 wt%, AC30 for 30 wt%, and AC40 for 40 wt%). The second category consisted of Sawbones® test materials; Saw-EP, Saw-PU20, and Saw-PU50 as defined at the chapter 2. The last category was bone samples; porcine mandibular bone and porcine femoral bone. Each material was processed to the desired geometry depending on mechanical testing.

5.2.2. Bending tests

The three-point bending tests were conducted using a universal testing machine (EZ-S, Shimadzu Corp., Japan), to obtain the flexural strength and modulus of acrylic-based specimens. Assuming the samples are homogeneous, the obtained strength and modulus can be equal to tensile strength and elastic modulus. Five types of only acrylic specimens including PMMA, AC10, AC20, AC30, and AC40 were produced with a geometry of 50 × 10 × 3 mm (length × width × thickness). Five samples in the identical geometry were prepared for each composition.

Bending tests were conducted under the following conditions; 40 mm for the support span, and the loading rate of 1 mm/min. The flexural strength and modulus were calculated from the obtained stress-strain curves.

5.2.3. Fracture toughness tests

Material removal during drilling can be related to fracture behavior of work piece. Since the penetration of drill bit along the evacuation of cutting chips can be affected by fracture behavior of work materials, the fracture toughness is considered to have impact drilling properties. Recently, Feldmann *et al.* adopted a new methodology for calculation of fracture toughness and related with machining of natural bone [179]. Cortical bone shows a quasi-brittle and not ductile behavior compared to metals. Besides, the anisotropy due to osteons provides a high fracture toughness to inhibit the crack growth, possibly resulting in larger cutting forces rather than polymeric materials.

Fracture toughness tests were carried out by applying linear-elastic fracture mechanics fracture toughness (K_{IC}) method referring to ASTM test standards [213,214]. Similarly to bending tests, five types of acrylic-based specimens including PMMA, AC10, AC20, AC30, and AC40 were prepared. Single edge (SE) notched bending samples were produced with a geometry of 50 × 10 × 4 mm (length × width × thickness), with a notch of 5-mm length and 2.6-mm width on a long side of specimens. The span length, *S*, was selected to be at least 4 times the width, *W*.

Fracture toughness tests were performed using a universal testing machine (EZ-S, Shimadzu Corp., Japan), same as bending tests. Strain speed of 0.05 mm/min was applied for all the tests. To measure the crack mouth opening displacement (CMOD), the whole tests were recorded by a digital camera (RX100 IV, Digital Still Camera Cyber-shot, Sony), and the crack width was calculated using an image processing software (Tracker 5.1).

In order to determine the stress intensity factor K_{IC}, firstly the critical stress-intensity factor, K_Q, was calculated based on the Eq. (1).

$$K_Q = \frac{P_Q \cdot S}{B \cdot W^{3/2}} \cdot f\left(\frac{a}{W}\right) \cdot \cdot \cdot (1)$$

where P_Q is a load corresponding to the 5% deviation from linearity, *B* specimen thickness, *f(a/W)* is the corresponding shape function as defined in the standard, the ASTM E399 [213]. The determination of K_{IC} values can be done upon agreement of small-scale yielding, as given in Eq. (2):

$$P_{max}/P_Q < 1.1 \cdot \cdot \cdot (2)$$

and plain strain conditions (*i.e.* the plastic zone must be small enough compared to the notch length, *a*, the uncracked ligament, $W - a$, and the thickness, *B*), as shown in Eq. (3):

$$B, a, (W - a) > 2.5\left(\frac{K_Q}{\sigma_y}\right)^2 \cdot \cdot \cdot (3)$$

5.2.4. Microindentation tests

The universal nanomechanical tester (ZwickRoell) with a diamond pyramid indenter, Berkovich type, of a face angle of 115.12º was used for a series of tests. In microindentation tests, the evolution of the applied force during a load/unload mode as a function of the indented depth is recorded. By applying the quasi continuous stiffness measurements (QCSM) technique, local deformation was generated along a harmonic load oscillation of the indenter during penetration.

The so-called "continuous stiffness measurement" method consisted in superimposing a small harmonic load oscillation of small amplitude (1.5 nm) at 32 Hz frequency. In fact, Young's modulus is generally obtained in the reduced form *E'**, which is given in [215] by Eq. (4)

$$E'^{*} = \mathrm{S}/2(\frac{\pi}{A_{\mathrm{ind}}})^{1/2} \cdot \cdot \cdot (4)$$

where *S* is the contact stiffness between the indenter and the specimen and A_{ind} is the indented area, which is given by Eq. (5)

$$A_{\mathrm{ind}} = 35.366(h_r' + h_0)^2 \cdot \cdot \cdot (5)$$

where h_r' means the plastic indented depth under the tip and h_0 indenter shape. The real Young's modulus of tested material can be calculated through Eq. (6) [216]

$$\frac{1}{E'^{*}} = \frac{(1-\nu^2)}{E} + \frac{\left(1-\nu_i^2\right)}{E_i} \cdot \cdot \cdot (6)$$

where *E* and *v* are Young's modulus and Poisson's ratio for the specimen and E_i and v_i the same parameters for the indenter. The elastic properties of the diamond indenter were E_i = 1131 GPa and v_i = 0.07. In this study, Young's modulus of both bone and PMMA based materials were calculated. Bone was assumed to be an isotropic material with a 0.3 Poisson ratio [86,92]. PMMA is considered to have 0.3 Poisson's ratio [217].

Using this technique, dynamic hardness and elastic modulus as a function of indentation depth were obtained. PMMA, AC20, and AC40 were used. The natural bones and Sawbones® test materials were also tested as controls. The polymeric specimens were cut into a thin block of a 5.0-mm height. A part of mandible bone was extracted. A surface parallel to the mandible base was located at the bottom for mandible bone samples considering the consistency of drilling direction in dental implant surgery. All the specimens were embedded in epoxy resin. The specimens were then polished with emery paper starting from P800 to 1200, 2400, and 4000, and then with diamond slurry of a diameter of 1.0 μm. The indentation was performed perpendicularly to the longitudinal axis of mandible base.

The indenter was loaded until 500 mN at the strain rate of 3.0×10^{-2} s^{-1}. The indenter was extracted from the test pieces when reaching the maximum force. Five times of indentations were conducted for each specimen.

5.2.5. DMA measurements

DMA measurements were carried out similarly using the 50-N 0.1-dB Metravib testing machine as presented at the section 3.3.2 in the chapter 3. The changes of the storage modulus, loss modulus, and the loss factor were plotted as a function of temperature within 25℃-200℃ at the heating rate of 1 ℃/min with the measurement frequency of 1 Hz.

5.3. Results and discussion

5.3.1. Bending test results

The representative stress-strain curve is illustrated in Fig. 5-1. The effect of additive concentration is observed; the more additives are put in acrylic composite materials, the less strain is required for their fracture. Along the increase in alumina cement, composite materials tend to show more brittle fracture mode. The averaged strength and modulus of acrylic resin and composite materials are plotted Fig. 5-2. Error bars represent the standard deviation from three measurements. The maximum strength exhibits almost constant regardless of the additive amount, while elastic modulus displays linear increase until 40 wt% of additive composition, ranging from 1.7 to 4.3 GPa.

Table 5-1 shows a list of tensile strength and elastic modulus from the literature [32,48,49,75,89–91]. It can be seen that acrylic specimens show drastically lower values for elastic modulus compared to natural bone, while strength is almost half to the lowest reference data of porcine cortical bone. The equivalent modulus and strength to those of arbitrary part of natural bone could be obtained by the replacement of acrylic resin with stronger mechanical properties. Although the similar values in torque and drilling feed rate were observed under constant load drilling, strength and elastic modulus are not directly corresponding between AC40 and natural bone.

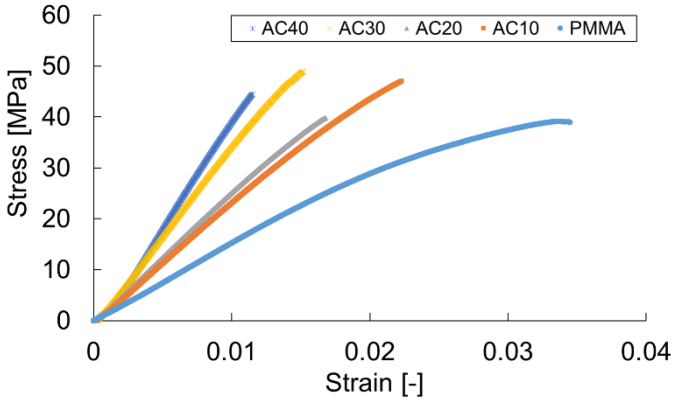

Fig. 5-1 Typical results of stress-strain curves obtained from bending tests

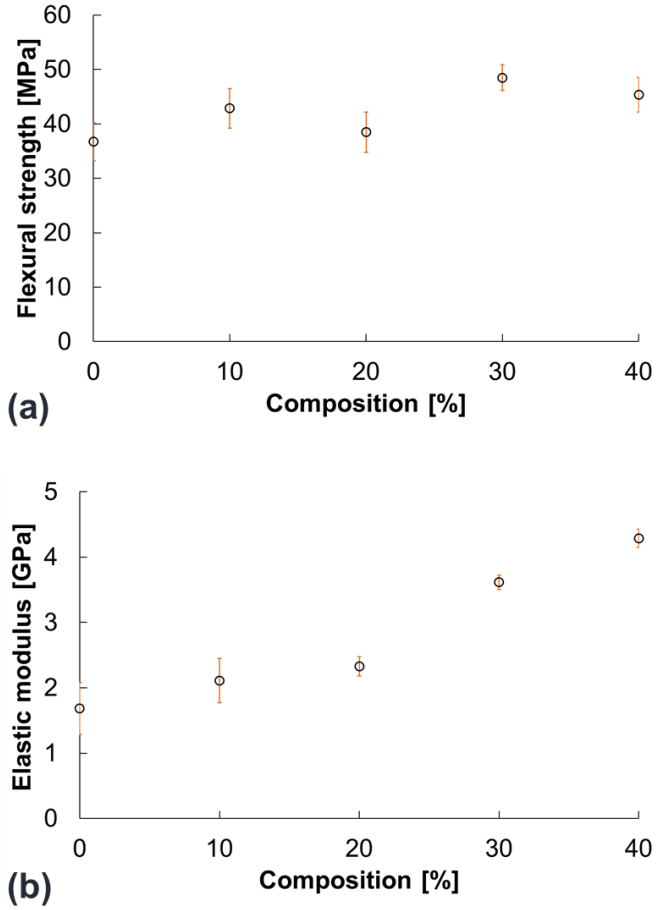

Fig. 5-2 Relationship between composition ratio of alumina cement and (a) flexural strength, and (b) flexural modulus

Table 5-1 List of mechanical properties from [a][48],[b][32],[c][89],[d][49],[e][75],[f][90],[g][91]

Material	Tensile strength [MPa]		Elastic modulus [GPa]	
	Axial (longitudinal)	Radial (traverse)	Axial (longitudinal)	Radial (traverse)
Sawbones #1522-03 (PU20)	5.6[a]		0.284[a]	
Sawbones #1522-27 (PU50)	27[a]		1.469[a]	
Sawbones #3401-06 (EP-S)	106[a]	93[a]	16.0[a]	10.0[a]
Human cortical bone	124 ± 1.1[b]		17.6[b]	
	132 ± 16.1[c]	57.9 ± 5.5[c]	17.7 ± 3.9[c]	13.1 ± 3.1[c]
	107.9 ± 12.3[d]		19.9 ± 1.8[d]	
Canine cortical bone	108.3 ± 20.5[e] (ultimate)		13.86 ± 1.17[e]	
	251.0 ± 49.1[f] (ultimate)		15.6 ± 2.6[f]	
Porcine cortical bone	194.5 ± 14.45[g]		17.4 ± 1.11[g]	
	88 ± 1.5[b]		14.9[b]	
PMMA (this study)	36.7 ± 3.5		1.68 ± 0.40	
AC20 (this study)	38.5 ± 3.7		2.33 ± 0.15	
AC40 (this study)	45.4 ± 3.2		4.29 ± 0.14	

5.3.2. Fracture toughness tests

The fracture toughness test results show the linear-elastic conditions as required by the standard [213]. Obtaining P_Q from bending of SE specimens, K_Q was calculated respectively, based on the Eq. (1). Then, the calculated K_Q values were confirmed as K_{IC} according to the Eq. (3).

Fig. 5-3 shows the obtained K_{IC} for acrylic specimens as a function of composition ratio of alumina cement up to 40 wt%. These obtained values are ranged between 1.18 ± 0.06 and 1.37 ± 0.08 MPa√m, and nearly corresponding to the values reported in the literatures for acrylic resin for clinical applications [218,219]. There seems to be little impacts of composition ratio of alumina cement on K_{IC} values of composite materials. From the results of bending tests, the composition ratio does not show large impacts on flexural strength. According to the Eq. (1), the K_{IC} values bear a proportionate relationship to the strength. Therefore, it can be considered that the K_{IC} values show similar trends as a function of additive amounts.

Table 5-2 shows a list of the K_{IC} values for test specimens in this study with literature data for cortical bone [220–222]. Comparing bovine and human bone, human bone relatively shows closer K_{IC} values to those of acrylic specimens. However, fracture toughness might have little effects on drilling behavior since drilling properties varies among materials with nearly corresponding K_{IC} values.

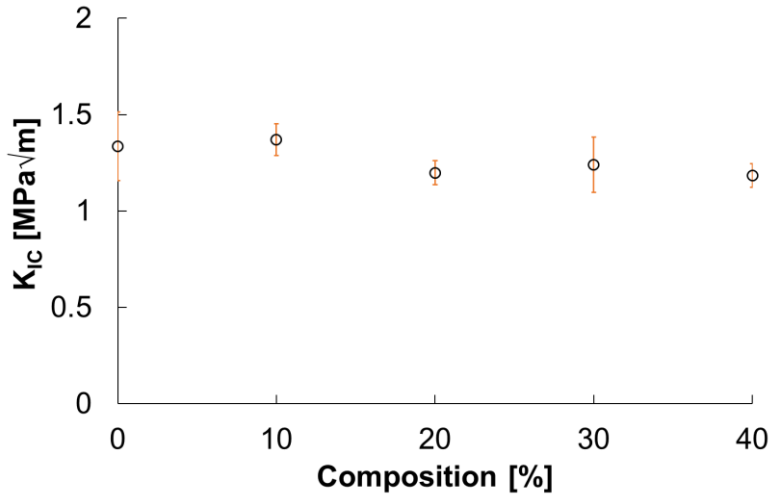

Fig. 5-3 Relationship between composition ratio of alumina cement and stress intensity factor, K_{IC}

Table 5-2 K_{IC} values for tested specimens with references for cortical bone from [221][a], [220][b], [222][c].

Material	K_{IC} [MPa√m]
PMMA (this study)	1.3 ± 0.2
AC10 (this study)	1.4 ± 0.1
AC20 (this study)	1.2 ± 0.1
AC30 (this study)	1.2 ± 0.1
AC40 (this study)	1.2 ± 0.1
Human cortical bone	1.6 to 2.5[a]
Bovine cortical bone	3.9 to 7.2[a]
	3.8 (dehydrated) to 5.5[b] (hydrated)
	4.4 ± 0.8[c]
Sawbones #1522-03 (Saw-PU20)	-
Sawbones #1522-27 (Saw-PU50)	-
Sawbones #3401-06 (Saw-EP-S)	-

5.3.3. Microindentation tests

Fig. 5-4 shows the averaged hardness and elastic modulus of acrylic specimens as well as controls. Error bars represent standard deviation for each property. Hardness shows significant difference between polymeric materials and natural bone tissue. Although EP-S shows the equivalent value to canine bone in hardness, other materials show drastically lower values in both hardness and

elastic modulus. Comparing PMMA, AC20, and AC40, the additives work to increase the stiffness. There is a small difference in stiffness found between AC20 and AC40. AC20 and AC40 shows almost two times higher values of hardness and elastic modulus compared to those of PMMA, and almost 3 times of difference in hardness and elastic modulus compared to natural bone.

The correlation between the drilling feed rate and stiffness is illustrated in Fig. 5-5. Globally, the similar trend can be found in Fig. 5-5(a) and (b). Until around 200 MPa of hardness, or 5 GPa of elastic modulus, the feed rate decreases along the increase in stiffness. After those values, the feed rate seems constant regardless of hardness and elastic modulus between AC40, EP-S, and natural bones.

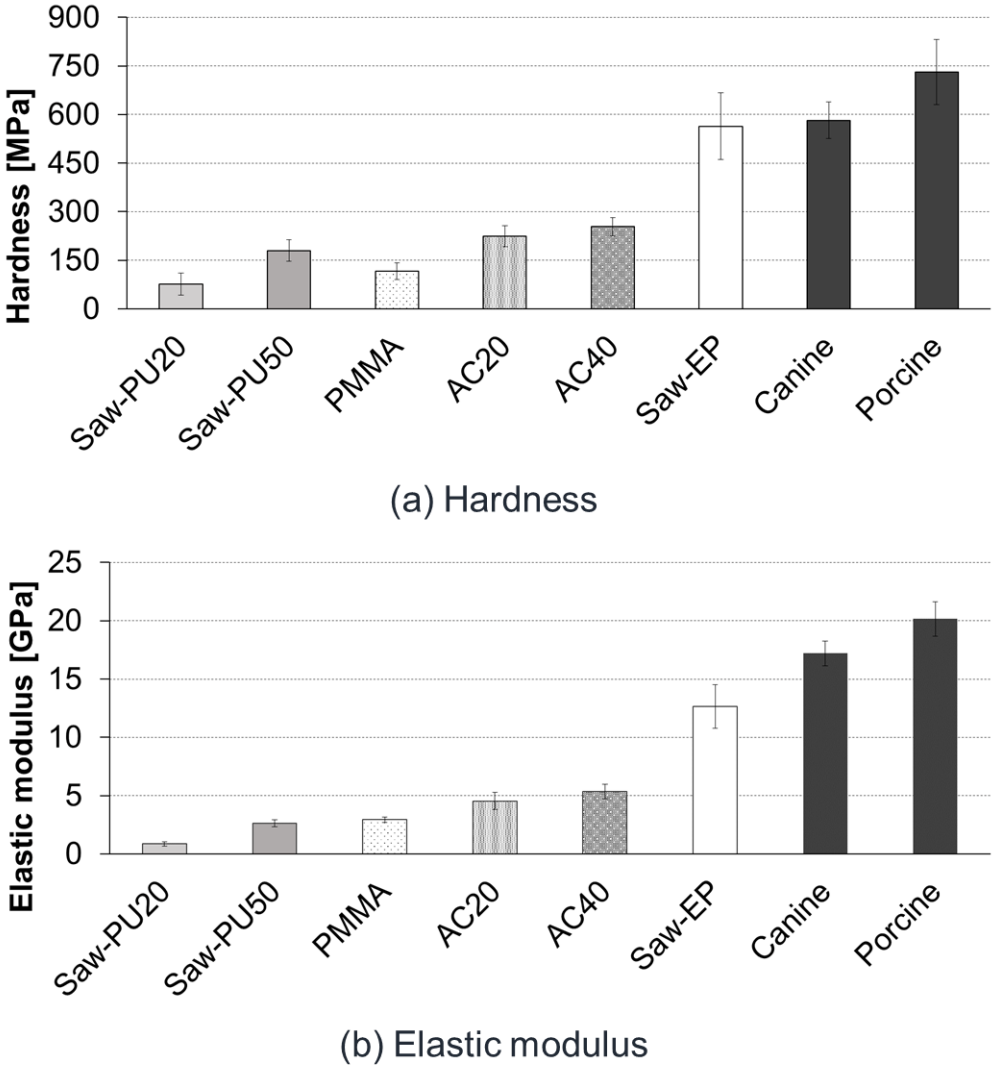

Fig. 5-4 The averaged hardness and elastic modulus

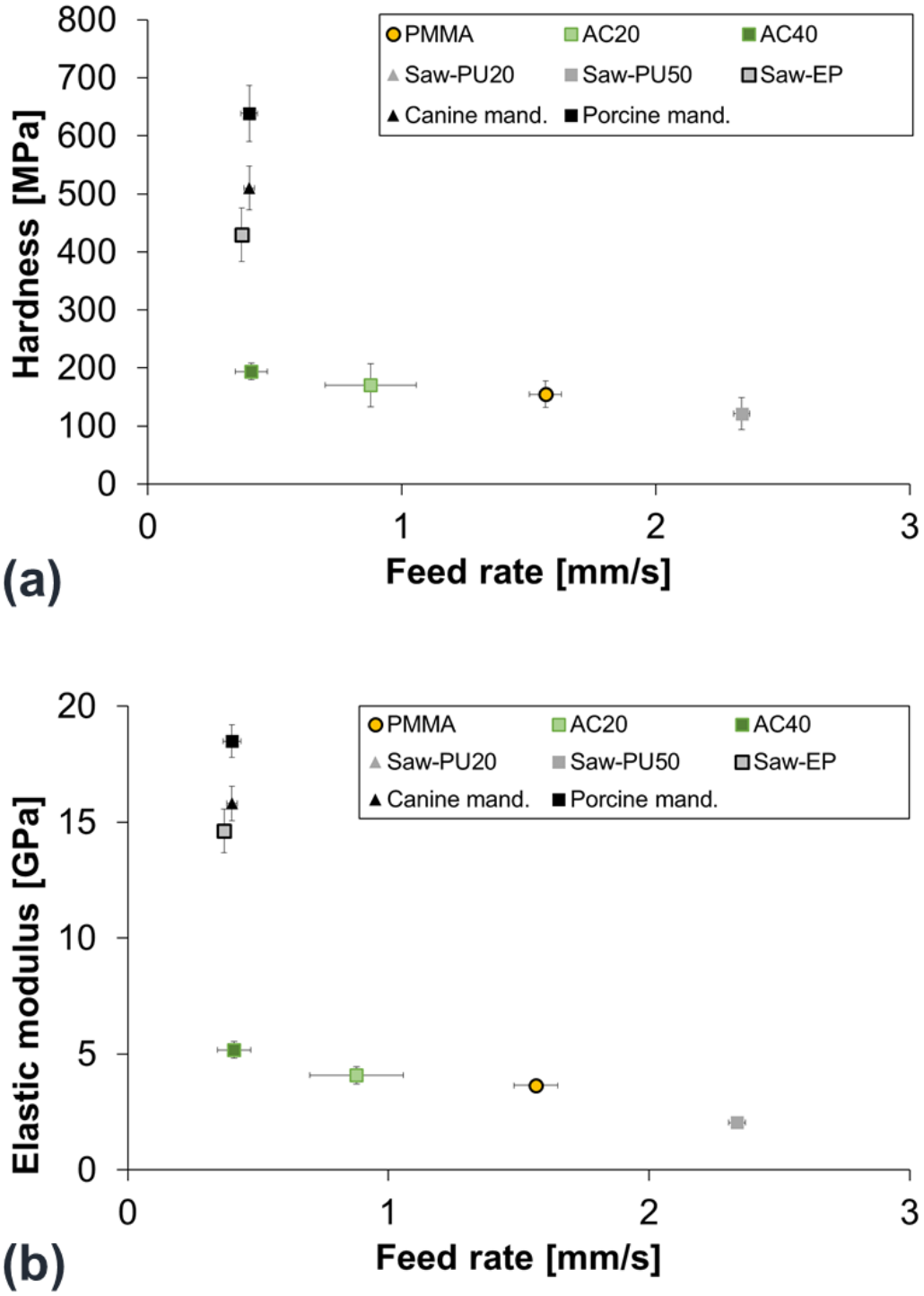

Fig. 5-5 Correlation between feed rate (under constant load drilling) and (a) hardness, and (b) elastic modulus

5.3.4. DMA measurement results

Fig. 5-6 shows representative DMA curves for acrylic, bone, and Sawbones specimens. Almost similar trend is observed among PMMA and ACs with slight difference in each modulus and tan δ. Among acrylic specimens as shown in the Fig. 5-6(a)~(e), both E' and E'' gradually decreases along the increase in temperature. There can be little effects of additive inclusion on the temperature dependency of mechanical properties.

As studied in the chapter 3, DMA curves for acrylic specimens are attributed to α-relaxation and β-relaxation. Likewise, the relaxation behavior can take place in polyurethane and epoxy resin, although the temperature that shows α-relaxation varies among polymers. According to the Fig. 5-6(f) and (g), polyurethane shows α-relaxation at about 145℃, while epoxy at about 75℃. On the other hand, bone shows the temperature-independent mechanical properties as is known.

Fig. 5-7 shows a comparison of the E' among acrylic specimens. The effect of additive amount on the E' as a function of temperature can be studied. Apparently, the E' continuously scores higher values along the increase in additive amount. It can be considered that alumina cement mixed in the acrylic matrix surrounds the polymer units inside the composite materials. Therefore, in addition to the enhancement in stiffness that can be brought by the alumina cement powder itself, the alumina cement powders consistently prevent the movement of molecules even at high temperature, resulting in high elasticity. The effect of the prevention of movements of acrylic molecules can get more dominant along the increase in additive amount, and so the composite materials have higher E' as the more additives are mixed.

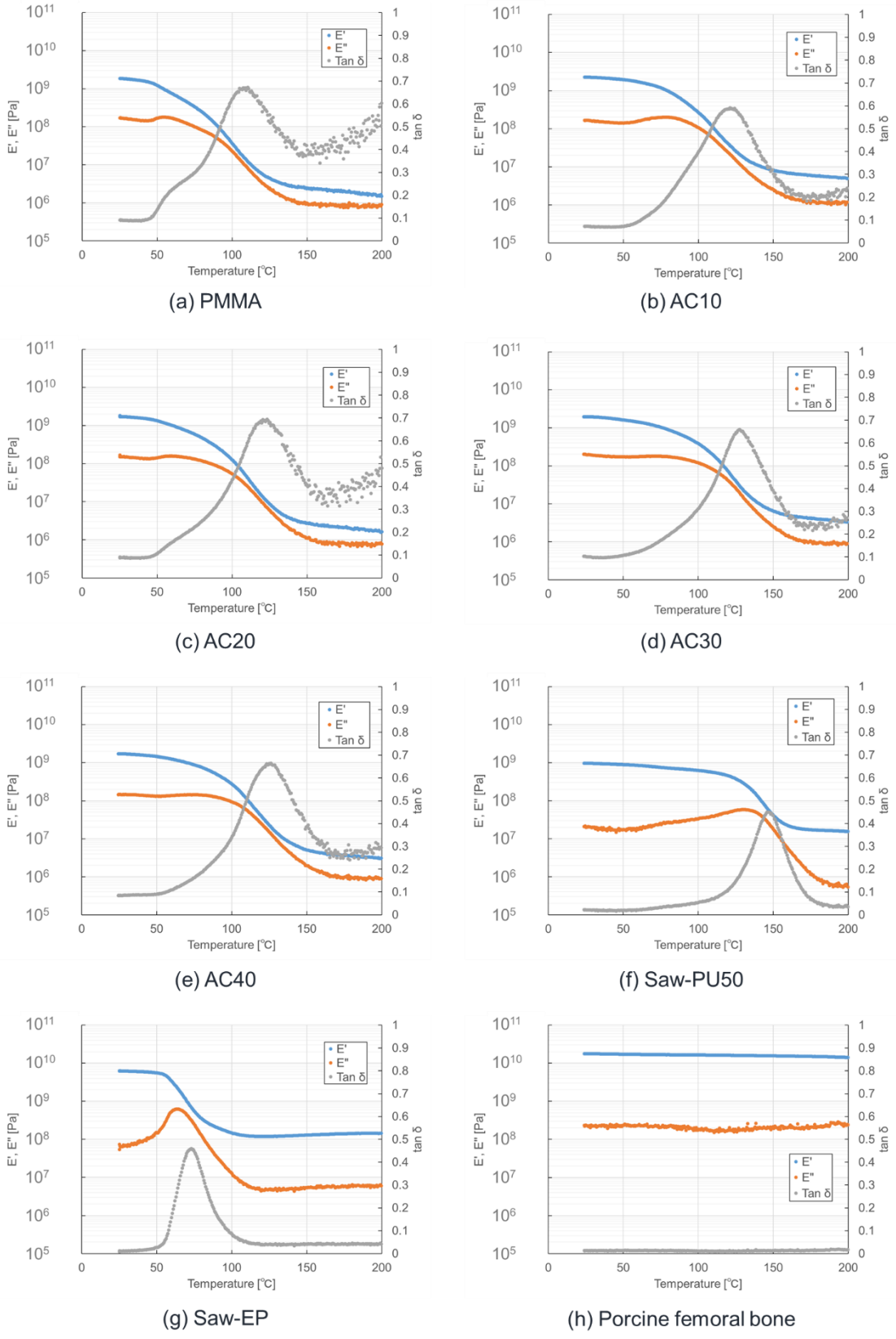

Fig. 5-6 Representative DMA curves

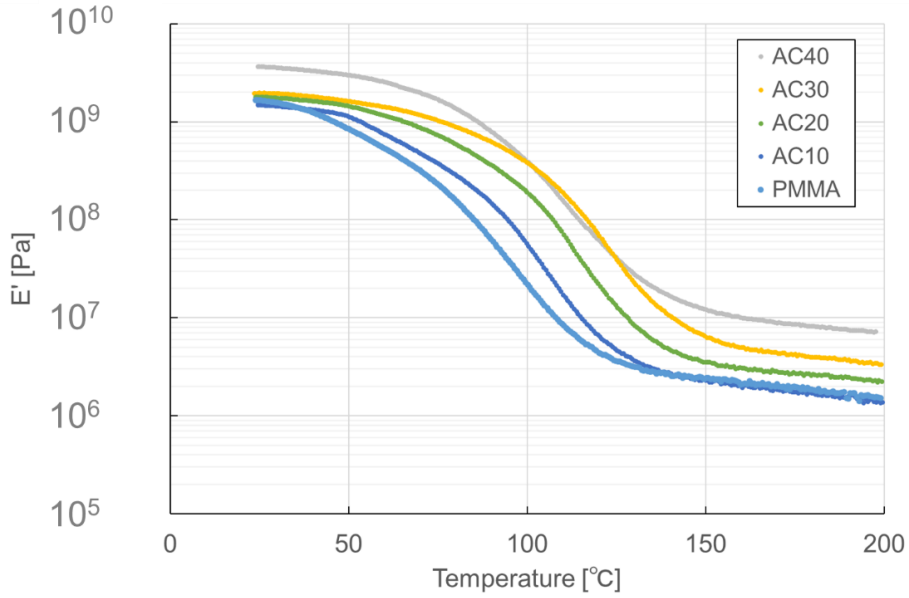

Fig. 5-7 Comparison of the E' curve depending on additive amount

5.4. Conclusions

In this chapter, mechanical tests using acrylic composite materials were performed in order to provide the effects of ceramic additives on mechanical properties. Mechanical properties that can be related to drilling properties were measured, such as strength, elasticity, hardness, and fracture toughness. Since drilling causes temperature elevation during drilling, the effects of additives on the temperature dependency of mechanical properties were also studied. A series of mechanical tests revealed findings as follows:

- The inclusion of alumina cement in acrylic resin causes higher hardness and elasticity, where the effects become larger along the additive amount up to 40 wt%. Instead of enhancing the stiffness, the composite materials tend to show more brittle fracture mode. The additives have little effects on alternation of flexural strength and fracture toughness.
- The presence of alumina cement in composite materials can prevent the movement of molecules at any temperature within 25℃-200℃. The additive amount has little effects on temperature dependency of the mechanical properties.
- Acrylic composite material including 40 wt% of alumina cement can show the comparable torque and feed rate under constant load drilling, but the stiffness of the composite materials is still lower than that of cortical bone. Thus, other mechanical properties rather than hardness or elasticity shall be dominant for determining drilling characteristics.

Chapter 6: Relationship between drilling properties and tactile feedback in drilling by surgeons

This chapter presents drilling experiments performed by surgeons. Using acrylic composite materials as well as natural bone and Sawbones® test materials, measurements of drilling properties such as thrust force and torque are carried out. Combining the measurement results of drilling properties and tactile feedback during drilling interviewed after drilling of test specimens, relationship between drilling properties and tactile feedback is discussed.

6.1. Introduction

The inclusion of ceramic additives in acrylic resin shows alternation of drilling properties with changes of mechanical properties such as hardness and elasticity as revealed in the previous chapters. These changes of mechanical and drilling properties are considered to affect resultant tactile feedback during drilling. The objective of this chapter is to see the relationship between drilling properties and tactile feedback. To do so, drilling experiments were performed by experienced surgeons using acrylic composite materials with controls of natural bone and Sawbones® test materials. During drilling by surgeons, drilling properties such as thrust force and torque were obtained using measurement system. After drilling of test specimens, tactile feedback was interviewed to surgeons, and the order of tactile sense of hardness during drilling was obtained using the ranking method. Combining the measurement results of drilling properties and the tactile feedback given by the surgeons, the relationship between drilling properties and the tactile feedback is studied.

6.2. Materials

For measurements of drilling properties, three categories of test materials were prepared as used in drilling tests, including natural bone, Sawbones® test materials, and acrylic composite materials. Seven kinds of specimens were selected; porcine femoral and mandible bone, Saw-PU50, Saw-EP, PMMA, AC20, and AC40. The same specimens as drilling tests under constant thrust force were used for drilling experiments by surgeons.

6.3. Experimental and analytical methods

Manual drilling tests were carried out by surgeons in both orthopedics and dentistry with more than 20-year career that required surgical operations including drilling of bone. Test specimens and measurement systems were brought to surgeons. Drilling was performed with recording cutting forces of thrust force and torque. Three measurements were performed for each test material. After drilling tests, tactile feedback for each material was interviewed, focusing on the similarity of tactile feedback compared to human cortical bone of men aged 30s to 40s as persona.

The tactile sense of hardness during drilling was ranked among Saw-PU50, Saw-EP, PMMA, AC20, and AC40. using the ranking method of the sensory analysis [223]. The ranking method is effective to qualitatively evaluate the magnitude of attributes among a small number (around six) of

specimens [224]. According to the rule of JIS Z 9080 [224], the preferable number of assessors is defined more than two for experts, while more than five for selected assessors, and more than ten for training assessors. In this test, we determined the bare minimum number of subjects is two, regarding the involved surgeons as experts considering the developed competence in drilling of bone. In advance of the drilling experiments, mutual understanding of the evaluation term of "the tactile sense of hardness during drilling" that describes the attribute of the resistance force to overcome drilling during material removal was obtained between the examiner and the assessors. Based on the questionnaire, the ranking of the attribute was obtained. Considering the number of participating subjects, the statistical test is not applied.

Fig. 6-1 shows an overview of experimental set-up for manual drilling tests. Drilling was performed on test specimens using surgical drill (Colibri II, DePuySynthes) and twist drill (Nobel Biocare Japan Co., Ltd.). A fresh drill bit was used for each test material. The measurement systems included a 6-axis sensor (CFS018CA101U, Leptrino), and a data loger (LGR101U, Leptrino). Drilling was performed on an epoxy plate on the sensor, and the cutting forces were recorded through a software (Virtual COM Port driver, ver1.3.1, STMicroelectronics) on a PC. The whole experiments were recorded by a camera (RX100 IV, Digital Still Camera Cyber-shot, Sony). Machining conditions such as 1,500 rpm of rotation speed were applied after the beginning of material removal. Penetration was performed until 10 mm of displacement in order to obtain full engagement of drill bit for material removal. Thrust force and torque were averaged from the maximum values after full engagement of drill bit. No irrigation was applied during drilling. For the statistical analysis of the difference among test specimens on thrust force and torque, the unpaired one-tailed Student's *t*-test was applied on Microsoft Excel 2016 (Microsoft Corp., Redmond, WA). The variance of results was considered significant at $p<0.05$.

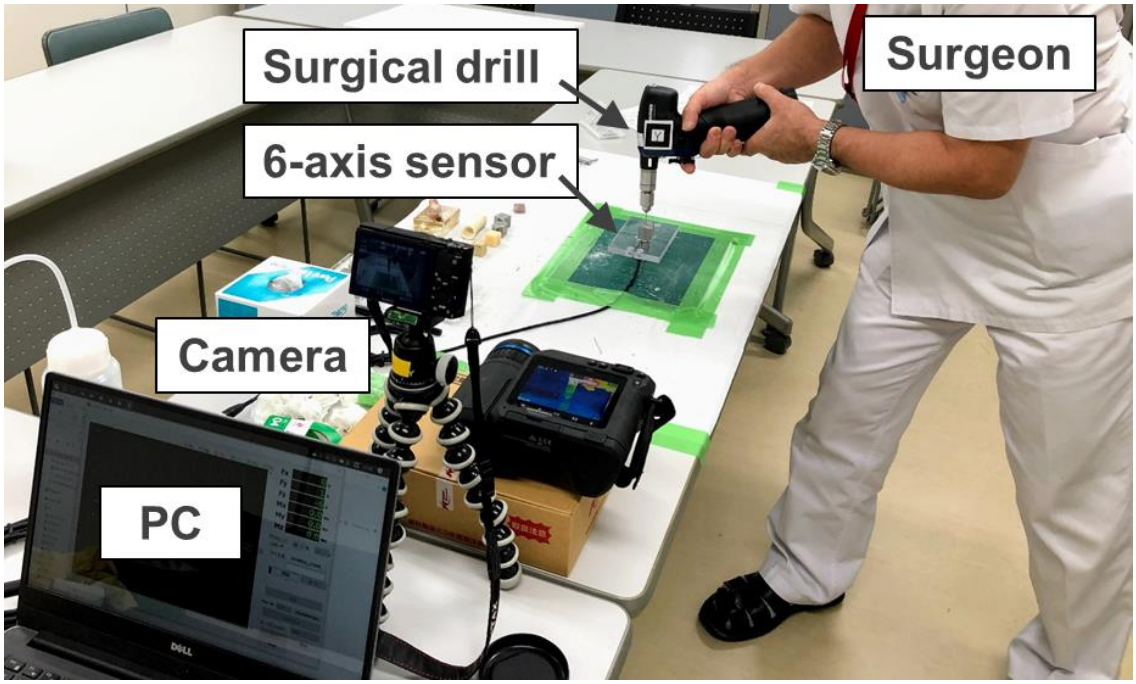

Fig. 6-1 Experimental set-up for drilling experiments by surgeons

6.4. Results and discussions

❖ **Tactile feedback and subjective evaluation ranking by surgeons**

Table 6-1 lists the comments given by surgeons after drilling of test materials. The comments by orthopedist and dentist are globally corresponding. Saw-PU50 and PMMA are commented to be softer in drilling compared to cortical bone, while Saw-EP and AC40 are relatively harder than bone. Among the test specimens, AC20 is reviewed to show good similarity to cortical bone in tactile feedback during drilling. Comparing PMMA and AC20, the surgeons commented that the specimens show hard tactile feedback at the beginning of drilling process, and gradually becomes softer along the progress of drilling process. The transition of tactile feedback can be influenced by the changes of dynamic viscoelasticity as revealed in the chapter 3, which is considered to happen also during drilling of AC20. Regarding the transition of tactile feedback, the dentist commented that the gap of tactile feedback between at the beginning and during drilling was less in AC20 compared to PMMA, and the gap was not obviously seen in drilling AC40. It is considered that the increase in additive amount in acrylic resin changed the tactile feedback during drilling.

Besides, the order of tactile sense of hardness during drilling among test materials based on the subjective evaluation of two surgeons are ranked as follows:

Saw-PU50<PMMA<AC20<AC40<Saw-EP

where the calculation of confidence interval between each material requires more numbers of subjects. According to the ranking, the inclusion of alumina cement can change the tactile feedback during drilling, to the direction that enhance tactile sense of hardness during drilling. It is assumed that the tactile feedback of natural bone locates either between PMMA and AC20, or AC20 and AC40 in the ranking, based on the comments by surgeons.

Table 6-1 Comments of surgeons after drilling of test specimens.

Materials	Orthopedist	Dentist
Saw-PU50	・Easy to drill	・Easy to drill
PMMA	・Soft to drill from the beginning. ・Softer than cortical bone.	・Hard at the first contact, but soft to drill inside specimen. ・Softer than cortical bone.
AC20	・Hard at the first contact, but gradually becomes soft during drilling. ・Good similarity to cortical bone.	・Hard at the first contact, but soft when drilling inside specimen. This gap is less in AC20 compared to PMMA. ・Relatively equivalent to human cortical bone, or possibly a little bit harder than cortical bone.
AC40	・Hard at the first contact, and stays hard throughout the drilling process. ・Relatively harder than cortical bone.	・Hard to drill throughout the cutting process; at the first contact, at the beginning of drilling, and during drilling. ・Harder than cortical bone.
Saw-EP	・Very hard to drill. However, softer than the way it looks. ・Harder than cortical bone.	・Too hard to drill. ・Much harder to cortical bone.

❖ **Measurement of drilling properties during drilling by surgeons**

Fig. 6-2 shows typical evolutions of thrust force and torque during manual drilling by the orthopedist. Both Fig. 6-2(a) and (b) shows that thrust force increases at the beginning of drilling to reach full engagement of drill bit, and then saturates at the specific value. This trend is similar to the results of drilling tests under constant feed rate. As described by Bertollo *et al.* [152], drilling by surgeon is thought to be quasi-constant thrust force after full engagement of drill bit, where the surgeon is considered to keep the constant value of thrust force. On the other hand, torque keeps increasing from the beginning of drilling until the end of drilling. The increase of torque is related to not only material removal by the tip of drill bit but also evacuation of cutting chips, and so torque is increased along the penetration depth meaning the much cutting chips are travelling through the drill flutes, the longer the penetration distance becomes. The trend of torque is also close to the typical evolution of torque under constant feed rate. The evolution of thrust force and torque was repeatable among test specimens, showing similar trend regardless of test materials with difference of magnitude of cutting forces.

Fig. 6-3 shows the average values of (a) thrust force and (b) torque for test specimens from the

drilling by the orthopedist. The order of x-axis is based on the ranking of tactile sense of hardness during drilling, where bone specimens are located after dot lines as reference values. Note that the highest peak of torque at the moment of penetration of drill bit through cortical bone was excluded for the extraction of maximum value in porcine bone specimens including mandibular and femoral bone. As for thrust force, Saw-PU50 and PMMA shows around 10 N, AC20 around 15 N, and AC40 and Saw-EP shows around 20 N for their maximum values. Bone specimens show between 10 and 15 N for thrust force. The measurement results imply that the inclusion of alumina cement in acrylic resin increases the applied force necessary for drilling, which can be estimated by the results of drilling tests under constant feed rate. PMMA and Saw-PU50 requires less force rather than porcine bones for drilling, while AC40 and Saw-EP requires relatively much force than bone specimens. Although Saw-PU50 and PMMA show the equivalent values, it turns out that the ascending order of thrust force among polymeric materials is corresponding to the ranking of tactile sense of hardness. It is considered that along the increase in the sense of hardness during drilling, the surgeon would put much thrust force for penetration of cutting tool. As for torque, bone specimens show relatively lower values between 10 and 20 N・mm, followed by Saw-EP around 20 N・mm, then acrylic-based materials and Saw-PU50 nearly more than 40 N・mm. Given that torque is related to tactile sense of hardness during drilling, the much the surgeon feels the tactile sense of hardness, the much torque would be applied. This trend is not observed for polymeric materials in the order of obtained ranking, implying that there is possibly little correlation between torque and tactile sense of hardness during drilling.

Fig. 6-4 shows the measurement results from drilling by the dentist. In the same manner to the drilling by the orthopedist, the required thrust force increase with the increase of additive amount as is seen in PMMA and acrylic composites. The ranking of tactile sense of hardness during drilling is corresponding to the ascending order of thrust force, except between Saw-PU50 and PMMA. It implies that the tactile sense cannot always be in response to thrust force applied during drilling. Less torque is required for Saw-EP and bone specimens, while much torque required for polymeric specimens especially for PMMA and Saw-PU50. Based on the hypothesis that much torque should be required for surgeons to feel much tactile sense of hardness during drilling, the measured values of torque is not corresponding to the order of the ranking, as torque is descending. Therefore, considering the dominant factors influencing tactile sense of hardness of surgeons, thrust force rather than torque is more likely to trigger surgeons' sense.

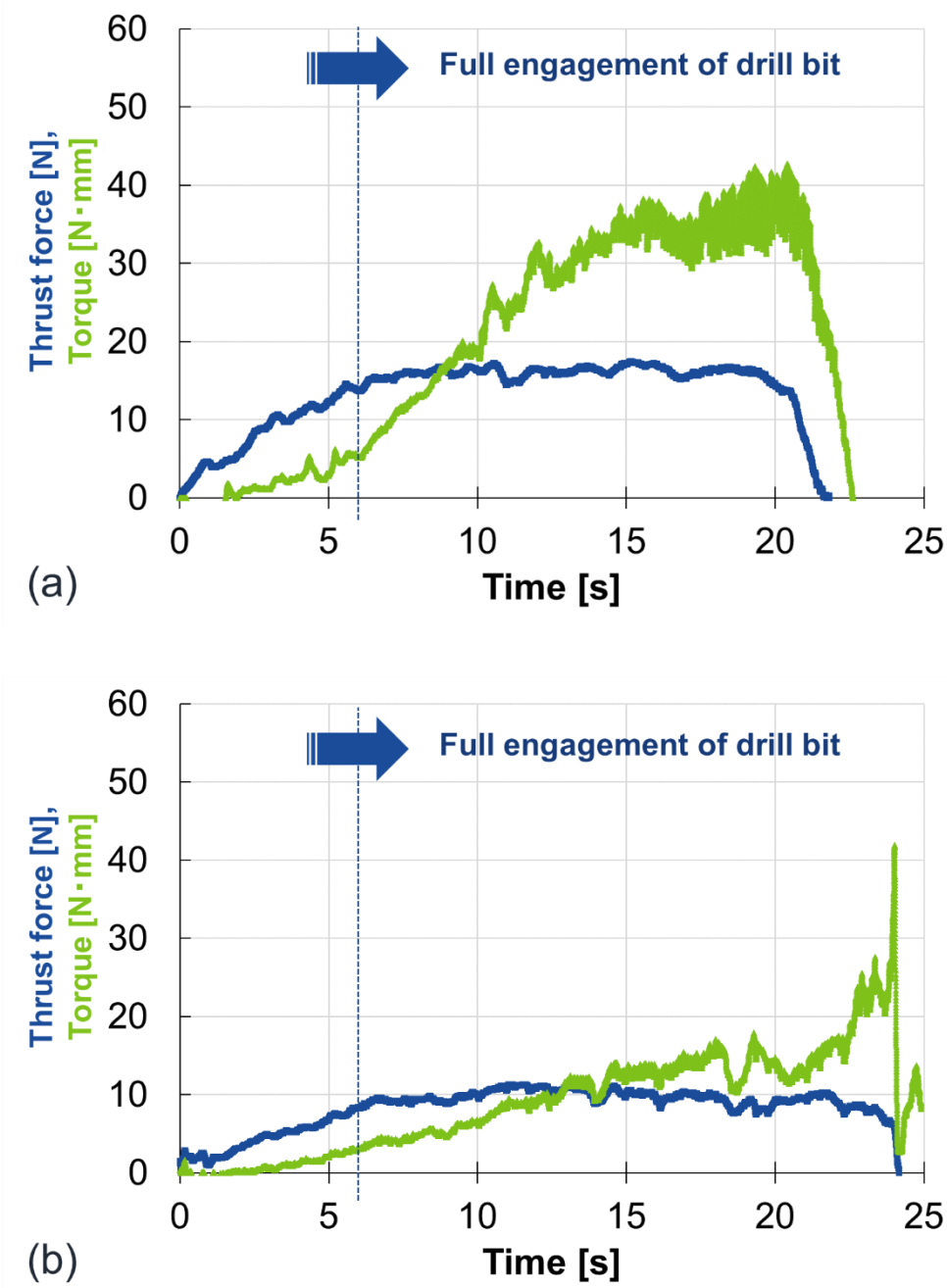

Fig. 6-2 Typical evolution of thrust force and torque during drilling: (a) AC20, (b) Porcine femur

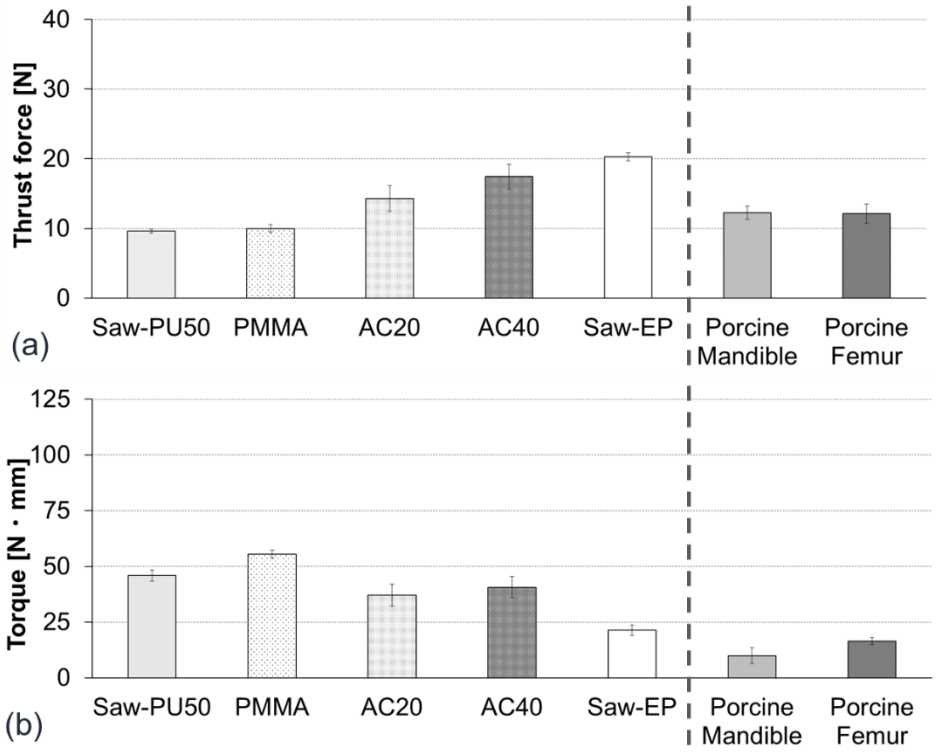

Fig. 6-3 (a) Thrust force and (b) torque (mean ±SD) in manual drilling tests by orthopedist.

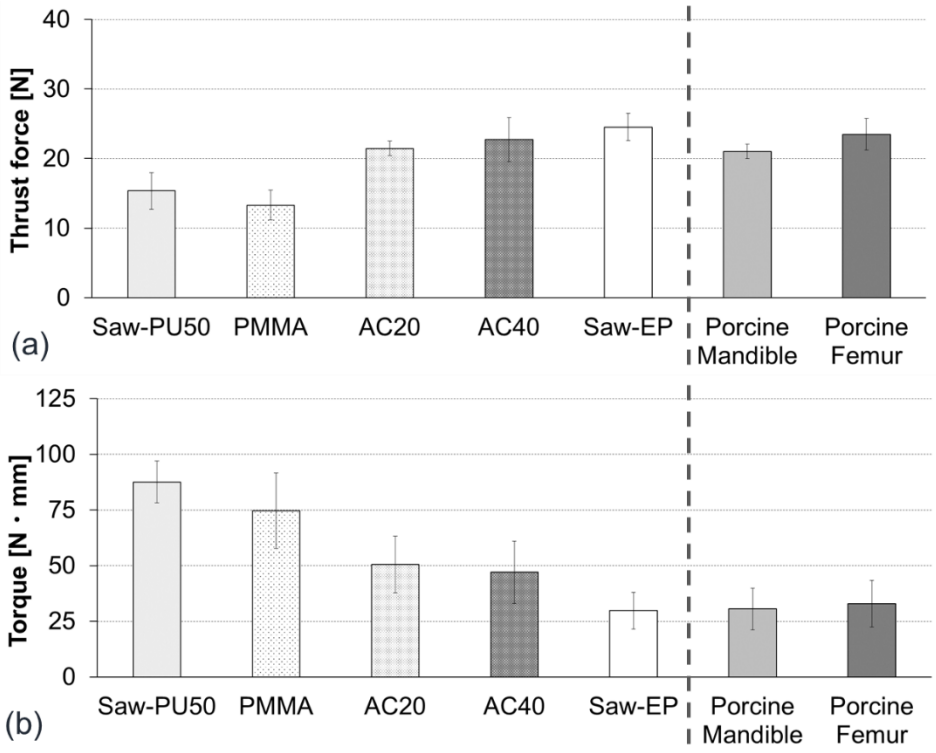

Fig. 6-4 (a) Thrust force and (b) torque (mean ±SD) in manual drilling tests by dentist.

❖ **Relationship between drilling properties and tactile feedback**

Combining the subjective evaluation ranking of the tactile sense of hardness during drilling with the measurement results of drilling properties during drilling by surgeons (Fig. 6-3 and Fig. 6-4), the evaluation ranking almost corresponds to the ascending order of thrust force except between PMMA and Saw-PU50 by dentist. However, according to both Fig. 6-3 and Fig. 6-4, there is no significant difference observed in thrust force between PMMA and Saw-PU50, indicating the equivalent magnitude of thrust force can be applied during drilling by surgeons. Thus, it could be estimated that the interval between PMMA and Saw-PU50 in the subjective evaluation ranking can be ignorable. The evaluation ranking is considered also partially equivalent to the descending order of torque. However, there are conflicts in the order of measurement results by surgeons both between PMMA and Saw-PU50, and AC20 and AC40, so the consideration of the relation of torque would require more numbers of subjects for the validation of the order of ranking. Taken together, it might be possible that thrust force rather than torque is more dominant on the determination of the subjective evaluation of the tactile sense of hardness during drilling.

Considering the vertical force applied by the surgeon is between 10 and 25 N, whereas lateral force applied by the surgeon to overcome drilling torque is almost 0.10 to 0.50 N, which can be calculated according to Fig. 6-3 and Fig. 6-4, assuming that the distance between the center of rotation of the power tool and the position of surgeon's hands was nearly 200 mm. Since the lateral force is almost double digits of magnitude lower than the applied vertical force, surgeons are likely to feel differences in thrust force rather than in torque. Therefore, it can be hypothesized that thrust force rather than torque can be dependent in describing the tactile feedback during drilling.

6.5. Conclusions

In this chapter, drilling experiments by skillful surgeons from both orthopedics and dentistry were performed in order to see the relationship between drilling properties and tactile feedback during drilling. The measurement of drilling properties was carried out while obtaining the tactile feedback by the surgeons. The results brought findings that the subjective difference in tactile feedback among synthetic materials can be resulting from the changes of thrust force rather than those of torque in drilling properties. This is implied by the fact that vertical force applied for drilling is almost one-hundred times larger the lateral force applied to overcome torque. In order to change the magnitude of thrust force applied by surgeons, the inclusion of ceramic additives such as alumina cement can be

effective in acrylic resin. The effect to modify the applied thrust force and torque becomes larger with the composition ratio up to 40 wt% of alumina cement. Toward development of bone biomodels that reproduce the similar tactile feedback to natural bone, the modification of thrust force during drilling can be one of the development approaches.

Chapter 7: Concluding remarks and perspectives

Bone biomodel is often used for surgical training of doctors or mechanical tests of medical devices. Along the progress of the super-aged society of our time, the usage of bone biomodels as the alternative practice or test materials instead of natural bone has caught more and more attentions especially for the specialties performing drilling of bone; orthopedics, dentistry, and neurosurgery. Compared to natural bones, bone biomodels have various merits such as the ease of handling, accessibility, and reproducibility. Although the usage of the bone biomodels are promising, previous studies revealed that Sawbones test materials, which are defined as the standard test materials in the standard specification in ASTM International F1839, cannot always show neither equivalent mechanical properties nor drilling characteristics. Therefore, there is a risk that surgeons or researchers are carrying out the surgical training or evaluation of medical devices under different situations from the realistic environments.

To overcome this situation, those who are aware of the gap between natural bone and conventional bone biomodels have been struggling to develop better bone biomodels. However, there has been a series of trials and errors in the development of bone biomodels because there used to be no reliable evaluation items except the perceptual evaluation of doctors.

Then, the main purpose of this study is to obtain the concrete direction toward future development of bone biomodels for the replication of drilling characteristics. To do so, this study applies the quantitative measurements of drilling properties of bone biomodel from the standpoint of engineering, in order to find out the relationship among mechanical and drilling properties, and tactile feedback during drilling. Assuming that drilling properties such as cutting forces, temperature elevation, machining conditions, or cutting chip morphology of work materials can be an outcome of mechanical properties that are related to drilling characteristics, this study adopts the development of composite materials. The effects of additives on both mechanical properties, the resultant drilling properties, and furthermore the perceptual feedback during drilling are studied.

The chapter 1 describes the research backgrounds and literature reviews concerning development of bone biomodels for drilling. The chapter 2, 3, and 4 describe the drilling aspects of natural bone, Sawbones bone biomodels, acrylic resin as a matrix, and then acrylic composite materials including ceramic additives. For the elucidation of the effects of additives on mechanical properties, a series of mechanical test results were reported in the chapter 5. Subsequently, the relationship between drilling properties and tactile feedback obtained during drilling by surgeons was studied in the chapter 6.

The chapter 2 describes the drilling characteristics of natural bone and Sawbones® test materials in order to obtain the target drilling properties of bone. Drilling tests were preliminarily performed under constant load machining conditions assuming that surgeons perform manual drilling under quasi-constant load in surgical operation, followed by drilling under constant feed rate. Drilling properties such as thrust force, torque, drilling time, and temperature elevation were recorded as well as the observation of cutting chips for the purpose of characterization of drilling in each material. Drilling tests provided the target information of drilling properties of mandibular and femoral bone, and revealed that Sawbones cortical model covers their drilling properties under the limited machining conditions. Since there is a wide range of material properties are available for cortical bone due to individual variance, the fabrication of cortical bone biomodels along the intended purpose should be necessary. From the standpoint of engineering, polymeric materials can easily get the effects of temperature rise during drilling, and so these characteristics should be taken into account for drilling of bone biomodel. Shear strength and fracture toughness of work material are also considered to affect drilling characteristics.

The chapter 3 describes the drilling of acrylic resin as a matrix for composite materials. From the drilling properties and observation of cutting chips, the temperature elevation during drilling can influence drilling of acrylic resin by stages. Due to the thermoplasticity of acrylic resin, when reaching the glass transition temperature around 100℃, there is a morphological change leading the slight decrease in torque that is associated with the decrease in viscoelasticity. Since the effects of mechanical changes due to temperature rise are confirmed on drilling characteristics, the acrylic composite materials are estimated also to show temperature-dependent drilling characteristics. The effects of temperature rise are negligible concerning drilling in acrylic-based bone biomodels.

Fabrication of acrylic composite materials and their drilling characteristics are described in the chapter 4. Ceramic additives were mixed to acrylic resin to form composite materials. After confirming the effects of ceramic additives on the alternation of drilling properties, the effects of additive amount were studied focusing alumina cement. The inclusion of alumina cement was useful for controlling drilling properties under both constant load and feed rate drilling. Thrust force, torque, and feed rate during drilling can be controlled along the amount of alumina cement; the much the additive is mixed, the more the effects become up to 40 wt% of additive composition. Moreover, acrylic composite materials including 40 wt% of alumina cement exhibits the comparable torque and feed rate under constant load drilling at 20-N thrust force and 1,000-rpm rotation speed. The similarity in drilling

properties can pertain to the similarity in mechanical properties related to drilling, and so mechanical tests were conducted.

Chapter 5 describes the relationship between drilling properties and mechanical properties of acrylic composite materials. The mechanical properties possibly dominant on determining drilling properties are focused on and measured in the mechanical tests. Considering previous studies, mechanical tests including bending tests, Microindentation tests, and fracture toughness tests were carried out. DMA tests were also performed to see the temperature dependency of mechanical properties of acrylic composite materials. The mechanical testing revealed that the inclusion of alumina cement in acrylic resin can enhance hardness and elasticity with showing more brittle behavior against the fracture. This effect becomes larger along the additive amount until 40 wt%. The enhancement of stiffness of acrylic composite materials can be resulting from the prevention of molecular movements by alumina cement. The additive amount has little effects on temperature dependency of mechanical properties. However, the hardness or elasticity of acrylic composite materials are still lower than that of cortical bone, and thus other mechanical properties rather than stiffness shall be dominant for determining drilling characteristics.

The chapter 6 describes the relationship between drilling properties and tactile feedback during drilling by surgeons. The drilling haptics by experienced surgeons were measured using the measurement system consisted of a 6-axis sensor. After drilling tests, tactile feedback was interviewed and the ranking of the tactile sense of hardness during drilling was obtained. The experimental results revealed that cutting forces represented by thrust force depends on work materials, and the resemblance of drilling haptics can be attributed to the similarity in the magnitude of thrust force rather than that of torque. The inclusion of ceramic additives such as alumina cement can be useful for the alternation of the perceptual feedback during drilling by promoting the changes in thrust force applied during drilling. Toward development of bone biomodels that can cover the similar tactile feedback to natural bone, one of the approaches is the modification of thrust force applied during drilling.

Through the whole chapters, the fabrication of composite materials made of acrylic resin as a matrix and ceramic powders as additives was established, and then the fabricated materials experienced a series of drilling and mechanical tests in order to provide quantitative information of drilling and mechanical properties considering the effects of the presence of additives. The relationship among drilling and mechanical properties, and tactile feedback during drilling was studied. The present study brought the following findings. The inclusion of alumina cement in a matrix of acrylic

resin enhances the stiffness of the matrix, and the effects becomes larger along the increase in the amount up to 40 wt%. The effect of the additive can be seen in drilling properties of acrylic composite materials as the thrust force, torque, and feed rate were altered to get closer to those of cortical bone. The alternation of drilling properties by alumina cement can be related to the alternation of mechanical properties dominant on determining drilling characteristics affected by alumina cement. The effects of alumina cement were observed in hardness and elasticity. However, since the obtained values of hardness, strength, fracture toughness, and elasticity of fabricated acrylic composite materials are not completely corresponding to those of cortical bone, other mechanical properties rather than the mechanical properties measured in this study may affect drilling properties. Shear strength and surface roughness are the prospective mechanical properties possibly influencing drilling properties based on cutting theory. Not only static but also dynamic mechanical properties might be other factors influencing drilling behavior. Furthermore, the acrylic composite materials including 20 wt% of alumina cement achieved the good agreement in the similarity in tactile feedback during drilling in comparison of human cortical bone. This agreement can be attributed to the equivalent thrust force to that of cortical bone during drilling by skillful surgeons. This finding implies that the similarity in thrust force during drilling can cause the close tactile feedback during drilling of natural bone. Therefore, toward the development of bone biomodels that reproduce the similar tactile feedback to natural bone, the modification of thrust force during drilling can be one of the development approaches, which is caused by the inclusion of alumina cement.

References

[1] The Statement on the Social Welfare Renovation n.d. https://www.mhlw.go.jp/stf/seisakunitsuite/bunya/hokabunya/shakaihoshou/kaikaku_1.html (accessed October 30, 2019).

[2] Cabinet Office The Government of Japan. The 2019 Edition White Paper on Aging Society. 2019.

[3] National Institute of Population and Social Security Research. Population Projections for Japan : 2016-2065 (With long-range Population Projections : 2066-2115). 2017.

[4] The Japanese Society of Arthroplasty Replacement. 2017 Annual Report. 2017. doi:10.1002/ejoc.201200111.

[5] National Joint Registry (NJR). 16th Annual Report. 2019.

[6] National Joint Registry (NJR). 15th Annual Report. 2018.

[7] Annual Report 2018. 2018. doi:10.3934/math.2019.1.166.

[8] Kurtz S, Ong K, Lau E, Mowat F, Halpern M. Projections of primary and revision hip and knee arthroplasty in the United States from 2005 to 2030. J Bone Joint Surg Am 2007;89:780–5. doi:10.2106/JBJS.F.00222.

[9] Lohfeld S, Barron V, Mchugh PE. Biomodels of Bone: A Review. Ann Biomed Eng 2005;33:1295–311. doi:10.1007/s10439-005-5873-x.

[10] Harrysson O La, Hosni YA, Nayfeh JF. Custom-designed orthopedic implants evaluated using finite element analysis of patient-specific computed tomography data: Femoral-component case study. BMC Musculoskelet Disord 2007;8. doi:10.1186/1471-2474-8-91.

[11] Arvier JF, Barker TM, Yau YY, D'Urso PS, Atkinson RL, McDermant GR. Maxillofacial biomodelling. Br J Oral Maxillofac Surg 1994;32:276–83. doi:10.1016/0266-4356(94)90046-9.

[12] D'Urso PS, Atkinson RL, Lanigan MW, Earwaker WJ, Bruce IJ, Holmes A, et al. Stereolithographic (SL) biomodelling in craniofacial surgery. Br J Plast Surg 1998;51:522–30. doi:10.1054/bjps.1998.0026.

[13] A Prosthetic Restoration Jaw Model, PRO2002-UL-UP-FEM-28, Nissin Dental Products, Inc. (accessed 2019.10.28) n.d. https://www.nissin-dental.net/products/DentalTrainingProducts/CrownBridge/PRO2002-UL-SP-FEM-28/index.html (accessed September 20, 2009).

[14] A Drilling Training Model, E7-X.1137, Nissin Dental Products, Inc. (accessed 2019.10.28) n.d. http://www.nissin-dental.jp/products/educationalmodels/inplant/E7-X.1137/index.html (accessed November 12, 2019).

[15] Blood vessel model (3DMed), Renaissance of Technology Corporation (R'Tech) (accessed 2019.10.28) n.d. http://www.r-tech.co.jp/en/product/3dmed/ (accessed September 28, 2019).

[16] Hochman JB, Kraut J, Kazmerik K, Unger BJ. Generation of a 3D printed temporal bone model with internal fidelity and validation of the mechanical construct. Otolaryngol - Head Neck Surg (United States) 2014;150:448–54. doi:10.1177/0194599813518008.

[17] Chae MP, Rozen WM, McMenamin PG, Findlay MW, Spychal RT, Hunter-Smith DJ. Emerging Applications of Bedside 3D Printing in Plastic Surgery. Front Surg 2015;2. doi:10.3389/fsurg.2015.00025.

[18] Tai BL, Rooney D, Stephenson F, Liao P, Sagher O, Shih AJ, et al. Development of a 3D-printed external ventricular drain placement simulator: technical note. J Neurosurg 2015;123:1070–6. doi:10.3171/2014.12.JNS141867.Disclosure.

[19] Shimizu Y, Tanabe T, Yoshida H, Kasuya M, Matsunaga T, Haga Y, et al. Viscosity measurement of Xanthan-Poly(vinyl alcohol) mixture and its effect on the mechanical properties of the hydrogel for 3D modeling OPEN 2018;8:16538. doi:10.1038/s41598-018-34986-4.

[20] Bento RF, Rocha BA, Freitas EL, Balsalobre F de A. Otobone®: Three-dimensional printed Temporal Bone Biomodel for Simulation of Surgical Procedures. Int Arch Otorhinolaryngol 2019. doi:10.1055/s-0039-1688924.

[21] Abbott JR, Netherway DJ, Wingate PG, Abbott AH, David DJ, Trott JA, et al. Computer generated mandibular model: surgical role. Aust Dent J 1998;43:373–8. doi:10.1111/j.1834-7819.1998.tb00193.x.

[22] Mizutani J, Matsubara T, Muneyoshi A, Ae F, Tanaka N, Iguchi H, et al. Application of full-scale three-dimensional models in patients with rheumatoid cervical spine. Eur Spine 2008;17:644–9. doi:10.1007/s00586-008-0611-3.

[23] Oliveira M, Sooraj Hussain N, Dias AG, Lopes MA, Azevedo L, Zenha H, et al. 3-D biomodelling technology for maxillofacial reconstruction. Mater Sci Eng C 2008;28:1347–51. doi:10.1016/j.msec.2008.02.007.

[24] Hieu LC, Zlatov N, Sloten J Vander, Bohez E, Khanh L, Binh PH, et al. Medical rapid prototyping applications and methods. Assem Autom 2005;25:284–92. doi:10.1108/01445150510626415.

[25] Alkhodary MA, Abdelraheim AEE, Elsantawy AEH, Al Dahman YH, Al-Mershed M. The development of a composite bone model for training on placement of dental implants. Int J Health Sci (Qassim) 2015;9:153–61.

[26] Fürst D, Senck S, Hollensteiner M, Esterer B, Augat P, Eckstein F, et al. Characterization of synthetic foam structures used to manufacture artificial vertebral trabecular bone. Mater Sci Eng C

2017;76:1103–11. doi:10.1016/j.msec.2017.03.158.

[27] Curcio R, Perin GL, Chilvarquer I, Borri ML, Ajzen S. Use of models in surgical predictability of oral rehabilitations. Acta Cirúrgica Bras -VolActa Cirúrgica Bras -Vol 2007;22.

[28] Krenn MH, Piotrowski WP, Penzkofer R, Augat P. Influence of thread design on pedicle screw fixation. J Neurosurg Spine 2008;9:90–5. doi:10.3171/SPI/2008/9/7/090.

[29] Kim Y-K, Kim Y-J, Yun P-Y, Kim J-W. Effects of the taper shape, dual-thread, and length on the mechanical properties of mini-implants. Angle Orthod 2009;79:908–14. doi:10.2319/071808-374.1.

[30] Clyde J, Kosmopoulos V, Carpenter B. A Biomechanical Investigation of a Knotless Tension Band in Medial Malleolar Fracture Models in Composite Sawbones. J Foot Ankle Surg 2013;52:192–4. doi:10.1053/j.jfas.2012.11.001.

[31] PMDA. Outline of Reviews and Related Services n.d. https://www.pmda.go.jp/english/review-services/outline/0001.html (accessed September 28, 2019).

[32] Subrata Pal. Design of Artificial Human Joints & Organs. Springer; 2014. doi:10.1007/978-1-4614-6255-2.

[33] Sedlin ED, Hirsch C. Factors Affecting the Determination of the Physical Properties of Femoral Cortical Bone. Acta Orthop Scand 1966;37:29–48. doi:10.3109/17453676608989401.

[34] Aerssens J, Boonen S, Lowet G, Dequeker J. Interspecies differences in bone composition, density, and quality: Potential implications for in vivo bone research. Endocrinology 1998;139:663–70. doi:10.1210/en.139.2.663.

[35] Pearce AI, Milz S, Schneider E. Animal Models for Implant Biomaterial Research in Bone : a Review. Eur Cells Mater 2007;13:1–10.

[36] ISO TC 150 / SC 5. International Organization for Standardization: ISO 9585:1990 — Implants for surgery — Determination of bending strength and stiffness of bone plates, 1990.

[37] ISO TC 150 / SC 1. International Organization for Standardization: ISO 5833:2002, Implants for surgery — Acrylic resin cements, 2014.

[38] ISO TC 150 / SC 4. International Organization for Standardization: ISO 14242-4:2018, Implants for surgery — Wear of total hip-joint prostheses-Part 4: Testing hip prostheses under variations in component positioning which results in direct edge loading, 2018.

[39] ISO TC 150 / SC 5. International Organization for Standardization: ISO 19213:2017 Implants for surgery — Test methods of material for use as a cortical bone model, 2017.

[40] ASTM. ASTM F543-07 Standard Specification and Test Methods for Metallic Medical Bone Screws, 2007. doi:10.1520/F0543-07E01.with.

[41] Japanese Standards Association. JIS T 0311 Mechanical Testing Methods for Bone Screws, 2009.

[42] Japanese Standards Association. JIS T 0312 Testing Methods for Bending Properties of Metallic Osteosynthesis Devices, 2009.

[43] Japanese Standards Association. JIS T 0313 Testing Method of Compression Bending Properties of Metallic Osteosynthesis Devices, 2009.

[44] Brown GA, McCarthy T, Bourgeault CA, Callahan DJ. Mechanical performance of standard and cannulated 4.0-mm cancellous bone screws. J Orthop Res 2000;18:307–12. doi:10.1002/jor.1100180220.

[45] Koistinen A, Santavirta SS, Kröger H, Lappalainen R. Effect of bone mineral density and amorphous diamond coatings on insertion torque of bone screws. Biomaterials 2005;26:5687–94. doi:10.1016/j.biomaterials.2005.02.003.

[46] Juvonen T, Nuutinen JP, Koistinen AP, Kröger H, Lappalainen R. Biomechanical evaluation of bone screw fixation with a novel bone cement. Biomed Eng Online 2015;14. doi:10.1186/s12938-015-0069-6.

[47] ASTM. ASTM F1839-08, Standard Specification for Rigid Polyurethane Foam for Use as a Standard Material for Testing Orthopaedic Devices and Instruments, 2008. doi:10.1520/F1839-08R16.

[48] Sawbones, Biomechanical Products Catalog 2019.

[49] Chong ACM, Miller F, Buxton M, Friis EA. Fracture toughness and fatigue crack propagation rate of short fiber reinforced epoxy composites for analogue cortical bone. J Biomech Eng 2007;129:487–93. doi:10.1115/1.2746369.

[50] Heiner AD. Structural properties of fourth-generation composite femurs and tibias. J Biomech 2008;41:3282–4. doi:10.1016/j.jbiomech.2008.08.013.

[51] Elfar J, Menorca RMG, Reed JD, Stanbury S. Composite bone models in orthopaedic surgery research and education. J Am Acad Orthop Surg 2014;22:111–20. doi:10.5435/JAAOS-22-02-111.

[52] Hausmann J-T. Sawbones in Biomechanical Settings - a Review. Osteo Trauma Care 2006;14:259–64. doi:10.1055/s-2006-942333.

[53] Cseke A, Heinemann R. The effects of cutting parameters on cutting forces and heat generation when drilling animal bone and biomechanical test materials. Med Eng Phys 2018;51:24–30. doi:10.1016/J.MEDENGPHY.2017.10.009.

[54] Inoue T, Shimada S, Hasegawa H, Sato K, Takabatake K, Tamura A, et al. Basics of Aneurysmal Clipping Surgery: The Importance of Wide Operative Field and Repeated Training. Surg Cereb Stroke 2013;41:163–9. doi:10.2335/scs.41.163.

[55] Ozawa K. Study on Mechanical Properties of Bone-Biomodeling. Tohoku Univ Master's Thesis 2010.

[56] Ryder MI, Morio I. Current challenges for dental education in Japan and the United States. Jpn Dent Sci Rev 2011;47:23–30. doi:10.1016/j.jdsr.2010.05.001.

[57] Reznick RK, MacRae H. Teaching surgical skills - Changes in the wind. N Engl J Med 2006;355:2664–9. doi:10.1056/NEJMra054785.

[58] Cosman P, Hemli JM, Ellis AM, Hugh TJ. Learning the surgical craft: A review of skills training options. ANZ J Surg 2007;77:838–45. doi:10.1111/j.1445-2197.2007.04254.x.

[59] NSW Department of Primary Industries and Animal Research Review Panel. Use of animals in post-graduate surgical training | Animal Ethics Infolink. ARRP Policies Guidel n.d. https://www.animalethics.org.au/policies-and-guidelines/animals-in-teaching/surgical-training (accessed October 31, 2019).

[60] Sokollik C, Gross J, Buess G. New model for skills assessment and training progress in minimally invasive surgery. Surg Endosc 2004;18:495–500. doi:10.1007/s00464-003-9065-1.

[61] James TP, Pearlman JJ, Saigal A. Predictive force model for haptic feedback in bone sawing. Med Eng Phys 2013;35:1638–44. doi:10.1016/J.MEDENGPHY.2013.05.012.

[62] Pourkand A, Zamani N, Grow D. Mechanical model of orthopaedic drilling for augmented-haptics-based training. Comput Biol Med 2017;89:256–63. doi:10.1016/j.compbiomed.2017.06.021.

[63] da Cruz JAS, dos Reis ST, Cunha Frati RM, Duarte RJ, Nguyen H, Srougi M, et al. Does Warm-Up Training in a Virtual Reality Simulator Improve Surgical Performance? A Prospective Randomized Analysis. J Surg Educ 2016;73:974–8. doi:10.1016/j.jsurg.2016.04.020.

[64] Cecil J, Kumar MBBR, Gupta A, Pirela-Cruz M, Chan-Tin E, Yu J. Development of a virtual reality based simulation environment for orthopedic surgical training. Lect. Notes Comput. Sci. (including Subser. Lect. Notes Artif. Intell. Lect. Notes Bioinformatics), vol. 10034 LNCS, 2017, p. 206–14. doi:10.1007/978-3-319-55961-2_21.

[65] A mandibular model for surgical training, Exsurg®, Tecno Cast Co., Ltd. n.d. https://www.3bs.jp/orthopaedic/exsurg/w65550.htm (accessed September 20, 2019).

[66] Kosukegawa H, Mamada K, Kuroki K, Liu L, Inoue K, Hayase T, et al. Measurements of Dynamic Viscoelasticity of Poly (vinyl alcohol) Hydrogel for the Development of Blood Vessel Biomodeling*. J Fluid Sci Technol 2008;3. doi:10.1299/jfst.3.533.

[67] Mamada K, Kosukegawa H, Fridrici V, Kapsa P, Ohta M. Friction properties of PVA-H/steel ball contact under water lubrication conditions. Tribiology Int 2011;44:757–63. doi:10.1016/j.triboint.2010.12.014.

[68] Ozawa K, Yamaguchi K, Shibata Y, Nakayama T, Hashida Y, Ohta M. Analysis of Mechanical Properties and Microstructures for Development of Bone-Biomodelling. 6th World Congr Biomech 2010:525.

[69] Tawara D, Nagura K, Tsujikami T, Adachi T. Bone Quality Evaluation Based On Bone Remodeling and Multi-scale Simulation. Mech Eng Congr Japan 2012.

[70] Shimizu Y, Yu K, Tupin S, Yoshida H, Matsunaga T, Masuda T, et al. Development of blood vessel model for bionic humanoid. Proc JSME Annu Conf Robot Mechatronics 2018;2018:1P1-J03. doi:10.1299/jsmermd.2018.1P1-J03.

[71] Marinho MM, Adorno BV, Harada K, Mitsuishi M. Active constraints using vector field inequalities for surgical robots. Proc. - IEEE Int. Conf. Robot. Autom., vol. 35, 2018, p. 5364–71. doi:10.1109/ICRA.2018.8461105.

[72] Maruyama H, Tsubaki M, Okuda K, Omata S, Masuda T, Arai F. Optical Measurement of Deformation Distribution on Retinal Model for Vitreoretinal Surgery Training. 2018 IEEE Int. Conf. Cyborg Bionic Syst. CBS 2018, Institute of Electrical and Electronics Engineers Inc.; 2019, p. 278–81. doi:10.1109/CBS.2018.8612175.

[73] Totora GJ. Principles of anatomy and physiology. 1987.

[74] Currey JD. The relationship between the stiffness and the mineral content of bone. J Biomech 1969;2:477–80. doi:10.1016/0021-9290(69)90023-2.

[75] Saha S, Martin DL, Phillips A. Elastic and strength properties of canine long bones. Med Biol Eng Comput 1977;15:72–4. doi:10.1007/BF02441578.

[76] Bonfield W, Grynpas MD. Anisotropy of the Young's modulus of bone. Nature 1977;270:453–4. doi:10.1038/270453a0.

[77] Martin RB. Determinants of the mechanical properties of bones. J Biomech 1991;24:79–88. doi:10.1016/0021-9290(91)90379-2.

[78] Martin RB, Boardman DL. The effects of collagen fiber orientation, porosity, density, and mineralization on bovine cortical bone bending properties. J Biomech 1993;26:1047–54. doi:10.1016/S0021-9290(05)80004-1.

[79] Evans FG. The mechanical properties of bone. Springfield, Ill, C C Thomas 1957:37–48.

[80] Carter DR, Hayes WC. Bone compressive strength: The influence of density and strain rate. Science (80-) 1976;194:1174–6. doi:10.1126/science.996549.

[81] Carter DR, Hayes WC. Compact bone fatigue damage-I. Residual strength and stiffness. J Biomech 1977;10:325–37. doi:10.1016/0021-9290(77)90005-7.

[82] Currey J. Measurement of the mechanical properties of bone: A recent history. Clin. Orthop. Relat. Res., vol. 467, 2009, p. 1948–54. doi:10.1007/s11999-009-0784-z.

[83] Turner CH, Rho J, Takano Y, Tsui TY, Pharr GM. The elastic properties of trabecular and cortical bone tissues are similar: results from two microscopic measurement techniques. J Biomech 1999;32:437–41.

[84] Zysset PK, Edward Guo X, Edward Hoffler C, Moore KE, Goldstein SA. Elastic modulus and hardness of cortical and trabecular bone lamellae measured by nanoindentation in the human femur. J Biomech 1999;32:1005–12. doi:10.1016/S0021-9290(99)00111-6.

[85] Hoc T, Henry L, Verdier M, Aubry D, Sedel L, Meunier A. Effect of microstructure on the mechanical properties of Haversian cortical bone. Bone 2006;38:466–74. doi:10.1016/j.bone.2005.09.017.

[86] Bala Y, Depalle B, Farlay D. Bone micromechanical properties are compromised during long-term alendronate therapy independently of mineralization. J Bone Miner Res 2012;27:825–34. doi:10.1002/jbmr.1501.

[87] Faingold A, Cohen SR, Wagner HD. Nanoindentation of osteonal bone lamellae. J Mech Behav Biomed Mater 2012;9:198–206. doi:10.1016/j.jmbbm.2012.01.014.

[88] Feng L, Chittenden M, Schirer J, Dickinson M, Jasiuk I. Mechanical properties of porcine femoral cortical bone measured by nanoindentation. J Biomech 2012;45:1775–82. doi:10.1016/j.jbiomech.2012.05.001.

[89] Bayraktar HH, Morgan EF, Niebur GL, Morris GE, Wong EK, Keaveny TM. Comparison of the elastic and yield properties of human femoral trabecular and cortical bone tissue. J Biomech 2004;37:27–35. doi:10.1016/S0021-9290(03)00257-4.

[90] Autefage A, Palierne S, Charron C, Swider P. Effective mechanical properties of diaphyseal cortical bone in the canine femur. Vet J 2012;194:202–9. doi:10.1016/j.tvjl.2012.04.001.

[91] Bonney H, Colston BJ, Goodman AM. Regional variation in the mechanical properties of cortical bone from the porcine femur. Med Eng Phys 2011;33:513–20. doi:10.1016/j.medengphy.2010.12.002.

[92] Imbert L, Aurégan J-CC, Pernelle K, Hoc T. Mechanical and mineral properties of osteogenesis imperfecta human bones at the tissue level. Bone 2014;65:18–24. doi:10.1016/j.bone.2014.04.030.

[93] Hansen U, Zioupos P, Simpson R, Currey JD, Hynd D. The effect of strain rate on the mechanical properties of human cortical bone. J Biomech Eng 2008;130. doi:10.1115/1.2838032.

[94] Johnson TPM, Socrate S, Boyce MC. A viscoelastic, viscoplastic model of cortical bone valid at low and high strain rates. Acta Biomater 2010;6:4073–80. doi:10.1016/J.ACTBIO.2010.04.017.

[95] Bushby AJ, Ferguson VL, Boyde A. Nanoindentation of bone: Comparison of specimens tested in liquid and embedded in polymethylmethacrylate. J Mater Res 2004;19:249–59.

doi:10.1557/jmr.2004.19.1.249.

[96] Mirzaali MJ, Schwiedrzik JJ, Thaiwichai S, Best JP, Michler J, Zysset PK, et al. Mechanical properties of cortical bone and their relationships with age, gender, composition and microindentation properties in the elderly. Bone 2016;93:196–211. doi:10.1016/j.bone.2015.11.018.

[97] van Haaren EH, van der Zwaard BC, van der Veen AJ, Heyligers IC, Wuisman PI, Smit TH. Effect of long-term preservation on the mechanical properties of cortical bone in goats. Acta Orthop 2008;79:708–16. doi:10.1080/17453670810016759.

[98] Stefan U, Michael B, Werner S. Effects of three different preservation methods on the mechanical properties of human and bovine cortical bone. Bone 2010;47:1048–53. doi:10.1016/j.bone.2010.08.012.

[99] Kaye B, Randall C, Walsh D, Hansma P. The Effects of Freezing on the Mechanical Properties of Bone. Open Bone J 2012;4:14–9.

[100] Szebényi G, Görög P, Török Á, Kiss RM. Effect of different conservation methods on some mechanical properties of swine bone. WIT Trans. Biomed. Heal., vol. 17, 2013, p. 225–33. doi:10.2495/BIO130201.

[101] Richmond BG, Wright BW, Grosse I, Dechow PC, Ross CF, Spencer MA, et al. Finite element analysis in functional morphology. Anat. Rec. - Part A Discov. Mol. Cell. Evol. Biol., vol. 283, 2005, p. 259–74. doi:10.1002/ar.a.20169.

[102] Raffaella A, Petrescu FIT, Petrescu RV V., Antonio A. Biomimetic finite element analysis bone modeling for customized hybrid biological prostheses development. Am J Appl Sci 2016;13:1060–7. doi:10.3844/ajassp.2016.1060.1067.

[103] Mielke M, Nyakatura JA. Bone microstructure in finite element modeling: the functional role of trabeculae in the femoral head of Sciurus vulgaris. Zoomorphology 2019;138:535–47. doi:10.1007/s00435-019-00456-2.

[104] Marco M, Rodríguez-Millán M, Santiuste C, Giner E, Henar Miguélez M. A review on recent advances in numerical modelling of bone cutting. J Mech Behav Biomed Mater 2015;44:179–201. doi:10.1016/J.JMBBM.2014.12.006.

[105] Takabi B, Tai BL. A review of cutting mechanics and modeling techniques for biological materials. Med Eng Phys 2017;45:1–14. doi:10.1016/j.medengphy.2017.04.004.

[106] An YH, Draughn RA. Mechanical testing of bone and the bone-implant interface. 1st editio. CRC Press; 1999. doi:10.1201/9781420073560.

[107] Chevalier J, Gremillard L. Ceramics for medical applications: A picture for the next 20 years. J Eur Ceram Soc 2009;29:1245–55. doi:10.1016/j.jeurceramsoc.2008.08.025.

[108] Abrão AM, Faria PE, Rubio JCC, Reis P, Davim JP. Drilling of fiber reinforced plastics: A review. J

Mater Process Technol 2007;186:1–7. doi:10.1016/j.jmatprotec.2006.11.146.

[109] Ohta M, Shibata Y, Katakura Y, Oikawa N. Bone model. P2008-250004A, 2008.

[110] Merchant ME. Mechanics of the metal cutting process. I. Orthogonal cutting and a type 2 chip. J Appl Phys 1945;16:267–75. doi:10.1063/1.1707586.

[111] Merchant ME. Mechanics of the metal cutting process. II. Plasticity conditions in orthogonal cutting. J Appl Phys 1945;16:318–24. doi:10.1063/1.1707596.

[112] Lee EH, Shaffer BW. The Theory of Plasticity Applied to Machining. vol. 18. 1951.

[113] Kobayashi A. Machining of Plastics. McGraw-Hill; 1967.

[114] Nakayama K. Cutting Theory (in Japanese). Tokyo, Japan: Corona Publishing; 1994.

[115] Sanda A. Ultrasonically assisted drilling of carbon fibre reinforced plastics and Ti6Al4V. J Manuf Process 2016;22:169–76. doi:10.1016/j.jmapro.2016.03.003.

[116] Vigneshwaran S, Uthayakumar · M, Arumugaprabu · V. Review on Machinability of Fiber Reinforced Polymers: A Drilling Approach. Silicon 2018;10:2295–305. doi:10.1007/s12633-018-9764-9.

[117] Mishra BP, Mishra D, Panda P. Drilling of glass fibre reinforced polymer /nanopolymer composite laminates: a review. vol. 8. 2018.

[118] Hocheng H, Puw HY. Machinability of Fiber-Reinforced Thermoplastics in Drilling. Trans ASME 1993;115:146–9.

[119] Mathew J, Ramakrishnan N, Naik NK. Investigations into the effect of geometry of a trepanning tool on thrust and torque during drilling of GFRP composites. J Mater Process Technol 1999;91:1–11.

[120] Lin S-C, Shen J-M. Drilling Unidirectional Glass Fiber-Reinforced Composite Materials at High Speed. J Compos Mater 1999;33:827–51. doi:10.1177/002199839903300903.

[121] Tsao CC, Hocheng H. The effect of chisel length and associated pilot hole on delamination when drilling composite materials. Int J Mach Tools Manuf 2003;43:1087–92. doi:10.1016/S0890-6955(03)00127-5.

[122] Mohan NS, Ramachandra A, Kulkarni SM. Machining of Fiber-reinforced Thermoplastics: Influence of Feed and Drill Size on Thrust Force and Torque during Drilling. J Reinf Plast Compos 2005;24. doi:10.1177/0731684405049865.

[123] Faria PE, Campos RF, Abrao a. M, Godoy GCD, Davim JP. Thrust Force and Wear Assessment When Drilling Glass Fiber-Reinforced Polymeric Composite. J Compos Mater 2008;42:1401–14. doi:10.1177/0021998308090456.

[124] Palanikumar K. Experimental investigation and optimisation in drilling of GFRP composites. Measurement 2011;44:2138–48. doi:10.1016/j.measurement.2011.07.023.

[125] Turki Y, Habak M, Velasco R, Aboura Z, Khellil K, Vantomme P. Experimental investigation of drilling damage and stitching effects on the mechanical behavior of carbon/epoxy composites. Int J Mach Tools Manuf 2014;87:61–72. doi:10.1016/j.ijmachtools.2014.06.004.

[126] John A. Hobkirk, Roger M. Watson LJJ. Introducing dental implants. 1st editio. Elsevier; 2003.

[127] Zimmer. Zimmer® NCB® Plating System Catalog. n.d.

[128] Zimmer. NCB® Distal Femur System Catalog. n.d.

[129] Natali C, Ingle P, Dowell J. Orthopaedic Bone Drills – Can They Be Improved? J Bone Joint Surg Br 1996;78-B:357–62. doi:10.1302/0301-620x.78b3.0780357.

[130] Motoyoshi M, Hirabayashi M, Uemura M, Shimizu N. Recommended placement torque when tightening an orthodontic mini-implant. Clin Oral Implants Res 2006;17:109–14. doi:10.1111/j.1600-0501.2005.01211.x.

[131] Erikssons AR, Albrekt T, Albrektsson B. Heat caused by drilling cortical bone. Acta Orthop Scand 1984:629–31.

[132] Augustin G, Zigman T, Davila S, Udilljak T, Staroveski T, Brezak D, et al. Cortical bone drilling and thermal osteonecrosis. Clin Biomech 2012;27:313–25. doi:10.1016/j.clinbiomech.2011.10.010.

[133] Pandey RK, Panda SS. Drilling of bone: A comprehensive review. J Clin Orthop Trauma 2013;4:15–30. doi:10.1016/j.jcot.2013.01.002.

[134] Abouzgia MB, Symington JM. Effect of drill speed on bone temperature. Int J Oral Maxillofac Surg 1996;25:394–9. doi:10.1016/S0901-5027(06)80040-8.

[135] Hillery MT, Shuaib I. Temperature effects in the drilling of human and bovine bone 1999;93:302–8.

[136] Folkman J. Heat generation during implant drilling: The significance of motor speed. J Oral Maxillofac Surg 2002;60:1160–9. doi:10.1053/joms.2002.34992.

[137] Bachus KN, Rondina MT, Hutchinson DT. The effects of drilling force on cortical temperatures and their duration: An in vitro study. Med Eng Phys 2000;22:685–91. doi:10.1016/S1350-4533(01)00016-9.

[138] Kim S-J, Yoo J, Kim Y-S, Shin S-W. Temperature change in pig rib bone during implant site preparation by low-speed drilling. J Appl Oral Sci 2010;18:522–7. doi:10.1590/S1678-77572010000500016.

[139] Lee JE, Ozdoganlar OB, Rabin Y. An experimental investigation on thermal exposure during bone drilling. Med Eng Phys 2012;34:1510–20. doi:10.1016/j.medengphy.2012.03.002.

[140] Palmisano AC, Tai BL, Belmont B, Irwin TA, Shih A, Holmes JR. Comparison of Cortical Bone Drilling Induced Heat Production Among Common Drilling Tools. J Orthop Trauma 2015;29:e188–93. doi:10.1097/BOT.0000000000000240.

[141] Noorazizi MS, Izamshah R, Kasim MS. Effects of Drill Geometry and Penetration Angle on Temperature and Holes Surfaces for Cortical Bovine Bone: An in Vitro Study. Procedia Eng 2017;184:70–7. doi:10.1016/j.proeng.2017.04.072.

[142] Sener BC, Dergin G, Gursoy B, Kelesoglu E, Slih I. Effects of irrigation temperature on heat control in vitro at different drilling depths. Clin Oral Implants Res 2009;20:294–8. doi:10.1111/j.1600-0501.2008.01643.x.

[143] Hou Y, Li C, Ma H, Zhang Y, Yang M, Zhang X. An Experimental Research on Bone Drilling Temperature in Orthopaedic Surgery. Open Mater Sci J 2015;9:178–88.

[144] Kirstein K, Dobrzyński M, Kosior P, Chrószcz A, Dudek K, Fita K, et al. Infrared Thermographic Assessment of Cooling Effectiveness in Selected Dental Implant Systems. Biomed Res Int 2016;2016. doi:10.1155/2016/1879468.

[145] Feldmann A, Gavaghan K, Stebinger M, Williamson T, Weber S, Zysset P. Real-Time Prediction of Temperature Elevation During Robotic Bone Drilling Using the Torque Signal. Ann Biomed Eng 2017;45:2088–97. doi:10.1007/s10439-017-1845-1.

[146] Ortmaier T, Weiss H, Döbele S, Schreiber U. Experiments on robot-assisted navigated drilling and milling of bones for pedicle screw placement. Int J Med Robot Comput Assist Surg 2006;2:350–63. doi:10.1002/rcs.

[147] Mitsuishi M, Sugita N, Harada K. Super-microsurgical robotic platforms and investigation of super-precise manufacturing technologies. Seimitsu Kogaku Kaishi/Journal Japan Soc Precis Eng 2014;80:36–41. doi:10.2493/jjspe.80.36.

[148] Bouazza-Marouf K, Browbank I, Hewit JR. Robot-assisted invasive orthopaedic surgery. Mechatronics 1996;6:381–97. doi:10.1016/0957-4158(96)00002-5.

[149] Nguyen Y, Bernardeschi D, Sterkers O. Potential of Robot-Based Surgery for Otosclerosis Surgery. Otolaryngol Clin North Am 2018;51:475–85. doi:10.1016/J.OTC.2017.11.016.

[150] Kawana H, Usuda S, Yu K, Nakagawa T, Ohnishi K. A remote controlled haptic drilling robot for oral and maxillofacial surgery. Int J Oral Maxillofac Surg 2017;46:207. doi:10.1016/J.IJOM.2017.02.704.

[151] Wazid M, Das AK, Lee J-H. User authentication in a tactile internet based remote surgery environment: Security issues, challenges, and future research directions. Pervasive Mob Comput 2019;54:71–85. doi:10.1016/J.PMCJ.2019.02.004.

[152] Bertollo N, Walsh WR. Drilling of Bone: Practicality, Limitations and Complications Associated with Surgical Drill-Bits. 2011.

[153] Augustin G, Davila S, Mihoci K, Udiljak T, Vedrina DS, Antabak A. Thermal osteonecrosis and bone

drilling parameters revisited. Arch Orthop Trauma Surg 2008;128:71–7. doi:10.1007/s00402-007-0427-3.

[154] Jacobs CH, Pope MH, Berry JT, Hoaglund F. A study of the bone machining process-Orthogonal cutting. J Biomech 1974;7. doi:10.1016/0021-9290(74)90051-7.

[155] Allotta B, Belmonte F, Bosio L, Dario P. Study on a mechatronic tool for drilling in the osteosynthesis of long bones: Tool/bone interaction, modeling and experiments. Mechatronics 1996;6:447–59. doi:10.1016/0957-4158(96)00005-0.

[156] Hobkirk JA, Rusiniak K. Investigation of variable factors in drilling bone. J Oral Surg (Chic) 1977;35:968–73.

[157] Bertollo N, Milne HRM, Ellis LP, Stephens PC, Gillies RM, Walsh WR. A comparison of the thermal properties of 2- and 3-fluted drills and the effects on bone cell viability and screw pull-out strength in an ovine model. Clin Biomech 2010;25:613–7. doi:10.1016/j.clinbiomech.2010.02.007.

[158] Larry S. M, Carl H. Temperatures Measured in Human Cortical Bone when Drilling. J Bone Joint Surg Am 1972;54A:297–308. doi:10.2106/00004623-197254020-00008.

[159] Matthews LS, Green CA, Goldstein SA. The thermal effects of skeletal fixation-pin insertion in bone. J Bone Jt Surg - Ser A 1984;66:1077–83. doi:10.2106/00004623-198466070-00015.

[160] Schmidt AO, Roubik JO. Distribution of Heat Generated in Drilling. Trans ASME 1949;71:245–52.

[161] Pandey RK, Panda SS. Modeling of temperature in orthopaedic drilling using fuzzy logic. Appl. Mech. Mater., vol. 249–250, 2013, p. 1313–8. doi:10.4028/www.scientific.net/AMM.249-250.1313.

[162] Tai BL, Palmisano AC, Belmont B, Irwin TA, Holmes J, Shih AJ. Numerical evaluation of sequential bone drilling strategies based on thermal damage. Med Eng Phys 2015;37:855–61. doi:10.1016/J.MEDENGPHY.2015.06.002.

[163] Al-Abdullah KIA lateef, Abdi H, Lim CP, Yassin W. Force and temperature modelling of bone milling using artificial neural networks. Meas J Int Meas Confed 2018;116:25–37. doi:10.1016/j.measurement.2017.10.051.

[164] Vilimek M, Horak Z, Goldmann T, Tichy P. Experimental Measurement and Numerical Simulation of Temperature During Drilling With Four Specific Dental Drills 2018:1–5.

[165] Feldmann A, Wili P, Maquer G, Zysset P. The thermal conductivity of cortical and cancellous bone. Eur Cells Mater 2018;35:25–33. doi:10.22203/eCM.v035a03.

[166] Chacon GE, Bower DL, Larsen PE, McGlumphy EA, Beck FM. Heat production by 3 implant drill systems after repeated drilling and sterilization. J Oral Maxillofac Surg 2006;64:265–9. doi:10.1016/j.joms.2005.10.011.

[167] Wiggins KL, Malkin S. Drilling of bone. J Biomech 1976;9:553–9. doi:10.1016/0021-9290(76)90095-6.

[168] MacAvelia T, Salahi M, Olsen M, Crookshank M, Schemitsch EH, Ghasempoor A, et al. Biomechanical measurements of surgical drilling force and torque in human versus artificial femurs. J Biomech Eng 2012;134:124503. doi:10.1115/1.4007953.

[169] Möhlhenrich SC, Modabber A, Steiner T, Mitchell DA, Hölzle F. Heat generation and drill wear during dental implant site preparation: Systematic review. Br J Oral Maxillofac Surg 2015;53:679–89. doi:10.1016/j.bjoms.2015.05.004.

[170] Lee J, Chavez CL, Park J. Parameters affecting mechanical and thermal responses in bone drilling: A review. J Biomech 2018;71:4–21. doi:10.1016/J.JBIOMECH.2018.02.025.

[171] Wang W, Shi Y, Yang N, Yuan X. Experimental analysis of drilling process in cortical bone. Med Eng Phys 2014;36:261–6. doi:10.1016/j.medengphy.2013.08.006.

[172] Tuijthof GJM, Frühwirt C, Kment C. Influence of tool geometry on drilling performance of cortical and trabecular bone. Med Eng Phys 2013;35:1165–72. doi:10.1016/j.medengphy.2012.12.004.

[173] L. Roseiro, C. Veiga, V. Maranha, A.Neto, N. Laraqi, A. Baïri NA. Induced Bone Tissue Temperature in Drilling Procedures: A Comparative Laboratory Study with and without Lubrication. Int J Medical, Heal Biomed Bioeng Pharm Eng 2014;8:828–31.

[174] Li S, Abdel-Wahab A, Demirci E, Silberschmidt V V. Penetration of cutting tool into cortical bone: Experimental and numerical investigation of anisotropic mechanical behaviour. J Biomech 2014;47:1117–26. doi:10.1016/J.JBIOMECH.2013.12.019.

[175] Sui J, Sugita N, Ishii K, Harada K, Mitsuishi M. Mechanistic modeling of bone-drilling process with experimental validation. J Mater Process Technol 2014;214:1018–26. doi:10.1016/j.jmatprotec.2013.11.001.

[176] Lughmani WA, Bouazza-Marouf K, Ashcroft I. Drilling in cortical bone: a finite element model and experimental investigations. J Mech Behav Biomed Mater 2015;42:32–42. doi:10.1016/j.jmbbm.2014.10.017.

[177] Khurshid A, Bahadur. IM, Ahmed. N. Cortical bone drilling, An experimental and numerical study. Technol Heal Care 2015;23:223–31.

[178] Liao Z, Axinte DA. On monitoring chip formation, penetration depth and cutting malfunctions in bone micro-drilling via acoustic emission. J Mater Process Technol 2016;229:82–93. doi:10.1016/j.jmatprotec.2015.09.016.

[179] Feldmann A, Ganser P, Nolte L, Zysset P. Orthogonal cutting of cortical bone: Temperature elevation and fracture toughness. Int J Mach Tools Manuf 2017;118–119:1–11.

doi:10.1016/j.ijmachtools.2017.03.009.

[180] Tai BL, Kao Y-T, Payne N, Zheng Y, Chen L, Shih AJ. 3D Printed composite for simulating thermal and mechanical responses of the cortical bone in orthopaedic surgery. Med Eng Phys 2018;61:61–8. doi:10.1016/J.MEDENGPHY.2018.08.004.

[181] Allan W, Williams ED, Kerawala CJ. Effects of repeated drill use on temperature of bone during preparation for osteosynthesis self-tapping screws. Br J Oral Maxillofac Surg 2005;43:314–9. doi:10.1016/j.bjoms.2004.11.007.

[182] Marciniak J, Paszenda Z, Kaczmarek M, Szewczenko J, Basiaga M, Gierzyńska-Dolna M, et al. Wear investigations of tools used in bone surgery New ceramic-polymer composite for epithesis with aluminum-silicate microspheres View project Wear investigations of tools used in bone surgery. J Achiev Mater Manuf Eng 2007;20:259–62.

[183] Tawara D, Tsujikami T, Okano Y. GS2-11 Verification of similarity of drilling properties between developed new artificial bone model and real bone(GS2: Orthopaedic Biomechanics II). Proc Asian Pacific Conf Biomech Emerg Sci Technol Biomech 2015;2015.8:154. doi:10.1299/jsmeapbio.2015.8.154.

[184] Tawara D, Toyono S, Tsujikami T, Okano Y. Analysis of drilling properties between the artificial bone models having different micro structure for surgery education. Proc Bioeng Conf Annu Meet BED/JSME 2018;2018.30:2C19. doi:10.1299/jsmebio.2018.30.2C19.

[185] Tai BL, Wang AC, Joseph JR, Wang PI, Sullivan SE, Mckean EL, et al. A physical simulator for endoscopic endonasal drilling techniques: technical note. J Neurosurg 2016;124:811–6. doi:10.3171/2015.3.JNS1552.

[186] Ina K, Takano N, Toyama K. Bone model. JPH06230717A, 1993.

[187] Alauddin M, Choudhury IA, El Baradie MA, Hashmi MSJ. Plastics and their machining: A review. J Mater Process Tech 1995;54:40–6. doi:10.1016/0924-0136(95)01917-0.

[188] Jagtap TU, Mandave HA. Machining of Plastics: A Review. Int J Eng Res Gen Sci 2015;3:577–81.

[189] Nassar MMA, Arunachalam R, Alzebdeh KI. Machinability of natural fiber reinforced composites: a review. Int J Adv Manuf Technol 2017;88:2985–3004. doi:10.1007/s00170-016-9010-9.

[190] Irisawa T, Iwamura R, Kozawa Y, Kobayashi S, Tanabe Y. Recycling methods for thermoplastic-matrix composites having high thermal stability in focusing on reuse of the carbon fibers. TANSO 2017;2017:175–81. doi:10.7209/tanso.2017.175.

[191] Tanaka K, Kashihara H, Katayama T. Vacuum assisted high speed compression molding and evaluation of mechanical properties of continuous carbon fiber reinforced polycarbonate composite. Zair Soc Mater

Sci Japan 2011;60:251–8. doi:10.2472/jsms.60.251.

[192] Yan X, Imai Y, Shimamoto D, Hotta Y. Relationship study between crystal structure and thermal/mechanical properties of polyamide 6 reinforced and unreinforced by carbon fiber from macro and local view. Polymer (Guildf) 2014;55:6186–94. doi:10.1016/j.polymer.2014.09.052.

[193] Rezaei F, Yunus R, Ibrahim NA, Mahdi ES. Development of short-carbon-fiber-reinforced polypropylene composite for car bonnet. Polym - Plast Technol Eng 2008;47:351–7. doi:10.1080/03602550801897323.

[194] Jagtap K, Pawade R. Experimental Investigation on the Influence of Cutting Parameters on Surface Quality in SPDT of PMMA. vol. 7. 2014.

[195] Abboud M, Vol S, Duguet E, Fontanille M. PMMA-based composite materials with reactive ceramic fillers: Part III: Radiopacifying particle-reinforced bone cements. J Mater Sci Mater Med 2000;11:295–300. doi:10.1023/A:1008981917653.

[196] Kurimoto M, Ozaki H, Yamashita Y, Funabashi T, Kato T, Suzuoki Y. Dielectric properties and 3D printing of UV-cured acrylic composite with alumina microfiller. IEEE Trans Dielectr Electr Insul 2016;23:2985–92. doi:10.1109/TDEI.2016.7736862.

[197] Saleh KJ, El Othmani MM, Tzeng TH, Mihalko WM, Chambers MC, Grupp TM. Acrylic bone cement in total joint arthroplasty: A review. J Orthop Res 2016;34:737–44. doi:10.1002/jor.23184.

[198] Currey JD. The mechanical consequences of variation in the mineral content of bone. J Biomech 1969;2:1–11. doi:10.1016/0021-9290(69)90036-0.

[199] Linde F, Sørensen HCF. The effect of different storage methods on the mechanical properties of trabecular bone. vol. 26. 1993. doi:10.1016/0021-9290(93)90072-M.

[200] Stelzle F, Frenkel C, Riemann M, Knipfer C, Stockmann P, Nkenke E. The effect of load on heat production, thermal effects and expenditure of time during implant site preparation - an experimental ex vivo comparison between piezosurgery and conventional drilling. Clin Oral Implants Res 2014;25. doi:10.1111/clr.12077.

[201] Surgical Manual BIOMET 3i. n.d.

[202] Matthews LS, Green CA, Goldstein SA. The thermal effects of skeletal fixation-pin insertion in bone. J Bone Jt Surg - Ser A 1984;66:1077–83. doi:10.2106/00004623-198466070-00015.

[203] Wu JW, Sung WF, Chu H Sen. Thermal conductivity of polyurethane foams. Int J Heat Mass Transf 1999;42:2211–7. doi:10.1016/S0017-9310(98)00315-9.

[204] Nakayama K. Classification of chips form. J Japan Soc Precis Eng 1976;42:74–80. doi:10.2493/jjspe1933.42.74.

[205] Ono K, Kawamura S, Kitano M, Shimamune T. Theoretical machining engineering. Gendai Kogaku Publisher; 1979.

[206] Charnley J. Anchorage of the Femoral Head Prosthesis. J Bone Jt Surg Br Vol 1960;42-B:28–30. doi:10.1302/0301-620X.42B1.28.

[207] Ashby MF. Materials Selection in Mechanical Design 3rd edition. 2005.

[208] Schmidt-Rohr K, Kulik AS, Beckham HW, Ohlemacher A, Pawelzik U, Boeffel C, et al. Molecular Nature of the β Relaxation in Poly(methyl methacrylate) Investigated by Multidimensional NMR. Macromolecules 1994;27:4733–45. doi:10.1021/ma00095a014.

[209] Merenga AS, Katana GA. Dynamic Mechanical Analysis of PMMA-Cellulose Blends. Int J Polym Mater 2010;60:115–23. doi:10.1080/00914030903538553.

[210] Gill PS, Marcozzi CL, Groves IF. The characterization of poly(methyl methacrylate), (PMMA), by dielectric analysis and the study of the effects of beta-alkyl substitution on the dielectric properties. Sixth Int Conf Dielectr Mater Meas Appl 1992:429–32.

[211] Ina K, Takano N, Toyama K. Bone model. JPH06230718A, 1994.

[212] Muramoto Y. Development of Bone Biomodel Made of Acrylic Composite Materials for Drilling. Tohoku University, 2017.

[213] ASTM. ASTM E399-12, Standard Test Method for Linear-Elastic Plane-Strain Fracture Toughness of Metallic Materials, 2012. doi:10.1520/E0399-09E02.2.

[214] ASTM. ASTM E1820-2011, Standard Test Method for Measurement of Fracture Toughness 2011. doi:10.1520/e1820-11.

[215] Roche S, Pavan S, Loubet J., Barbeau P, Magny B. Influence of the substrate characteristics on the scratch and indentation properties of UV-cured clearcoats. Prog Org Coatings 2003;47:37–48. doi:10.1016/S0300-9440(03)00017-1.

[216] Oliver WC, Pharr GM. An improved technique for determining hardness and elastic modulus using load and displacement sensing indentation experiments. J Mater Res 1992;7:1564–83. doi:10.1557/adv.2015.9.

[217] Murphy BP, Prendergast PJ. Measurement of non-linear microcrack accumulation rates in polymethylmethacrylate bone cement under cyclic loading n.d.;1:7–9.

[218] Saha S, Pal S. Mechanical properties of bone cement: A review. J Biomed Mater Res 1984;18:435–62. doi:10.1002/jbm.820180411.

[219] Alhareb AO, Akil HM, Ahmad ZA. Impact strength, fracture toughness and hardness improvement of PMMA denture base through addition of nitrile rubber/ceramic fillers. Saudi J Dent Res 2017;8:26–34.

doi:10.1016/j.sjdr.2016.04.004.

[220] Vashishth D, Behiri JC, Bonfield W. Crack growth resistance in cortical bone: Concept of microcrack toughening. J Biomech 1997;30:763–9. doi:10.1016/S0021-9290(97)00029-8.

[221] Yan J, Daga A, Kumar R, Mecholsky JJ. Fracture toughness and work of fracture of hydrated, dehydrated, and ashed bovine bone. J Biomech 2008;41:1929–36. doi:10.1016/j.jbiomech.2008.03.037.

[222] Libonati F, Vergani L. Understanding the structure–property relationship in cortical bone to design a biomimetic composite. Compos Struct 2016;139:188–98. doi:10.1016/j.compstruct.2015.12.003.

[223] International Standard. Sensory analysis-Methodology-Ranking Analyse sensorielle-Méthodologie-Classement par rangs. vol. 8587. 2006.

[224] Japanese Standards Association. JIS Z 9080: 2004 Sensory analysis-Methodology. 2004.

Acknowledgements

This study was performed in Graduate School of Biomedical Engineering, Tohoku University, and in Laboratoire de Tribologie et Dynamique des Systèmes (LTDS), Ecole Centrale de Lyon. Since I joined in a Double Degree (DD) Ph.D. Program between Tohoku University and Ecole Centrale de Lyon, and in a Leading Graduate School Program, my research life as a Ph.D. student, from April 2017 to March 2020, was full of wonderful experiences and opportunities to meet a lot of extraordinary people. I could have finished this work and immensely grown as a person thanks to the encounter with those whom I wish to express hereafter my feelings of gratefulness.

First of all, I wish to express my sincere gratitude to Prof. Makoto Ohta (Institute of Fluid Science, Tohoku University), for his generous support and encouragement throughout this work. I truly appreciate his hospitality to have welcomed me as a DD Ph.D. student and willingly sent me to France. I learned many things from him, about how to progress research, and how to act as a Ph.D. student in a laboratory, and how to communicate with people more agreeably. I was fortunate in having him as my supervisor, and will keep in mind what he taught me.

I wish to express my sincere gratitude to Dr. Vincent Fridrici (Laboratoire de Tribologie et Dynamique des Systèmes, Ecole Centrale de Lyon), for being not only my supervisor in French side, but also a great supporter and patron of my life as an international student in Lyon. He generously received me from Japan and let me in his team. His thoughtful support continuously enabled me to concentrate on my research works, and his insightful feedback and comments on my outputs always opened the right way. His open-minded attitude taught me a lot of things.

Secondly, I wish to express my cordial gratitude to Dr. Hitomi Anzai (Institute of Fluid Science, Tohoku University), co-supervisor of my thesis. Her ingoing comments and suggestions based on theoretical thinking and intellectual interest brought me a huge reinforcement on this work.

I wish to send my cordial gratitude to Prof. Philippe Kapsa (Laboratoire de Tribologie et Dynamique des Systèmes, Ecole Centrale de Lyon), co-supervisor of my thesis in French side. His professional guidance backed by the long career in tribology allowed me to observe the experimental outputs from the basic principle.

Thirdly, I wish to show my great appreciation for my thesis advisors. Prof. Shinji Kamakura (Graduate School of Dentistry, Tohoku University) willingly consent not only to give his assistance on sensory evaluation of bone biomodels, but also to be a part of my thesis committee member. Prof. Koshi Adachi (Graduate School of Engineering, Tohoku University) and Prof. Mami Tanaka (Graduate School of Biomedical Engineering, Tohoku University) are kindly willing to take part in my thesis committee. Their

invaluable, insightful, and thoughtful questions and comments have been huge help for me to improve and brush up this Ph.D. thesis.

Furthermore, I wish to cordially thank those who helped me perform a series of experiments related to this work. I wish to send my great thanks to Dr. Toshihiro Mata (Jujo Takeda Rehabilitation Hospital) for his keen cooperation on our sensory evaluation, with distinct understanding of the necessity of the evaluation of tactile feedbacks of bone biomodel as one of the users. Dr. Seiya Ishii (Department of Orthopaedic Surgery, Juntendo University) kindly explained us about the current situation of medical education, which was helpful to set the research objective. Prof. Hiroaki Yoshida (Faculty of Textile Science and Technology, Shinshu University) kindly suggested us the suitable methods for evaluation of tactile feedback based on his major in human engineering. Mr. Yukihiko Shibata (Tecno Cast Co., Ltd.) helped us understand the technical aspects in dentistry, including the use of acrylic resin for fixation of teeth. Drilling tests under constant feed rate were performed with generous help of Mr. Takeshi Kubo (Tanoi MFG. Co., Ltd.) and his colleagues. Mr. Yoichi Watanabe (Industrial Technology Institute, Miyagi Prefectural Government) is also acknowledged for helping us perform drilling tests for measurements of thrust force under constant feed rate drilling.

I also wish to thank Mr. Keisuke Wakui and his colleagues at IFS factory on the technical supports for processing acrylic specimens, Mr. Takeshi Sato (Institute of Fluid Science, Tohoku University) for helping perform compression tests, and also Dr. Hiroyuki Kosukegawa (Institute of Fluid Science, Tohoku University), for helping perform pull-out tests.

These acknowledgements would not reach completion without mentioning my word of thanks to heartening assistance from staffs in my school. I particularly wish to thank Ms. Hiromi Wakabayashi (Graduate School of Biomedical Engineering) for her generous supports on managing administrative works about scholarships and class registration.

I also appreciate the consistent supports from staffs in my laboratory. I wish to show my special gratitude to Dr. Simon Tupin (Institute of Fluid Science, Tohoku University) for his professional technical support based on his enthusiastic interests in engineering. I wish to thank Mr. Atsushi Totsuka (Institute of Fluid Science, Tohoku University) for managing technical works in our laboratory. I wish to thank Ms. Yasuno Emori (Institute of Fluid Science, Tohoku University) for her routinely kind assistance on managing administrative works, in my case particularly about frequent business trips and exportation of materials and instruments related to my work in France. My gratitude also goes to Dr. Yasutomo Shimizu (Institute of Fluid Science, Tohoku University) for his far-sighted advice, and to Dr. Kaihong Yu (Institute of Fluid Science, Tohoku University), and Dr. Mingzi Zhang (Institute of Fluid Science, Tohoku University) for their willingness to offer suggestions and feedbacks on this work.

While in France, Prof. Eric Viguier (VetAgro Sup, University of Lyon, France) kindly offered bone specimens from his veterinary school. Dr. Michelle Salvia (Laboratoire de Tribologie et Dynamique des Systèmes, Ecole Centrale de Lyon) offered her technical support on the Dynamic Mechanical Analysis

measurements of acrylic specimens and shared her knowledge about polymers. Dr. Bruno Berthel (Laboratoire de Tribologie et Dynamique des Systèmes, Ecole Centrale de Lyon) offered his technical support on the temperature measurements and analysis in drilling. Ms. Sophie Pavan (Laboratoire de Tribologie et Dynamique des Systèmes, Ecole Centrale de Lyon) offered her help on indentation tests. Their supports were indispensable to properly conduct my research works at LTDS, so are deeply acknowledged.

I also wish to thank Ms. Sylvie Navarro and Ms. Hélène Schoch (Laboratoire de Tribologie et Dynamique des Systèmes, Ecole Centrale de Lyon) for managing administrative tasks to work in LTDS. I wish to thank cordially Mr. Gaëtan Bouvard (Laboratoire de Tribologie et Dynamique des Systèmes, Ecole Centrale de Lyon) for his technical support on experiments at LTDS. Without his help, my experiments could not have been performed within an acceptable time span. Whenever I had problems in dealing with my experiments, he stopped his own work and came to see the situation. Above all, their supports were indispensable to properly conduct this work. Dr. Julien Fontaine (Laboratoire de Tribologie et Dynamique des Systèmes, Ecole Centrale de Lyon) taught me how to use optical microscope. Mr. Thomas Malhomme not only supported me as a technician, but also sometimes organized sports activities for relaxation time in LTDS.

I should not forget to show my heartfelt gratitude to all my colleagues. I wish to thank you particularly all of my seniors in both Japan and France: Dr. Yujie Li, Dr. Narendra Kurnia Putra, Dr. Marième Fall, and Dr. Ding Haohao, for being great examples and supporting my both research activity and everyday life. Hope I could have done to my youngers what you have done to me. Thank you all of my Ph.D. colleagues: Mr. Kazuhiro Watanabe, Mr. Gaoyang Li, Mr. Haoran Wang, Mr. Muhammad Shiddiq Sayyid Hashuro, Mr. Zi Wang, and Ms. Méghane Decroocq for being good mates and sometimes rivals. Thank you all of my junior colleagues: Mr. Ren Takahashi, Mr. Makoto Ito, Mr. Masami Matsuura, Mr. Ko Kitamura, Mr. Ryota Nagano, Ms. Fanjia Pan, Mr. Dominik Huesener, Mr. Naohiro Kobayashi, Mr. Kazuyoshi Jin and the following generations, for being nice to me and accompanying with me.

In France, despite being far away from my home, I could keep up my mental stability and motivation with the assistance of a lot of associates. I was fortunate in having such good LTDS-mates: Ms. Vilayvone Saisnith, Mr. Amaury Guillermin, Ms. Mayssa Al kharboutly, Ms. Nasrya Kossoko, Mr. Valentin Salinas, Mr. Yun Long, and Ms. Mariana de Souza. Dr. Sho Takeda, Mr. Tadashi Oshio, Mr. Takeshi Kunishima, and Mr. Kazuki Ozawa spent some time with me over a cup of coffee in the lab, or over a table of *cuisine française*. As a Japanese, their presence was a great reassurance to me. I wish to send my special thanks to Dr. Adrien Pyskir for our friendship, always showing his interests in Japanese culture with his outstanding Japanese skills, and to Mr. Pradeep Mohanasundaram, also a DD Ph.D. student in a same program, who spent funny moments with me over Indian curry. I am willing to thank Ms. Laura Jay, also a DD Ph.D. student, and her partner Mr. Louison Trémeaux for caring and supporting me as my best friends. It was truly my pleasure to spend our time both in France and Japan. I wish to thank all the encounters during my Ph.D. works in France and appreciate all the laughs, smiles, and helps you have shared with me.

Huge thanks should be sent to the Program for Leading Graduate Schools, “Inter-Graduate School Doctoral Degree Program on Global Safety", by the Ministry of Education, Culture, Sports, Science and Technology, for its generous supports through a full scholarship and research grant. Their financial supports enabled me to concentrate on my study and to work during these years. I would also like to thank the ImPACT Program of Council for Science, Technology and Innovation (Cabinet Office, Government of Japan) for their funding throughout my research works.

This study was partially supported by the IFS collaborative research project, and also by the JSPS Core-to-Core Program, A. Advanced Research Networks, “International research core on smart layered materials and structures for energy saving”. I would like to express my gratitude to Professor Toshiyuki Takagi (Institute of Fluid Science, Tohoku University) for offering this support. Besides, this research work was carried out on a framework of ELyT lab (CNRS LIA between Tohoku University, INSA Lyon and Ecole Centrale de Lyon). Parts of this study were also covered by the LABEX MANUTECH-SISE (ANR-10-LABX-0075) of Université de Lyon, within the Program "Investissements d'Avenir" (ANR-11-IDEX-0007) operated by the French National Research Agency. LIA ELyT Global is also cordially acknowledged.

Finally, I would like to express my greatest gratitude to dearest friends all over the world. I would like to thank particularly those who have been generous and supportive to me in Sendai and Lyon. I would like to appreciate also my old friends in my hometown, for still keeping in touch and hanging out with me. Having a relaxing time with you has been irreplaceable in my student life.

Last but not least, I would like to express my heartfelt gratitude to my lovely family, younger brothers and sisters, my grandparents, and of course my parents, for their consistent, uncountable and invaluable affection from my birth up until today.

Yuta Muramoto

February 3rd, 2020

List of Publications

Publications with Peer Reviewed Process

International Journals

1. **Yuta Muramoto**, Vincent Fridrici, Philippe Kapsa, Gaëtan Bouvard, Makoto Ohta, *Effects of Temperature Increase During Surgical Drilling in Acrylic Resin.* Technology and Health Care, vol. Pre-press, no. Pre-press, pp. 1-12, 2019. doi: 10.3233/THC-191870 (Chapter 3)

International Conference's Proceedings

1. **Yuta Muramoto,** Vincent Fridrici, Philippe Kapsa, Gaëtan Bouvard, Makoto Ohta, *Fabrication, observation, and tribological characterization of acrylic composite materials for bone biomodel for surgical drilling.* Procédés et Génie civil, JIFT2018 (Journées Internationals Francophones de Tribologie 2018), 16-18 May 2018, Mines ParisTech CEMEF, Sophia Antipolis, France (Accepted) (Chapter 2 and 4)
2. **Yuta Muramoto,** Vincent Fridrici, Philippe Kapsa, Gaëtan Bouvard, Makoto Ohta, *Tribological aspects of drilling bone biomodel*. Procédés et Génie civil, JIFT2015 (Journées Internationals Francophones de Tribologie 2015), 27-29 mai 2015, Nantes, France, Edited by M. -T. Do, V. Cerezo, Ph. Kapsa, pp. 81-89, 2016 (Chapter 4)

***Publications with non-Peer Reviewed* Process**

Journals

1. Makoto Ohta, Dominik Huesener, **Yuta Muramoto,** Simon Tupin, *Biomodel of Hard Tissue for Dynamic Mechanical Testing of Medical Device.* The reports of the Institute of Fluid Science, Tohoku University, Vol. 29 (2017) Sendai, Japan

International Conference Proceedings & Abstracts

1. **Yuta Muramoto**, Vincent Fridrici, Philippe Kapsa, Gaëtan Bouvard, Makoto Ohta, *Drilling properties of acrylic composite materials for modeling of bone drilling in*

dry conditions, International Tribology Conference (ITC) Sendai 2019, September 17-21, 2019, Sendai, Japan

2. **Yuta Muramoto**, Vincent Fridrici, Philippe Kapsa, Gaëtan Bouvard, Makoto Ohta, *The effects of additive amount of acrylic composite materials on drilling properties towards development of bone biomodels*, 46th Leeds-Lyon Symposium on Tribology, September 2-4, 2019, Lyon, France
3. **Yuta Muramoto**, Gaëtan Bouvard, Vincent Fridrici, Philippe Kapsa, Makoto Ohta, *Drilling of PMMA-based bone biomodel: The effects of temperature elevation during drilling*, 8th World Congress of Biomechanics, July 8-12, 2018, Dublin, Ireland
4. **Yuta Muramoto**, Gaëtan Bouvard, Makoto Ohta, Vincent Fridrici, Philippe Kapsa, *Fabrication, Observation and Tribological Characterization of Acrylic Composite Materials for Bone Biomodel for Surgical Drilling*, 30ème Journées Internationals Francophones de Tribologie (JIFT2018), May 16-18, 2018, Sophia Antipolis, France
5. **Yuta Muramoto**, Gaëtan Bouvard, Vincent Fridrici, Philippe Kapsa, Fredrik Lundell, Makoto Ohta, *Research of high-speed contact with medical devices*, The 17th International Symposium on Advanced Fluid Information, November 1-3, 2017, Sendai, Miyagi, Japan
6. **Yuta Muramoto**, Vincent Fridrici, Philippe Kapsa, Gaëtan Bouvard, Fredrik Lundell, Makoto Ohta, Drilling of *PMMA based bone biomodel: effect of additives*, 6th World Tribology Congress (WTC2017), September 17-22, 2017, Beijing, China
7. **Yuta Muramoto**, Makoto Ohta, Vincent Fridrici, Philippe Kapsa, and Gaëtan Bouvard, *Study of Mechanical Properties of Acrylic Composite for Drilling Bone Biomodel*, International Tribology Conference, (ITC 2015), September 16-20, 2015, Tokyo, Japan
8. **Yuta Muramoto**, Makoto Ohta, Vincent Fridrici, Philippe Kapsa, and Gaëtan Bouvard, Tribological aspects of drilling of bone biomodels, 27ème Jornées Internationals Francophones de Tribologie (JIFT2015), May 27-29, 2015, Nantes, France
9. Makoto Ohta, Wataru Sakuma, **Yuta Muramoto**, Hitomi Anzai, Toshio Nakayama, Modeling of Cortical Bone and Bone Marrow, 11th International Conference on Flow Dynamics (ICFD2014), Sendai, Oct. 8-10, 2014

International Symposium Abstracts

1. **Yuta Muramoto**, Vincent Fridrici, Philippe Kapsa, Gaëtan Bouvard, Makoto Ohta, *Tribological Characterization of natural bones and bone substitutes for simulating bone drilling in dry conditions*, ELyT Workshop 2019, March 11-12, 2019, Naruko, Osaki, Japan
2. **Yuta Muramoto**, Vincent Fridrici, Philippe Kapsa, Gaëtan Bouvard, Makoto Ohta, *Tribological aspects of composite materials for bone biomodels: the effects of temperature elevation during drilling*, Second Workshop Lyon Center, November 20, 2018, Lyon, France
3. Makoto Ohta**, Yuta Muramoto,** Ryota Nagano, *Model for fluid evaluation of medical devices*, Second Workshop Lyon Center, November 20, 2018, Lyon, France
4. **Yuta Muramoto**, Vincent Fridrici, Philippe Kapsa, Gaëtan Bouvard, Makoto Ohta, *Tribological aspects of acrylic composite materials: The effects of additives*, ELyT Global-LyC seminar: Bio-tribology, bio-materials and biomedical engineering, July 6, 2018, Lyon, France
5. **Yuta Muramoto**, Dominik Hüsener, Gaëtan Bouvard, Makoto Ohta, Vincent Fridrici, Philippe Kapsa, *Drilling of Acrylic Composite Materials Towards the Development of A New Bone Biomodel*, Swansea Univ. Symposium, March 13, 2018 Swansea, England
6. **Yuta Muramoto**, Dominik Hüsener, Gaëtan Bouvard, Makoto Ohta, Vincent Fridrici, Philippe Kapsa, *Effects of temperature elevation on drilling of acrylic composite materials for bone biomodel*, ELyT Workshop 2018, March 6-8, 2018, La Gentilhommière, Satillieu, France
7. **Yuta Muramoto**, Joanna Seiller, Vincent Fridrici, Gaëtan Bouvard, Philippe Kapsa, Makoto Ohta, *Drilling under constant feed rate for bone biomodel made of acrylic composites*, TFC ELyT Workshop 2016, October 6-8, 2016, Tohoku University & Miyagi Zao Royal Hotel, Japan
8. **Yuta Muramoto**, Joanna Seiller, Vincent Fridrici, Gaëtan Bouvard, Philippe Kapsa, Makoto Ohta, *Comparison of drilling behavior of acrylic materials measured by tribometer*, Beijing-Tohoku Biomechanics Symposium, November 25, 2015, Beijing, China

9. Makoto Ohta, Kaihong Yu, Ren Takahashi, **Yuta Muramoto**, Wataru Sakuma, Taihei Onishi, Hitomi Anzai, *Development of in-vitro and in-silico model for evaluating medical devices*, Beijing-Tohoku Biomechanics Symposium, November 25, 2015, Beijing, China
10. Makoto Ohta, **Yuta Muramoto**, Vincent Fridrici, Kaihong Yu, Philippe Kapsa, *Research of Friction and Drilling on Bio-composite Model (third report)*, AFI-TFI, Oct. 27-29, 2015, Sendai, Japan
11. **Yuta Muramoto**, Gaëtan Bouvard, Vincent Fridrici, Philippe Kapsa, Makoto Ohta, *Production and characterization of composite materials for bones-biomodeling*, 2015 ELyT lab Workshop, Feb. 18-21, 2015, Matsushima, Japan
12. Makoto Ohta, Wataru Sakuma, **Yuta Muramoto**, Hitomi Anzai, Toshio Nakayama, *Modeling of Cortical Bone and Bone Marrow*, 11th International Conference on Flow Dynamics (ICFD2014), Oct. 8-10, 2014, Sendai, Japan

Domestic Symposium Abstracts

1. **Yuta Muramoto**, Vincent Fridrici, Philippe Kapsa, Gaëtan Bouvard, Fredrik Lundell, Makoto Ohta, *An approach to fabricate bone biomodels made of acrylic composite materials for drilling*, Tohoku – Shinshu – Hirosaki University Joint Symposium, 7th August, 2017, Tohoku University, Sendai, Japan

Talks

1. 太田 信，清水康智，Simon Tupin, 大西泰平，**村元雄太**，Joanna Seiller, 于凱鴻，安西 眸, *血管内治療のための血管モデル開発*, 日本機械学会 2016 年度年次大会, 9 月 11-14 日, 2016, 九州大学，福岡

Others

1. **村元雄太,** 医工学研究科リーフレット・在校生の声, 2017

Achievements

Scholarship

1. A Full Ph.D. Scholarship and Research Grant from the Program for Leading Graduate Schools, “Inter-Graduate School Doctoral Degree Program on Global Safety", by the Ministry of Education, Culture, Sports, Science and Technology
2. A Scholarship for Short-term Study Abroad from the Cooperative Laboratory Study Program (COLABS) from 31st August to 16th Sept. 2019, intended for research stay in Laboratoire de Tribologie et Dynamique des Systèmes, Ecole Centrale de Lyon, France.
3. A Scholarship for Long-term Study Abroad in the framework of the Integration Research Center for Materials and Fluid Sciences, at the Lyon Center (LyC) from the Institute of Fluid Science (IFS), from 16th March to 22nd May 2019, intended for research stay in LTDS, ECL, France.
4. A Scholarship for Long-term Study Abroad provided from IFS, supported by the JSPS Core-to-Core Program, A. Advanced Research Networks, “International research core on smart layered materials and structures for energy saving”, from 16th Oct. 2016 to 24th Nov. 2016, intended for research stay in LTDS, ECL, France.
5. A Scholarship for Long-term Study Abroad provided from IFS, supported by the JSPS Core-to-Core Program, A. Advanced Research Networks, “International research core on smart layered materials and structures for energy saving”, from 19th Sept. 2014 to 13th Sept. 2015, intended for research stay in LTDS, ECL, France.